Procedures for Automated Building Energy Model Production for Urban and Early Design

by

Timur Dogan

MDES, Sustainable Design
Harvard Graduate School of Design, 2012.

Dipl. Ing. with Distinction, Architecture
Technische Universität Darmstadt, 2010.

Submitted to the Department of Architecture
In Partial Fulfillment of the Requirements for the Degree of

Doctor of Philosophy in Architecture: Building Technology

at the

Massachusetts Institute of Technology

September 2015

Signature of Author: Signature redacted

Department of Architecture
08.13.2015

Certified by: Signature redacted

Christoph F. Reinhart
Associate Professor of Building Technology
Massachusetts Institute of Technology
Thesis Supervisor

Accepted by: Signature redacted

Chair of the Committee on Graduate Students
Professor Takehiko Nagakura

Thesis Committee:

Christoph F. Reinhart
Associate Professor of Building Technology
Massachusetts Institute of Technology
Thesis Supervisor

Leslie K. Norford,
Professor of Building Technology
Massachusetts Institute of Technology
Thesis Reader

Panagiotis Michalatos,
Assistant Professor of Architectural Technology,
Harvard Graduate School of Design
Thesis Reader

Procedures for Automated Building Energy Model Production for Urban and Early Design

by Timur Dogan

Submitted to the Department of Architecture on August 13, 2015 in Partial Fulfilment of the Requirements for the Degree of Doctor of Philosophy in Architecture: Building Technology

Abstract

This research is meant to facilitate a wider use of energy simulation in urban and schematic building design. The major contribution is the development and validation of software algorithms that can manage, automatically produce and execute building energy models for urban and schematic design. Modeling approaches for building performance simulation engines such as EnergyPlus and TRNSYS have been developed. The first approach introduces an algorithm that automatically converts arbitrary building massing models into multi-zone thermal models following the ASHRAE 90.1 Appendix G prescribed perimeter and core discretization schema. This method yields geometrically resolved multi-zone models and provides a streamlined workflow for single and multi-building energy evaluation. The second approach dissects an urban massing model that may consist of hundreds of buildings with various architectural programs into a discrete number of "typical room" energy models. It is shown that for standard interior partitions and fully conditioned spaces the method yields results that are comparable to conventional perimeter and core simulations in terms of accuracy as well as temporal and spatial resolution at a fraction of the calculation time. This speed-up facilitates interactive urban level design evaluations. The third approach explores the energetic consequences of using a zoning methodology that goes beyond generic perimeter and core subdivisions. Based on a review and categorization of real floor plan designs it is shown that key characteristics of interior subdivisions have a decisive effect on building energy use and present a largely untapped opportunity for architects to reduce building energy use in schematic design. Each approach is documented and simulation results are compared against conventional modeling workflows for a real-world urban case study. As a proof of concept, the mentioned methods have been implemented as plug-ins for the widely used CAD modeling software Rhinoceros3d (Rhino) and its parametric scripting environment Grasshopper.

Thesis supervisor: Christoph F. Reinhart
Title: Associate Professor of Building Technology

Acknowledgements

First and foremost, I wish to thank my Ph.D. advisor Professor Christoph Reinhart. Since the days I began my Master in Design Studies in Harvard, Christoph was overwhelmingly supportive regarding my research and professional career and became a good friend. Working on this thesis has been a great pleasure and I hope we will continue the great discussions and collaborative work. I would also like to thank the members of my thesis committee. Professor Leslie Norford's feedback on my research was incredibly valuable and his expertise appreciated. I am especially thankful to Professor Panagiotis Michalatos for introducing me to the art of programming and computational design. Without the countless hours of his support, this thesis would not have been possible.

I further would like to thank Stefan Holst and Wolfgang Kessling at Transsolar, Munich for giving me the opportunity to work on several exciting projects, the numerous productive discussions and their hospitality.

Friends and colleagues at the Harvard GSD Sustainable Design Lab and MIT Building Technology research groups have made the efforts towards my degree infinitely more pleasant. Thank you, Aiko, Alstan, Carlos, David, Cody, Diego, Holly, Irmak, Jeff, Julia, Madeline, Nathan, Nathaniel, Tarek, Tea and Tianyi. A special thanks to Manos Saratsis for the exceptionally good collaboration on numerous papers. I would also like to thank Kathleen Ross and Renee Caso, who kept the administrative process running smoothly.

I am indebted to my family and friends for their unlimited and unconditional support that incented me to strive towards my goals.

The MIT Presidential Fellowship and Transsolar Energietechnik GmbH have generously funded this research.

Table of Contents

List of Figures

List of Tables

1 Introduction

Population growth, urbanization and related space constraints require new construction and densification of urban centers around the world. With drastically increasing building-related CO_2 emissions in developing countries, urbanization is widely recognized as a key liability and opportunity to fight climate change and to build new livable and energy-efficient habitats. However, energy modeling tools that could inform the design process of these future urban centers are underutilized. Substantial research efforts have gone into the development of building performance simulation tools to ensure that individual building designs can provide "high comfort spaces" while having a "minimum environmental impact." Using these tools to model the energetic implications of existing cities and master-plan proposals with hundreds of buildings, vaguely defined interiors and complex micro-climates can currently not be done effectively. The importance of simulation tools that can inform the urban design process, however, is self-evident given that urban design decisions largely predetermine the intrinsic environmental performance of a building. Providing a new generation of simulation tools that can reliably model cities and master-plan proposals within feasible working hours is an aspect that existing research has yet to address. Accordingly, this thesis concentrates on the development of software that can manage and rapidly produce building energy models for urban-scale simulations. A vision for an enhanced urban energy modeling workflow and its applicability in design is provided.

1.1 Urbanization and its impact on greenhouse gas emissions

The earth's urban population is expected to nearly double by 2050 (Figure 1-1), requiring the construction of hundreds of new cities [UN, 2012]. With building-related CO2 emissions having tripled and quintupled since 1970 in developing countries such as China and Turkey (Figure 1-2) [World Bank, 2015], urbanization is widely recognized as a key liability and opportunity to fight climate change. Building new livable and energy-efficient urban areas can thus be seen as the defining planning challenge of this century.

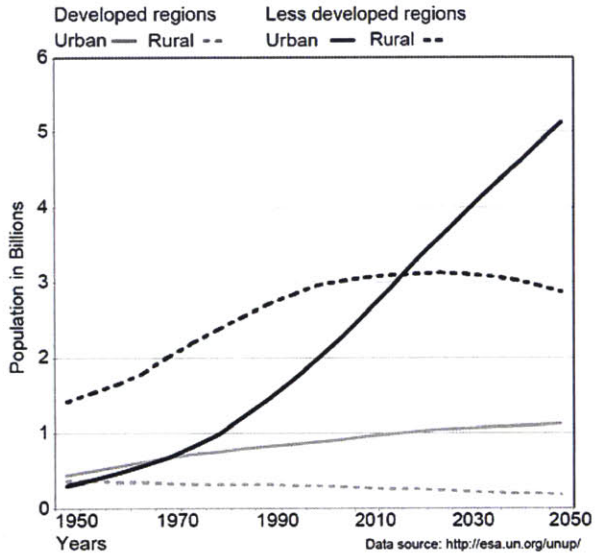

Figure 1-1: Urban and rural population projection

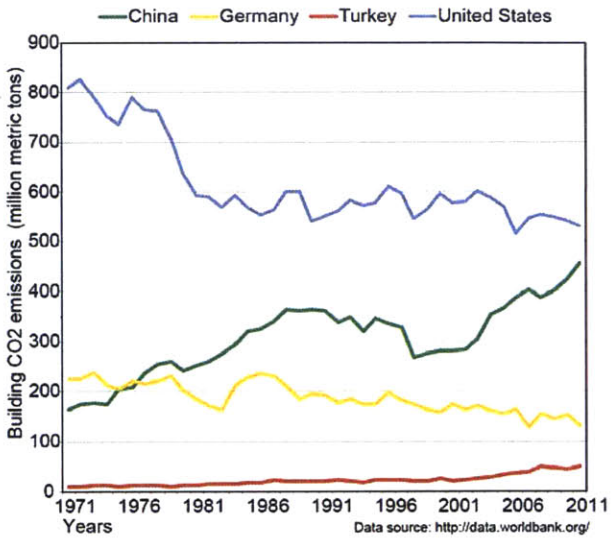

Figure 1-2: Building related CO2 emissions.

1.2 Energy, Environment and Buildings

Buildings serve multiple societal needs. Among their most fundamental function is the provision of a comfortable and safe human habitat. Meeting these needs requires the use of energy resources. In the US and other western countries about 40% of the overall energy use can be attributed to buildings. Out of this 40% an estimated 60% and 47% are used for space conditioning and lighting in residential and commercial buildings, respectively. Building-related energy demand is thus responsible for 38% of US [EERE, 2015] and approximately one-third of global [UNEP, 2015] greenhouse gas (GHG) emissions. In addition to municipal initiatives [The City of New York, 2015] [City of Boston, 2014], efforts such as the "Carbon Roadmap" of the

European Union aim at a 90% reduction of CO2 emissions by 2050 in comparison to 1990 levels [European Commission, 2015]. Similarly, the US Department of Energy has committed to reducing GHG emissions by 28% compared to a 2008 baseline [DOE, 2015]. Meeting this goal will require, among other measures, a fundamental rethinking of architecture and architectural practice.

1.3 Sustainable design process

The goal of a so-called *sustainable design* process is the development of buildings that "meet the needs of the present without compromising the ability of future generations to meet their own needs" [World Commission on Environment and Development, 1987]. In order to approach this overarching ideal, economic, social and environmental viability are considered [UN, 2015]. In the architectural realm these three themes often translate into goals such as ecological and economic efficiency, consistency and sufficiency [Hegger et al., 2013] including considerations regarding energy conservation and generation, minimized material use, efficient space use, higher built densities, recyclability of materials, longevity and flexibility of spaces to reflect changing societal needs.

Within the context of sustainable design, several construction standards and green building rating systems have emerged to frame and evaluate the efforts of creating a more sustainable building sector (LEED [USGBC, 2008], DGNB [DGNB, 2014] BRREAM [BRREAM, 2004] Minergie [Beyeler et al.,2009], EnEV [Bundesrepublik Deutschland, 2007], ASHRAE 90.1 [ANSI/ASHRAE/IES, 2013]).

A popular voluntary residential construction standard evolved out of a research initiative in 1989 [Feist 1989]. The so-called "Passivhaus" standard limits a building's energy demand to ≤15 kWh/m²/a in heating and ≤15 kWh/m²/a in cooling energy and its total primary energy consumption to 120 kWh/m²/a. In comparison, the mandatory building code in Germany at that time prescribed a heating energy demand of ≤150 kWh/m²/a [WSVO 82]. Buildings mostly achieve these specifications through a super-insulated and airtight building envelope and an efficient ventilation system. A more recent initiative postulates the "Active House," which in its most ambitious form allows ≤ 30kWh/m²/a end-use energy and an annual net-zero primary energy balance with 100% on-site renewable energy production [ActiveHouse, 2015]. Besides

operational energy efficiency, the Active House also sets elevated indoor environmental quality standards for daylight availability and quality, thermal comfort, indoor air quality and material selection. The combination of overall resource efficiency and occupant comfort and health is increasingly demanded and leads to a more complete evaluation of the environmental performance of a building.

In order to help architects and engineers design buildings with such ambitious specifications, multidisciplinary design processes are required. These processes are increasingly supported by computer-based building performance simulations (BPS) and models that predict the environmental performance of different design choices and building operation. The so-called building energy models (BEM) can be generated with tools such as TRNSYS [Klein, 1979], ESP-r [Clarke et al., 1993], DOE-2 [Birdsall et al., 1990] and EnergyPlus [Crawley et al., 2000]. The outputs of these models range from energy consumption and renewable energy production to indoor environmental conditions including thermal comfort and daylight availability. Based on these outputs, assumptions about the environmental quality and impact of spaces and buildings can be made.

1.4 The urban scale

In the context of urbanization, designers and environmental engineers have recently broadened their interests and efforts to larger scales [Keirstead et al., 2012] and a new field that applies BEMs to urban scales emerged. Besides technology-driven energy-efficiency improvements that traditionally focus on the building envelope and building level heating, ventilation and air conditioning (HVAC) improvements, urban level solutions may offer various new opportunities and challenges, some of which are listed below.

Building improvement and load mitigation: Urban BEMs (UBEM) can be used to understand and improve energy demand and resilience of new and existing urban areas [USGBC, 2011]. At the urban scale, the sensitivity of several buildings to climate change and related phenomena such as heat waves can be analyzed. Spatially resolved models can then reveal vulnerable buildings and can help to identify the most effective mitigating measures to make the existing building stock future-proof [Jentsch et al., 2008]. Besides load mitigation and increased resource efficiency through retrofits, municipal governments and policy makers may

use the findings of simulated scenarios to target their efforts in order to increase policy impact [Hutchinson et al., 2006].

District energy management and energy supply networks: District energy supply systems and heating, cooling and electricity cogeneration can significantly lower GHG emissions. The utilization of waste heat that incurs during the electricity production increases fuel efficiency and thus can decrease the overall primary energy consumption of a city [UNEP 2015]. When shifting from the building scale to the neighborhood, synergies that may occur among multiple buildings can be identified. Many cities, especially mixed-use urban areas [Gaine &Duffy 2010], as well as campuses such as Stanford University [2015] have incurring simultaneous heating and cooling loads. Interconnected distribution networks can maximize efficiency by allowing buildings to share excess energy with other connected buildings. The use of thermal storage can further help to shift heating or cooling demand by hours, days or even months. This leads to smaller and smoother demand curves that are beneficial for the operation of district-energy-supply-systems. Planners of such systems often require high-resolution time series of end-use heating, cooling and electric loads from the consumer buildings. UBEMs can provide this data when detailed demand profiles are not available, e.g., for new neighborhoods. If the data is spatially resolved, it can be used to optimally lay out and dimension distribution networks. Efficient systems often strategically place power centers to shorten distribution paths to the end-user.

Density and urban environmental quality: Urban densification is often linked to higher economic profitability and enhanced urban-scale sustainability by preserving land and resources, minimizing transportation footprint and fostering socially cohesive urban communities [Owen, 2009]. However, densification can also severely affect environmental quality. This is especially true for ad hoc urban growth, manifested in informal, overcrowded and smog-plagued neighborhoods that deny their inhabitants crucial ingredients of human well-being such as access to fresh air and daylight both inside and around buildings. Urban daylight modeling tools can be used to find a compromise between good annual daylight availability and urban density [Compagnon, 2004], [Strømann-Andersen & Sattrup, 2011] [Dogan et al., 2012] [Saratsis et al., 2015]. Similarly, energy modeling tools can be used to study natural ventilation,

passive solar heating potential and energy conservation measures to minimize fossil fuel use and related emissions as well as indoor and outdoor comfort implications of urban design.

BPS and urban design: However, modeling tools are underutilized when it comes to understanding and predicting the energetic implications of urban form [Besserud and Hussey, 2011]. Current BPS tools have mainly been optimized to accurately evaluate finalized single-building design projects. Modeling districts, urban areas or entire master-plan proposals containing hundreds of buildings with vaguely defined interiors and complex micro-climatic implications cannot be accomplished at an appropriate effort level using current BPS tools. Tool limitations include unjustifiably high model setup and simulation times when used for urban projects. This requires urban energy modelers to introduce various workarounds and simplifications with unknown implications on model accuracy. The importance of simulation tools that can inform urban design and renewal processes, however, is self-evident. Design decisions involve project goals, sustainability statutes, local building code and land development plans that prescribe densities, construction standards, energy supply concepts and urban massing morphology. The massing morphology in turn significantly influences solar, daylight and natural ventilation potentials. Hence, master planning largely predetermines the intrinsic environmental performance of a neighborhood and its buildings. Providing a new generation of UBEM tools is an aspect, that existing research has yet to address. Accordingly, this dissertation concentrates on the development of software that can manage and rapidly produce BEMs for urban-scale simulations. A vision for an urban energy modeling workflow and its applicability is provided.

1.5 Thesis outline

The thesis introduces three methods for rapid BEM generation. Chapter 1 provides a brief overview of the scope of this thesis and its motivation. Further, use case examples of urban BEM applications are discussed. After a brief summary of early design building energy modeling in Chapter 2, the reader is introduced to current urban building energy modeling practice. Manual methods for model abstraction, the so-called Archetype Approach and dedicated urban modeling tools are reviewed and their shortcomings and limitations are

identified. Further, currently available methods to automatically generate and zone energy models are reviewed.

Chapter 3, 4 and 5 explore new paths to generate early design BEMs and UBEMs. A diagram that sketches these paths is provided in Figure 1-3. Chapter 3 aims to automate the status quo of early-design energy-model generation in order to make a large-scale application of such models feasible. An algorithm is introduced that automatically creates "whole building" multi-zone BEMs that are subdivided into perimeter and core regions as prescribed by ASHRAE 90.1 Appendix G [ANSI/ASHRAE/IES, 2013] from urban massing models and building designs with yet unknown floor plans. The method yields geometrically resolved energy models that can consider complex heat and mass-flow interactions between zones. It is applied to various building shapes to validate the algorithm's robustness. Chapter 4 describes a method that is capable of abstracting an arbitrary building-massing model into a meaningful group of "typical room" energy models. The method aims to approximate results of perimeter and core multi-zone BEMs in a more efficient manner. The method is inspired by the so-called "shoebox studies" where modelers use simple box-shaped single-zone energy models to quickly generate design feedback. Key improvements are added and a fully automated procedure that makes informed simplifications by clustering buildings by their internal program and building form-factor is introduced. Further, facade segments are clustered based on micro-climatic boundary conditions. The method considers context geometry and can report results at a high spatial and temporal resolution. The method is tested and validated with a real-world urban design case study by thoroughly comparing it to results that have been computed with the method introduced in Chapter 3. Further examples for the application of the introduced methods in design and energy modeling practice are provided. In Chapter 5 the perimeter and core zoning paradigm, which is fundamental to current BEM modeling approaches including those in Chapters 3 and 4, is validated but also critically reviewed from an architectural perspective. The zoning paradigm's accuracy and usefulness in early design are discussed and an enhanced design workflow that incorporates key typological characteristics such as the horizontal and vertical circulation layout is presented.

Chapter 6 summarizes the results of this dissertation.

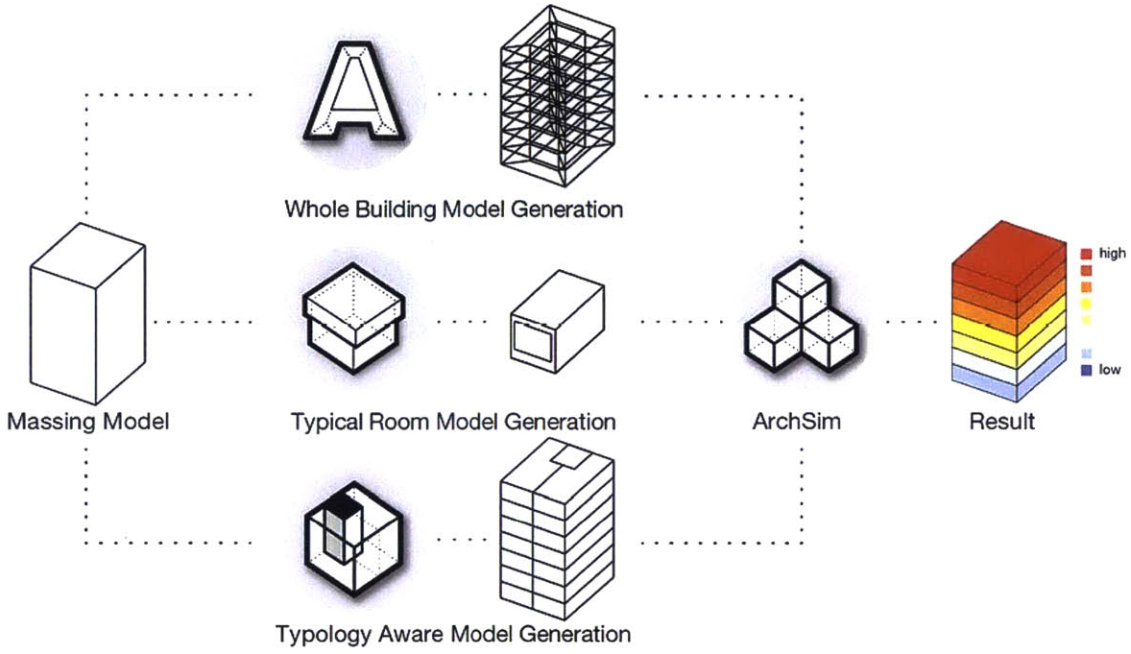

Figure 1-3: Main contributions of this thesis

1.6 Research hypotheses

The hypotheses underlying this thesis are that the development of automated building energy model generators at the individual building and city-level is feasible and that the use of these generators can be introduced into current planning practice at a justifiable effort level while providing relevant results for early building design and urban planning processes.

Feasibility

- The current practice of implementing the ASHRAE 90.1 Appendix G thermal zoning guideline that prescribes a perimeter and core subdivision for buildings with yet undefined interiors is justifiable for the use in the majority of urban energy modeling tasks.
- It is possible to develop a robust, fully automated thermal zoning algorithm that converts arbitrarily shaped planar-surface massing models into ASHRAE 90.1 Appendix G compliant multi-zone "whole building" energy models.
- For fully conditioned spaces, urban massing models can be automatically translated into a meaningful set of "typical room" energy models to approximate simulation results of the ASHRAE 90.1 Appendix G compliant perimeter and core BEMs at a fraction of the computational cost.

Justifiable effort

- If BEM space templates and digital 3D massing models are available, the additional effort that is required to produce urban energy models with automatic building energy model generators is marginal and their utilization is hence realistic and justifiable for modelers who are interested in building level energy simulations.

Relevance

- Improved modeling methodologies can provide relevant energy performance related insights in a high spatial and temporal resolution, which can help to evaluate sustainable design strategies.

2 Urban-Scale Building Energy Modeling

The following chapter reviews the current state of the art of urban building energy modeling. A brief overview of urban energy modeling and two different urban building energy-modeling approaches that rely on traditional BEM simulation engines are given. Their limitations are described thoroughly and a lack of efficient workflows and tools to rapidly generate building energy models for urban and early design is identified as a major gap in the literature towards urban building performance modeling and integrated urban design.

2.1 Introduction

Several urban energy-modeling methodologies are available and an overview is given by Swan and Ugursal [2009]. The authors identify three types of modeling techniques that follow either a top down, a bottom-up-statistical or a bottom-up-engineering approach. The top-down approach, primarily implemented for coarse energy demand forecasts, uses widely available aggregate economic, real estate, climate and historic energy consumption data as inputs and regress how they affect energy demand. A pitfall of this approach is its lack of detail and inability to account for non-linear technological improvements. Both bottom-up approaches utilize detailed input datasets that include geometry, materiality, construction standard, equipment and appliances, weather data as well as set-point temperatures, occupancy profiles and conditioning equipment utilization. The extensive input data that is required allows modelers to make more differentiated projections such as end-use-related energy demand. Statistical approaches implement techniques such as regression analysis or neural networks to formulate an energy model. A drawback of the statistical approach is that it requires historical energy data to generate results and hence cannot be used in planning and design processes where such data is not available. In contrast, the engineering approach utilizes the detailed inputs to explicitly simulate the energy demand with BEMs. A key advantage of this approach is that besides end-use-related energy demand forecasts, scenarios, retrofitting options and contextual implications such as a change of urban form can be taken into account. These characteristics are favorable in design and planning processes since they allow modelers to prevent planning errors and to identify potentials for design improvement and energy saving. The following sections hence focus on reviewing the engineering approach for urban energy modeling.

2.2 Single Building Energy Modeling: A brief summary

Building-related heat flows are well understood and models are extensively described by Hensen & Lamberts [2011], Underwood & Yik [2008] and Clarke [2000]. Figure 2-1 provides an overview of key energy flows that are considered in buildings. The figure shows a room that is influenced by its environment due to envelope transmission losses, infiltration, ventilation and solar gains. The indoor climate is, however, also influenced by multiple internal energy flows

such as plug loads as well as emitted heat from occupants. These flows are not always in balance and hence heating, cooling and ventilation systems are required to provide a comfortable indoor environment.

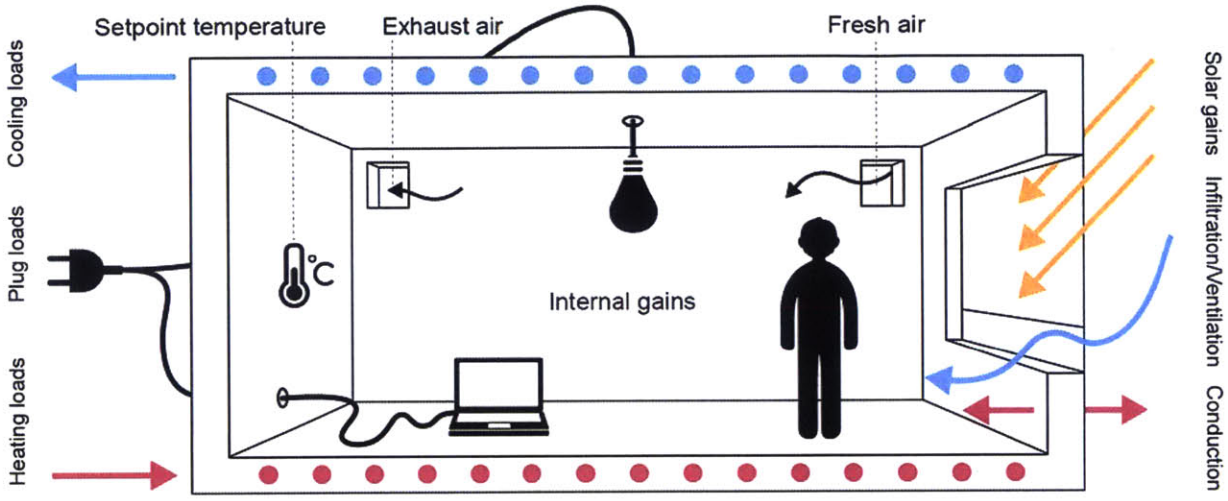

Figure 2-1: Main heat and mass transfers considered in a room

In order to accurately model these constantly changing and dynamically interacting flows, substantial research efforts have gone into the development of dynamic building-performance-simulation engines. The first generation of BPS engines emerged in the eighties and nineties to overcome limitations of the until then common steady-state single room heat balance models. The purpose of "dynamic" models using computational heat transfer methods such as response functions or finite-difference methods was to model transient thermal-mass effects [Clarke, 2000]. BPS engines such as TRNSYS [Klein, 1979], ESP-r [Clarke et al., 1993], DOE-2 [Birdsall et al., 1990], EnergyPlus [Crawley et al., 2000], IDA-ICE [Kropf & Zweifel, 2001] and IES-VE [IES, 2015] have been thoroughly validated and tested in practice so that whole buildings and their HVAC systems can be modeled reliably [Samuelson et al., 2014][ANSI/ASHRAE, 2011] and in great detail. An overview that contrasts the differences between modeling engines in detail is given by Crawley et al. [2008].

The use of multi-zone models was driven by the idea to further spatially resolve micro-climatic and functional differences within buildings such as space orientation and programmatic use. Such differences have significant impact on the load behavior of a space and thus also on the specifications for an HVAC system that serves it [Bobenhausen, 1994]. To simplify the

simulation and system layout, multiple rooms may be joined together into one zone if they share similar load profiles. However, lumping spaces of different character together in one zone can lead to significant load under-predictions [Smith et al., 2011]. For example, a localized heat surplus that may occur during the winter near a south-facing façade may be absorbed by a space to the north that is underserved by solar gains. Consequently, the predicted energy demand according to the one-zone thermal model would be dampened due to load cancellation compared to a spatially resolved multi-zone model. In early design, when the room layouts that would provide the basis for thermal zoning are yet unknown, ASHRAE 90.1 Appendix G prescribes a zoning methodology stating that a floor should be divided into core and perimeter regions. The perimeter is defined as the space along the facade with a depth of five meters. Further, perimeter spaces with more than one orientation should be subdivided proportionally. The leftover region in the center of the floor forms the core [ANSI/ASHRAE/IESNA, 2013].

In order to create a BEM, several inputs are required. The geometry of a building needs to be provided in an abstract form. External obstructions and the geometric building blocks of a thermal zone such as walls, slabs, roofs, and windows are provided as zero-thickness simple convex polygons. The geometric data is used to compute contextual shading, the surface orientation and areas of building elements and to establish interior and exterior view factors for radiation exchange. The geometry is paired with physical properties of materials and constructions that are required for the envelope heat transfer and absorption calculations. Further, the boundary conditions of the building elements must be defined. Elements can for example be facing the outdoor environment, the ground or another room. Besides its enclosing elements, a thermal zone also requires information on its mode of operation. This information includes internal gains, occupancy profiles, controls, set-point temperatures and HVAC systems. In addition to the building-related inputs provided in a BEM, simulation engines must be provided with the environmental boundary conditions of a building. These boundary conditions include site location, outdoor air temperature, humidity, solar irradiance and illuminance, cloud cover, wind speed and direction and ground temperatures. Preferably, this data is recorded directly at the project site and is given in short time intervals that capture rapid weather-related fluctuations [Barnaby & Crawley, 2011]. In reality, commonly used weather data is aggregated to represent typical weather years in hourly time steps. The data is often recorded at airports or other major weather stations. Several methods to generate weather data

and various file formats exist. A few examples are International Weather for Energy Calculations (IWEC) [ASHRAE, 2001], Solar and Wind Energy Resource Assessment (SWERA) [SWERA, 2009] and Typical Meteorological Year 3 (TMY3) [Wilcox & Marion, 2008]. Climate change [Remund et al., 2010] [Jentsch et al., 2013] as well as urban micro-climates [Bueno et al., 2011, 2012] can be considered. An overview of key BPS inputs and the flow of information are shown in Figure 2-2. The outputs of a BEM simulation range from energy consumption and renewable energy production to indoor environmental conditions including thermal comfort and daylight, based on which the environmental quality and energy use of buildings can be assessed.

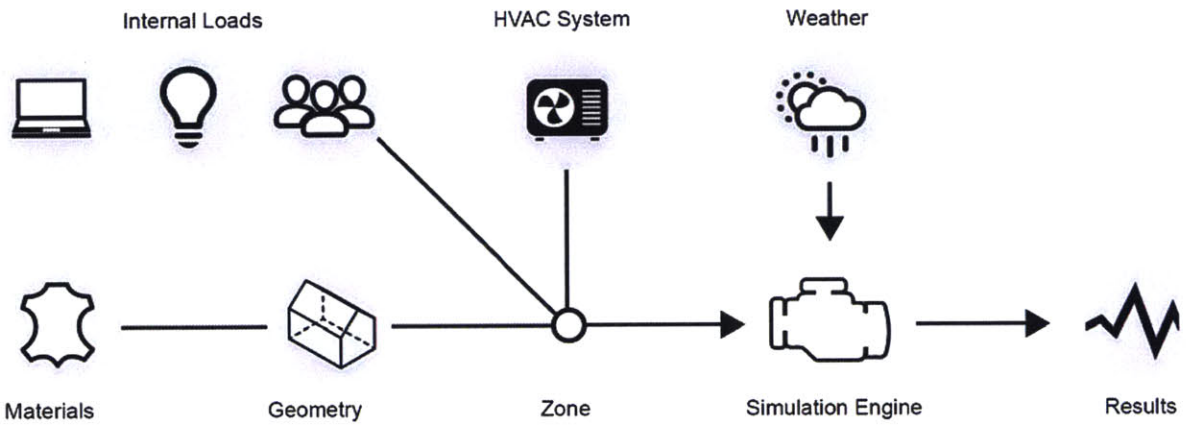

Figure 2-2: BEM Input Flow Chart

Interfaces and users: Besides reliable inputs and simulation engines, multidisciplinary and intuitive design processes are required. Until recently, the most common framework of collaboration foresaw a clear division of labor where engineers were largely in charge of implementing a given environmental concept for a building while the architect concentrated on design tasks. This division of responsibilities has recently started to blur and the American Institute of Architects (AIA) is actively promoting the use of energy simulations by architects [AIA, 2012]. This development is largely facilitated by a new generation of software interfaces. Visual geometric scripting environments such as Rhinoceros 3D's Grasshopper [McNeel, 2010] have evolved to become powerful generative tools and are widely used by architects to formulate design intentions parametrically. These environments have also attracted developers of environmental performance simulation tools that provide intuitive interfaces for daylight

simulation engines [Jakubiec & Reinhart, 2011] [Roudsari et al., 2013]. A recently developed plug-in for Grasshopper called Archsim [Dogan, 2013] enables users with limited energy modeling experience to run dynamic energy simulations in EnergyPlus. Besides its ease of use, the integration of Archsim in the Grasshopper visual scripting environment significantly changes how users can provide simulation inputs. The current BEM interfaces require users to specify thermal model geometry and to manually attach properties to each geometric element in the model. In Archsim, geometry can be modeled explicitly or parametrically. The non-geometric inputs are hierarchically organized and interchangeable (e.g., a zone setting container contains other containers that describe constructions, zone use and conditioning systems) and can be generated with a classic user interface (containing drop-down menus, text and check boxes) or through visual and code based scripting. Both geometric and non-geometric data is then linked either explicitly though a direct reference or parametrically through grouping, filter and search functions. This allows users to combine data at very high levels without limiting functionality for exceptions at lower levels. Once a link between geometric and non-geometric data is established, Archsim automatically builds the adjacency graph and boundary conditions. A tree analogy is given in Figure 2-3. (A) represents a classic BEM user interface where the user must traverse the hierarchical levels of the thermal model tree manually to edit properties to geometric elements. In Archsim (B) the user cannot edit the tree directly but manipulates higher level information in the roots that then are automatically propagated into the tree and its branches. In the case of exceptions, the user can replicate an entire branch in the roots (C) to directly modify lower level information. This input organization hides complexity from the user and allows to automate many aspects of BEM generation. One remaining question is how to provide adequate thermal zone geometry automatically.

With the availability of tools that allow fluid and interactive design workflows [Lagios et al., 2010] integrated design and its earlier implementation in the design process is significantly facilitated. It is widely acknowledged that this can increase impact and effectiveness of BPS [Schlueter and Thesseling, 2009] [de Wilde et al., 2002].

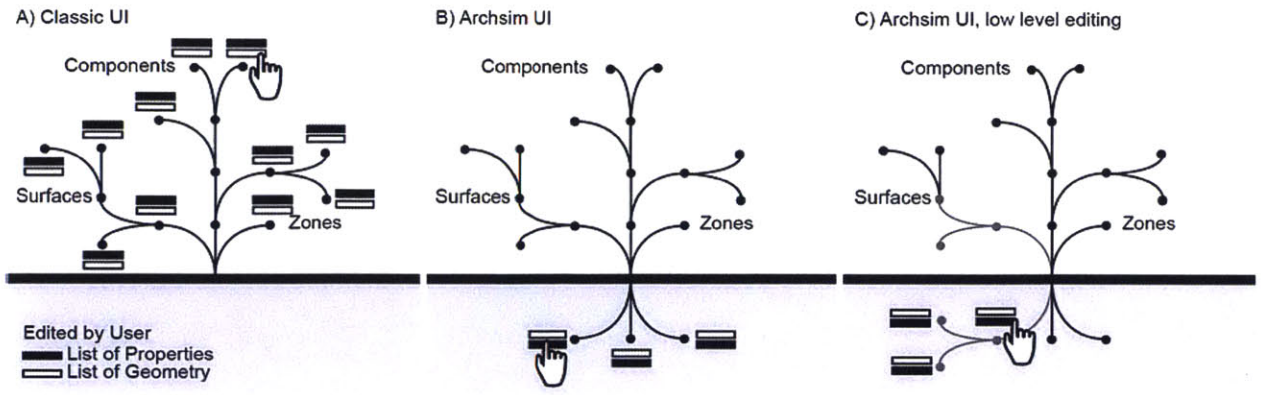

Figure 2-3: BEM Input Flow Chart

2.3 Urban building energy modeling

While the use of the previously described building-performance-simulation tools for urban level analysis has been rare, it recently became an active field of research. A general review of urban building energy modeling (UBEM) approaches shows that several engineering type simulation workflows that utilize traditional building energy modeling are emerging [Mata et al., 2013] [Reinhart & Cerezo, 2015]. The authors identify manual workflows that reduce urban models to a representative set of archetypical BEMs and urban simulation tools that model each building explicitly. The following paragraphs provide a focused literature review on the different approaches.

2.3.1 Archetype approach

Urban areas may contain hundreds or thousands of buildings. Hence, manually setting up an energy model for each building with traditional BPS tools is not feasible. Consequently, modelers use workarounds and abstractions to simplify the urban modeling task in three steps that Mata et al. [2014] label as segmentation, characterization and quantification.

Usually, urban areas are broken down into a set of archetypical buildings or typical space type clusters (Segmentation). The modelers then set up representative energy models for each cluster (Characterization). For existing cities, several researchers have defined typical building types and databases that include building properties that are relevant for energy simulations [Loga et al., 2012]. For new developments the SIA Merkblatt 2024 [S. I. A., 2006] or the DOE reference models [Deru et al., 2011] may serve as a starting point for energy model inputs. The

results of each archetype building are then scaled by area or building count to represent the entire building group/cluster (Quantification).

The approaches mainly differ in the level of detail and the heat balance method of the thermal models. Several researchers implemented lumped single-zone models for each building archetype utilizing steady state calculations [Filogamo, et al., 2014] and dynamic simulations [Mata et al. 2014]. Others [Tuominen et al., 2014] [Korolija et al.,2013] [Griffith & Crawley, 2006] [Huang & Brodrick, 2000] explicitly modeled dynamic multi-zone energy models of archetypical buildings.

In contrast to the multi-zone models, the lumped single-zone models cannot simultaneously model different space uses within one building. This can lead to load cancellation and significant underestimation of energy loads, especially in mixed used buildings. In addition, all previously mentioned approaches ignore the implications of contextual shading. Research on optimal building orientation, spatial interrelationships of buildings, form finding and implications of urban layout and density is hence not possible.

Therefore, the design consulting practice and design focused research work on urban modeling tasks in "section-view". Instead of archetypical buildings, typical street sections or "urban canyons" are identified. Strømann-Andersen & Sattrup [2011] parametrically alter height-to-width ratio of the canyon form to study its implications on energy demand. Since in early and urban design the interior subdivision (floor plan) of a building is unknown, modelers often do not model a full building but instead focus on typical rooms for each possible building use case and shading situation. The results of the street sections are then combined and extrapolated according to the land-use-allocation-plan.

In practice, the segmentation and classification and the following extrapolation are often done manually and lead to interminable and error-prone accounting procedures. Furthermore, it is unclear how many archetypes are necessary to accurately simulate the urban energy demand of a neighborhood in a per-building resolution. If the sampling of archetypes is too coarse, one can expect that within one archetype group the surface areas (of façade, floor, ground-slab and roof) and their relationships are significantly different from building to building. All archetype simulation approaches intrinsically ignore these differences. The error introduced by this simplification, however, remains unknown. In addition, a response to micro-climatic

details that are influenced by the geometry of an urban environment is very difficult since the geometric simplification breaks nearly all ties with the original 3D nature of a design or urban district.

An argument in favor of the typical room models, however, is their computational efficiency. Unlike, "whole building multi-zone" models with their complexity and computational overhead, the shoebox models are practical when it comes to parametric searches. In such a search, various window-to-wall ratios, overhangs, construction types, fenestration and shading systems can be tested. In addition, efficient energy distribution systems as well as further load optimization by reducing plug-loads and the potential for natural ventilation can be explored. Such workflows can make use of genetic algorithms or other optimization software like that introduced by Wetter [2011] to work through the search-space more efficiently.

2.3.2 Urban modeling tools

Due to the previously mentioned limitations of archetype modeling workflows, several research tracts have turned their attention to developing dedicated urban energy analysis tools that can model all buildings and can thus skip the segmentation and classification routine.

The software "GSOL" is one of the first computational urban tools for energy evaluations and passive solar design [Goretzki, 1993]. It uses a steady state heat balance method to calculate heating demand of buildings in a given neighborhood. The same calculation is repeated without context to report potential solar optimization strategies. The tool focuses on heating-dominated climates and has been used for various master-plan evaluations in Germany [Goretzki, 2013]. A newer development called "SIMSTADT" [Nouvel et al., 2013] [Strzalka et al. 2011] processes semantic urban 3D models in the CityGML format [Kolbe et al., 2005] and performs single-zone steady state heat balance calculations. Both modeling approaches produce spatially resolved building simulation results. Their steady-state heat balance methods, however, impose limitations since thermal inertia effects cannot be modeled. A detailed discussion on the relevance these effects and their implications on modeling accuracy is given by Clarke [2001, p. 8].

With SUNtool and CitySim, Robinson et al. [2007] introduced a multi-criteria urban energy-modeling platform that includes a simplified, dynamic thermal simulation engine and

behavioral models for occupancy profile generation. The custom engine has been thoroughly validated for a single-zone and multi-zone scenario [Kämpf & Robinson, 2007] but the achieved computational efficiency benefits remain unknown.

While SIMSTADT relies on the existence of CityGML models, GSOL and SUNtool require the user to manually build the energy model geometry for each building within their provided interfaces. Especially the thermal model discretization into multiple zones does not seem feasible for urban projects with hundreds of buildings. Figure 2-4 shows a series of increasingly complex floor plans that are divided into thermal zones according to ASHRAE 90.1 Appendix G. Figure 2-4 (a) and (b) show that complying with Appendix G is unambiguous and straightforward for simple building shapes. However, for more complex shapes such as (c) and (d), following Appendix G zoning rules quickly evolves into a tedious and somewhat ambiguous process. Finding the subdivision (d') in a floor plan such as (d), ceases to be practical by hand even for just one building.

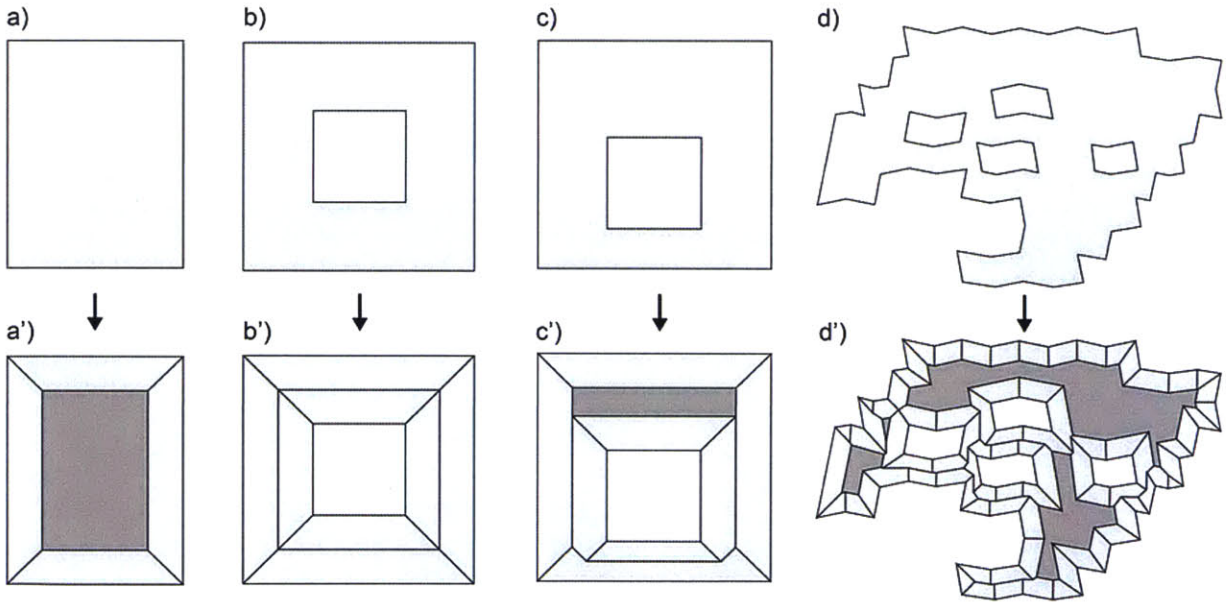

Figure 2-4: Floor plans zoned according to ASHRAE 90.1 Appendix G

While algorithms for automatic zoning exist in tools such as EQuest [Hirsch, 2010], Bentley AECOsim [Bentley, 2013] and UMI [Reinhart et al., 2013], they are limited to simple geometric shapes such as Figure 2-2 (a) (Polygons without holes). Autodesk Vasari [Autodesk, 2013], a schematic design tool for architects, can automatically split up a 3D building massing

into perimeter and core zones. It is fairly robust and only fails occasionally on concave geometries with sharp angles and narrow inner regions. A major pitfall of Vasari is that it cannot consider building adjacencies. This makes it difficult to use for urban applications. Further, details of the zoning algorithm and its implementation have not been publicly released.

2.3.3 Automated Architectural Model Translation and Automatic Zoning

In order to facilitate building-energy-model setup several researchers have focused on automatically converting architectural 3D models into building energy models. Van Treeck et al. [2006] introduced a method that performs a dimensional reduction of 3D building information models (BIM) using graph theory. Similarly, O'Donnell et al. [2013] worked on a semi-automated BIM to BEM conversion process implementing automated space boundary identification. Pratt et al. [2012] presented a geometric modeling protocol and framework that included geometry correction and surface heuristics that would allow the conversion of more traditional 3D CAD models with interior space subdivisions into BEMs. Later that same group refined this approach, presenting additional methods for "cleaning up" real world architectural models by removing small holes, reducing the number of interior surfaces and using a view-factor based method to identify zones and their adjacencies [Jones et al., 2013].

All previous studies assume that a detailed BIM or CAD model with defined interior spaces is available for conversion to a BEM. While such models may be available later in the design process, in urban design the interior subdivision of a building is typically unknown and therefore not geometrically modeled.

2.4 Conclusion

The previous sections showed that BPS tools can reliably model energy flows in buildings and that there are several ways to use BPS tools to create UBEMs. The archetype approach models a few representative buildings and extrapolates the results. The main shortcomings of this approach are related to the required effort and uncertainty that is introduced with the segmentation of an urban model into a meaningful set of archetypes. Further, geometric over-simplification of a 3D problem limits its useful application in design processes.

Urban modeling approaches that model every building explicitly can overcome the shortcomings of the archetype approach. However, currently available urban modeling tools use simplified single zone, mostly steady state, simulation models to keep the computational overhead at a feasible level. With the exception of SunTool, they hence cannot model thermal mass effects, which may have a significant impact on results in cooling-dominated climates. Further, it is widely known that the use of single zone models (and single zone per floor) can lead to significant load underestimation [Smith et al. 2011]. It is however not feasible to expect that modelers of a master plan can thermally zone hundreds of buildings manually. Methods that can automate this task for arbitrary building designs do not exist.

Urban building energy modeling remains a difficult task due to the lack of good workflows and tools for rapid urban energy model creation. Hence, this thesis focuses on the development and validation of procedures for rapid building-energy-model production for urban and early design simulations.

3 Automated "Whole Building" Model Generation

In this chapter a general algorithm to automatically convert arbitrary building massing models into multi-zone BEMs is presented. The algorithm follows current guidelines for thermal zone discretization when actual interior space boundaries are yet undefined. Envisioned applications are rapid model generation for schematic building design as well as for urban massing studies. An argument that current recommendations for separating core from perimeter zones effectively follow a straight-skeleton subdivision is presented. Following a step-by-step explanation of the procedure, a number of example building shapes of varying complexity are shown to demonstrate the algorithm's robustness and suitability for automated multi-zone BEM generation.

Elements of this chapter have been published in the Journal of Building Performance Simulation:
Dogan, T., Reinhart, C., Michalatos, P. (2015). Autozoner: An algorithm for automatic thermal zoning of buildings with unknown interior space definitions. Journal of Building Performance Simulation.
http://dx.doi.org/10.1080/19401493.2015.1006527

3.1 Introduction

This chapter introduces a method that can automate the status quo of early-design energy-model generation. The goal of this method is to significantly reduce BEM setup times in order to facilitate urban BEM applications. Given the complexity of thermal zoning for arbitrary shapes and the absence of a published, general and automatic zoning methodology, this chapter introduces an algorithm called the Autozoner. It is proposed that the prescribed proportional space subdivision suggested by the ASHRAE Appendix G can be related to a topological skeleton of a polygon and that it is therefore possible to formulate a general and robust algorithm to obtain Appendix G compliant space partitioning automatically. A proof of concept implementation that is designed to convert an arbitrarily shaped architectural massing model into a multi-zone thermal model that can be used in energy modeling engines such as EnergyPlus and TRNSYS is presented.

3.2 Methodology

The following section is divided into three parts. Following a step-by-step description of the Autozoner algorithm, a testing procedure is described along with a proof of concept implementation and simulation workflow.

3.2.1 Automated zoning:

Input: Architectural 3D models that are frequently used in urban and schematic design processes can be categorized into three main types. During the earliest stages, individual buildings are modeled as a single volume (Figure 3-1(a)). This form of representation helps the designer to understand basic morphologic features such as the massing and the proportions of a design. Another very common representation involves "stacking" floor-volumes. This adds a notion of "scale" since it immediately allows one to read floor-to-floor heights from the model and it facilitates the distribution volumes during the design process (Figure 3-1(b)). At a slightly later stage, the stacked volumes can be further subdivided and differentiated by program/function as shown in Figure 3-1(c). At this point, more complex spatial arrangements within a building such as split-levels or atria spanning over multiple floors can be introduced as well. It should be noted that all three input geometries shown in Figure 3-1 still fall under what

can be considered as schematic or early design. The Autozoner algorithm supports all three geometry types. In the case of a single volume model (Figure 3-1(a)), the algorithm requires a list of closed poly-surfaces, each representing a single building, as well as a user-defined floor height. The latter is used to subdivide the building into floor volumes. The floor-to-floor distance can also be given as an array to consider varying floor heights. For models that already have a floor- or programmatic subdivision (Figure 3-1(b) and (c)), the algorithm requires groups of stacked volumes for each building or programmatic subdivision. These volumes can be organized in a tree data structure where each branch represents a user-defined group (Figure 3-2). As an example, Figure 3-2 shows three data tree representations of the massing models shown in Figure 3-1. In Figure 3-2(c), the entire model is grouped into buildings with further sub-groups for each building that reflect the different programs within it. The volumes representing the floors are stored inside of these programmatic sub-groups. The organization (the structure and depth of the branches) of such a tree is arbitrary and thus allows the user to pick any grouping schema. The algorithm stores the given tree structure and reflects it in the outputs. The starting point for all following steps is hence a data tree of arbitrary depth containing closed poly surfaces representing floor volumes.

For convenience and clarity, it makes sense to convert this purely geometric data into objects that allow one to attach further information to them and that facilitate querying the data later. Therefore, two constructs called "unit" and "face" are introduced. A unit contains a floor volume and its position in the input data tree. It further holds a list of all surfaces of the floor volume in form of the face construct. Since all essential steps of the zone subdivision are produced based on a 2D floor plan, one must be able to distinguish between the faces that define the floor volume. This is done by checking the face-normal orientation. If the face-normal points downwards, a floor plate is identified, if it points up, one is dealing with a ceiling or roof. All other normal orientations must then be walls or facades. This information is stored in the form of a type label in each face. To correctly handle sloped surfaces, the user may specify a maximum tilt angle to distinguish floors and ceilings from possibly tilted facades. For each unit the 2D floor plan is computed by collecting its faces labeled as floor plate, projecting them onto the XY-Plane (to eliminate slopes) and merging them with a Boolean addition.

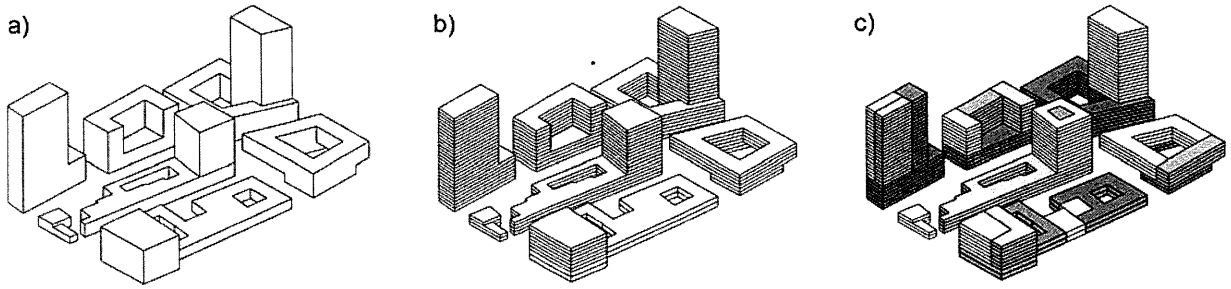

Figure 3-1: Typical modeling styles of massing models

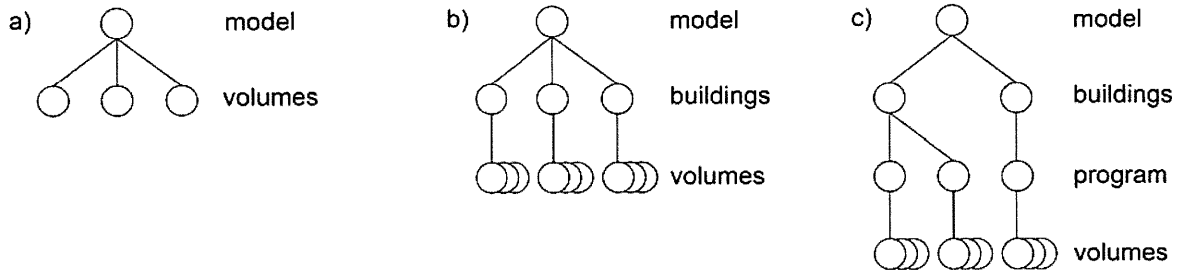

Figure 3-2: Data tree structure for the three possible input cases

2D Zoning: The next step is to subdivide each unit into thermal zones. The perimeter and core zone subdivision of the 2D floor plan, as described by the previously mentioned ASHRAE 90.1 Appendix G guideline, is computed first. In the simplest case the core region can be found by offsetting the outer edge of the floor plan. Then a search for the closest point from the outer polygon vertices to the inner ones can yield the desired subdivision. This is shown in Figure 3-3(a). For more complicated cases, the above-mentioned approach fails. Figure 3-3(b) shows a convex floor plan with a core region that retreated completely from the left part of the polygon due to a series of collapsing edges during the offset. It subdivides parts that have good "core visibility" as intended but leaves the entire left half undivided. However, with a certain thickness of the remaining polygon-tip it might be desirable to split the tip into single sided zones instead of a lumped region with access to multiple cardinal directions. This would require a partition somewhere along the medial axis [Preparata, 1977] of the polygon. A medial axis approximation is shown in Figure 3-3(c). However, the medial axis does not consist of straight-line segments and can instead involve parabolic curves. This is not desirable since the final output of the algorithm is a set of 3D thermal zones that should ideally consist of as few planar

surfaces as possible. Very similar to the medial axis, but involving just straight lines, is the "straight skeleton" that was first described by Aichholzer et al. [1996; Aichholzer and Aurenhammer, 1996; Barequet et al., 2003]. The straight skeleton of a polygon, as shown in Figure 3-3(d), divides the polygon into one cell per outer edge and is thus fulfilling the requirement of proportionally splitting the perimeter region by orientation. In order to obtain a core and a valid thermal zone subdivision, a couple of simple steps have to be added. After the skeletonization (Figure 3-4(a)), the algorithm produces the core region by performing an offset of the outer and hole-polygons (see Figure 3-4(b)). In step (c) the core overlap is removed from each skeleton cell by a 2D Boolean difference operation. If the thermal zones have to be strictly convex, such as required by the "detailed" radiation distribution algorithms of EnergyPlus and TRNSYS, the resulting perimeter and core zones have to be further subdivided if they are concave. Various polygon-partitioning techniques exist for this task and have been described in detail [O'Rourke, 1998]. Since the resulting perimeter regions are guaranteed to be hole-free, a simple split at each concave vertex to the closest point on the exterior edge of the polygon delivers the desired result (Figure 3-4(d)). The core regions, however, can consist of polygons with holes. One simple example is a donut-shaped floor plate with a circular core region. Here, triangulating the shape of the core and then subsequently removing mesh diagonals lets one obtain strictly convex zones [Hertel & Mehlhorn, 1983]. Enforcing convexity as described before can yield perimeter regions without facade access or zones that are unrealistically small and narrow. It is therefore important to split non-convex spaces only virtually by placing a partition that is permeable for air and radiation. The result of the previous steps is a set of 2D regions for the perimeter and the core of each floor plate. As underlying data structure a doubly connected edge list (DCEL) is used. The DCEL data structure is a planar graph that allows efficient topological manipulation of the core and perimeter cells [De Berg et al., 2000].

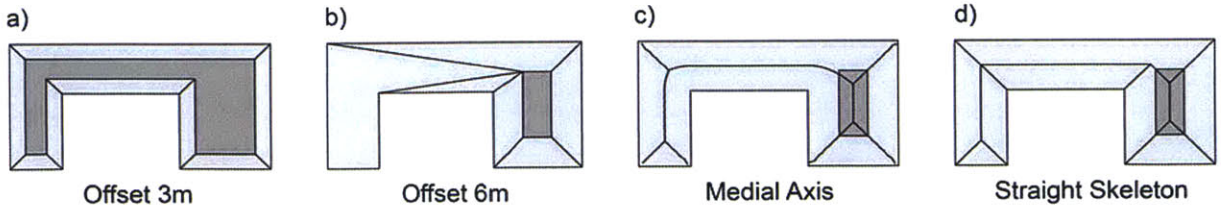

Figure 3-3: From a simple and limited to a general cell finding method based on Straight Skeleton

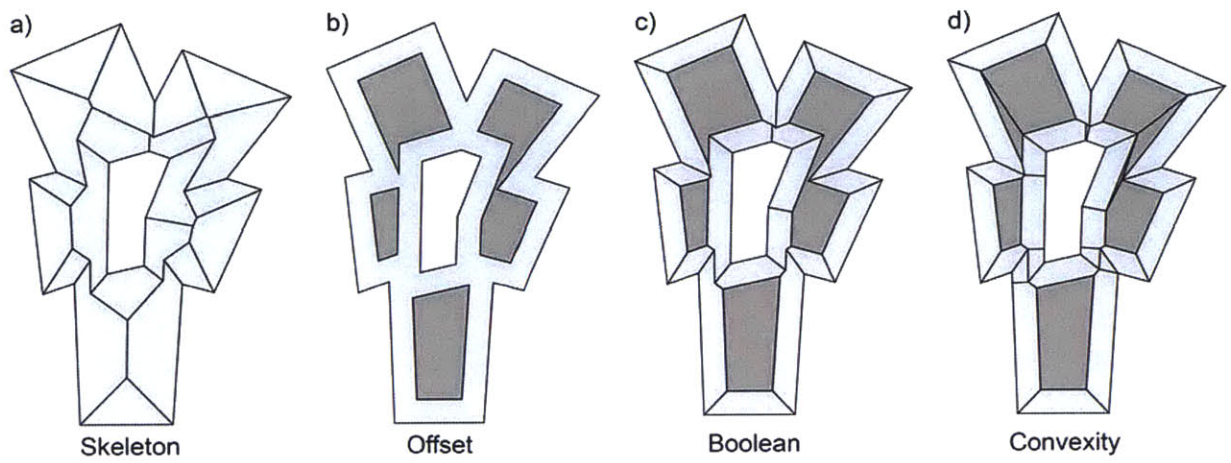

Figure 3-4: Step by step visualization of the 2D zoning procedure

From 2D to 3D zones: The 2D core and perimeter cells resulting from the previous steps have to be further processed to obtain the final 3D volumes that represent a thermal zone. The simplest and fastest approach is to extrude the cells by the floor height. This, however, is only possible, without significantly altering the building shape, if the facades of the initial envelope are strictly vertical. In order to overcome this limitation, the algorithm can use the floor volumes stored in each unit as a basis to cut out a zone volume with the correct façade geometry. In addition to the floor volume, cutting volume needs to be constructed. The required procedure is shown in Figure 3-5(e) whereas Figure 3-5(a) to (d) depict the initial Autozoner steps discussed above. In Figure 3-5(e) the DCEL data structure from the 2D zoning step is queried for all edges of each perimeter cell that have a congruent neighboring edge in an adjacent cell. This yields only the interior edges of the perimeter zones. They are then extracted in form of a poly-line and the endpoints are extended outwards. If the extensions intersect, the polygon is closed at the intersection point (which may happen in the case of two following convex corners in the floor plan shape); otherwise, a line between the two endpoints is drawn. The extension is necessary to span beyond any outward tapering of the facade. The algorithm then begins to extrude the cutting volume to match the height of the bounding box of the currently processed floor volume (Figure 3-5(f)). A Boolean intersection of the floor volume and the cutting volume follows as shown in Figure 3-5(g). Since the cutting volume might intersect in multiple regions, e.g., in convex corner regions where another facade is in close proximity, the footprint of each volume that is returned by the intersection is checked and only added to the list of zone

volumes if it corresponds to the perimeter cell region that is currently processed. This method unfortunately does not guarantee convex volumes at all times. An example where this method would yield a concave space is a floor volume with a facade that zig-zags up multiple times. For the implementation, this considered as an exception and the algorithm relies on the user to prevent such a case when zone convexity is a requirement.

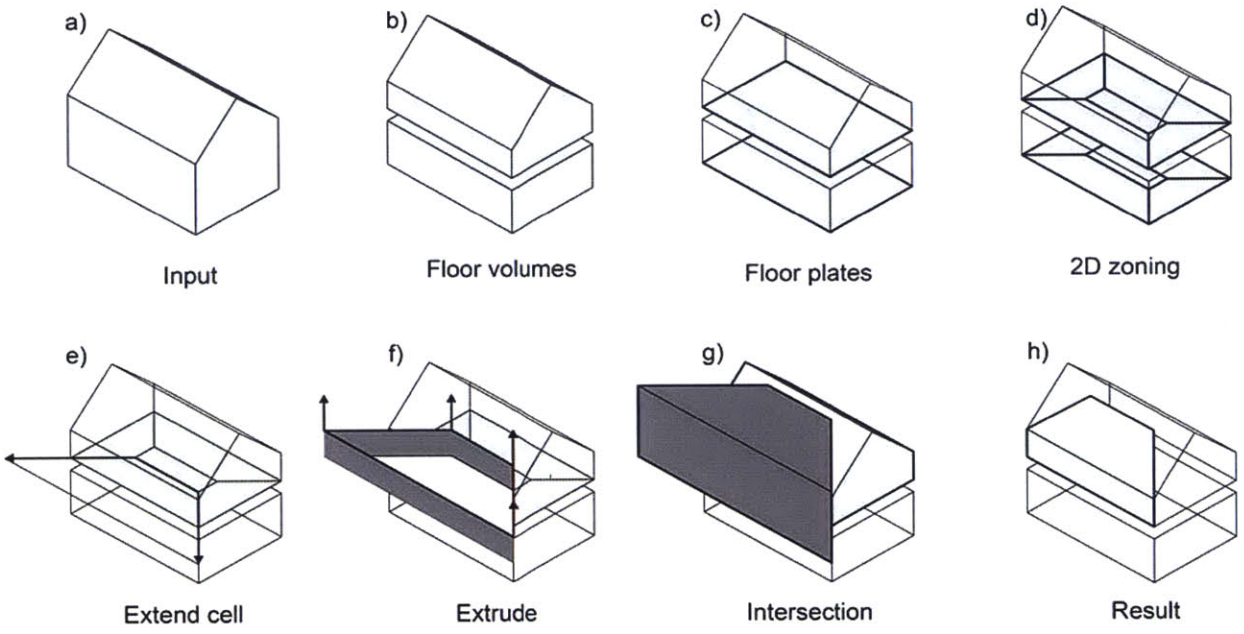

Figure 3-5: Graphic representation of the main algorithmic steps

Adjacency: In urban models, it is quite common that buildings touch each other and not every face with horizontal orientation is a facade. Similarly, the programmatically subdivided volumes (Figure 3-1(c)) have interior partition walls. A simple 2D example is shown in Figure 3-6(a) where adjacent regions with interior walls are represented by a thick stroke. In such a case, the algorithm presented thus far would build perimeter cells at each inter-building and program-separating partition such as shown in Figure 3-6(b). In 2D, a simple trick to avoid this is to join all neighboring floor plans into a single one before the cellular subdivisions are computed. Following the subdivision, one can use the original floor plans to crop the computed results to obtain core and perimeter cells corresponding to the original floor plans. The cropping operation can produce perimeter cells without any exterior edge. However, by keeping track of the type of cell and its parent floor plan in the DCEL data-structure, one can detect these cells

and merge them with neighboring perimeter cells (if there is no neighboring perimeter cell they are merged with the core). The result is a 2D cellular subdivision as shown in Figure 3-6(c). The dotted lines indicate edges that have been removed during the merging.

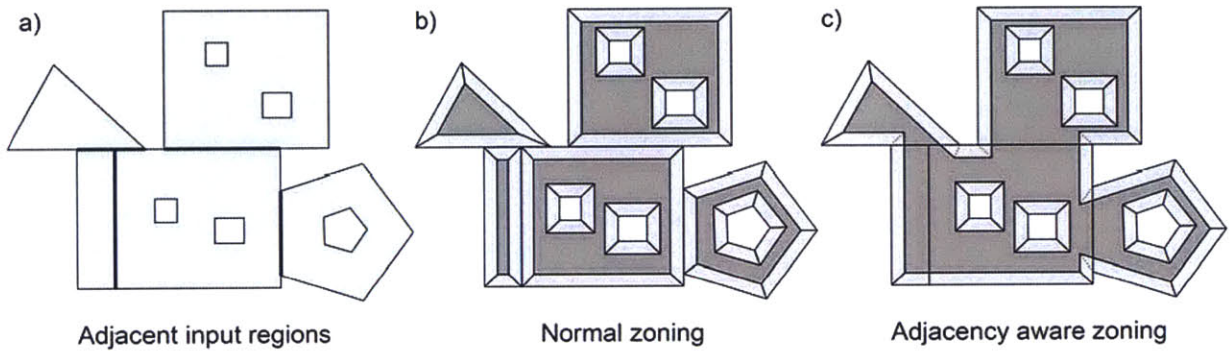

Figure 3-6: Zoning for adjacent regions.

In 3D, the adjacency problem is far more complex. One must be able to detect horizontal adjacencies of the units in order to selectively join only neighboring floor plans. Thus, the algorithm tests for a potential overlap of all unit faces with all other unit faces labeled as wall/facade. The algorithm first checks if the face pair resides in the same plane and has opposite face orientation. If both tests are positive a 2D polygon intersection is computed. If an intersection is encountered and the two faces overlap, both parent units are adjacent. Then, the algorithm loops over each unit, joins the unit floor plan with all floor plans in adjacent units, computes the 2D zoning and then crops the result back as described for the simple case in Figure 3-6. Figure 3-7 visualizes these steps. For the input shown in (a) the final result (c) is computed. The core volumes are shown separately for clarity in (b). The process is highlighted for the face f_1 in (d) and its parent unit u_1 shown in (a). The adjacent floor plans are merged into the polygon set p_1 in (e). Figure 3-7(e) also shows the result of the cropped zoning as shaded surfaces. Figure 3-7(f) shows the resulting 3D zones.

The user can further specify a minimum overlap area and a maximum floor plan distance in order to cull small overlaps and overly distant floor plans in the adjacency test. The importance of both parameters is highlighted in (g), (h) and (i) where both parameters are deliberately set so that all adjacencies are found. The face f_2 has a clearly visible neighbor but

its parent unit u_2 is slightly higher and thus overlaps with other unit faces from higher and lower floors. Thus, faces $f_{3\text{-}6}$ are also detected as adjacent. If the geometry is tapering (f_3) or changing drastically from floor to floor (f_5) the geometry of such floor plans should not be added to the floor plan union (p_2) since it widens or alters the core region at the adjacent edge and would thus produce unexpected zoning (Figure 3-7 (h) and (i)).

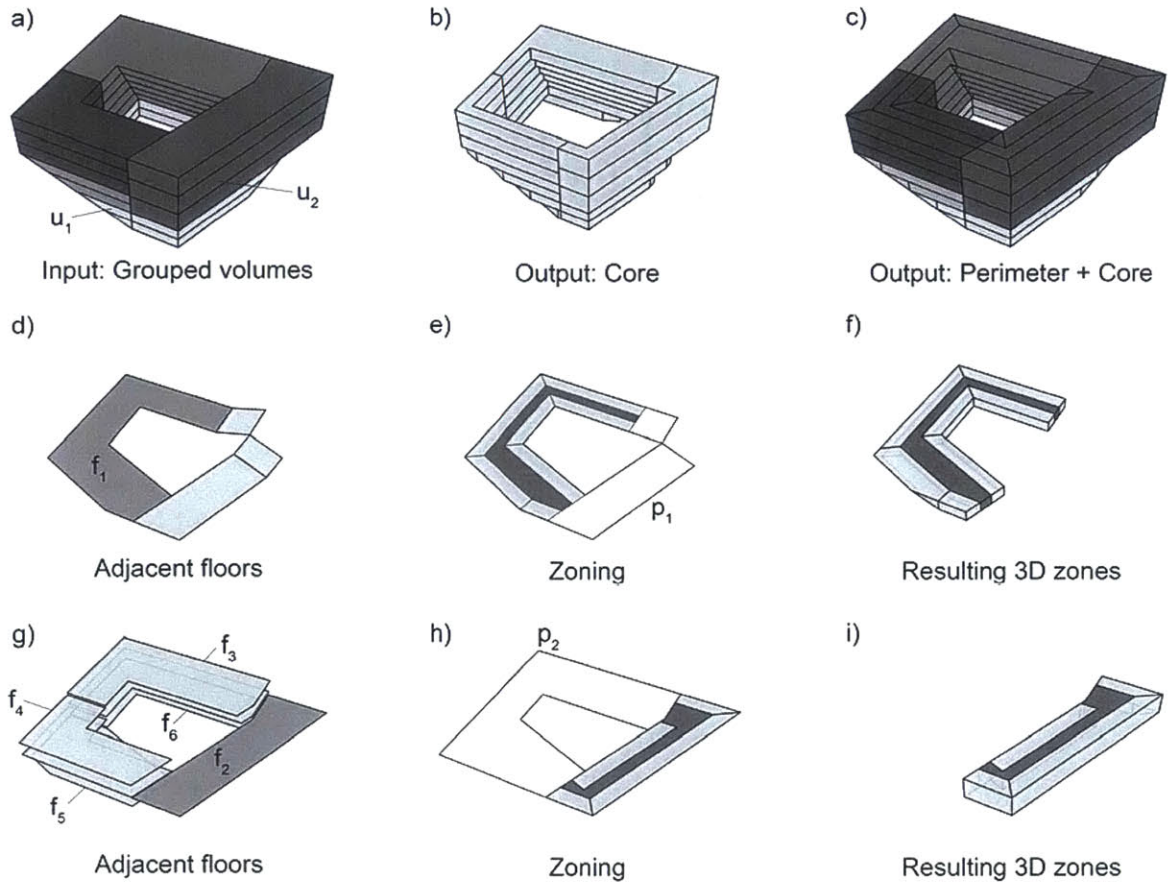

Figure 3-7: 3D adjacency detection and adjacency aware zoning.

Modeling of windows: After the zone geometry is modeled, one has to further articulate the facades. In this implementation, the user can specify orientation dependent window-to-wall-ratios that are then used to model the windows. As a basis to construct the window geometry, all unit faces that are outward facing facades are retrieved (labeled wall/facade and no overlaps with other faces). Then they are sorted by face normal orientation, copied and scaled by the

specified window-to-wall-ratio. Based on the window geometry one can also model horizontal and vertical shades by extruding the edges of the widow geometry along the face normal with a user specified magnitude. This magnitude can be orientation dependent and can be specified for the horizontal and vertical edges separately. For more specific design ideas such as punched-hole facades, horizontal window stripes or more complicated shading devices, this implementation can easily be overridden. Manual intervention is also possible after the 3D geometry is produced and before the energy model is written out.

3.2.2 Testing the algorithm:

In order to test the algorithm's capability, subdivisions for various floor plan outlines of varying complexity (Figure 3-8) are computed. Starting with a simple rectangle (a), convex (c) and non-convex holes (d) are added and the overall edge count of the polygons is increased (g). The time required to compute the Zones was recorded on a Macbook Pro from early 2011 with a 2.3 GHz Intel Core i7 chip, 8GB of RAM and SSD hard drive. How and when the results from the automated procedure could be different from potential manual zoning was analyzed next. Therefore, each shape in Figure 3-8 was zoned by hand according to how energy modelers may subdivide the shapes into core and perimeter cells. There is certainly a high degree of subjectivity associated with this approach. To quantify the geometric difference between the automatically and the manually zoned versions, they are compared based on the zone floor area A_i normalized by the zone facade length lf_i given as ω_i in Formula 1a. An area weighted Root Mean Square Error AW-RMSE as given in Formula 1b and 1c, where ω_{Ai} is the normalized area for the automated zoning and ω_{Mi} is the normalized area for the manual zoning, was computed. In order to understand the implications of the possible geometric difference on a thermal simulation, three different annual load calculations for the shapes in Table 3-1 are compared. First the same material and internal gain settings as given in the DOE Commercial Reference Buildings 'Small Office - New Construction' case [DOE, 2013] are used. For the second case, the materiality is changed to a heavy weight construction without insulation and single glazing. For the third case insulation and triple glazing are added. Results are given as percentage error labeled $E\%_{DOE}$, $E\%_{LOW}$ and $E\%_{HIGH}$ respectively. All simulations were simulated in the Boston climate.

Further, the runtimes of the algorithm to compute the zone subdivision of the shapes in Figure 3-8 and the runtimes of Energy Plus to run an annual energy simulation for each zoned model were monitored.

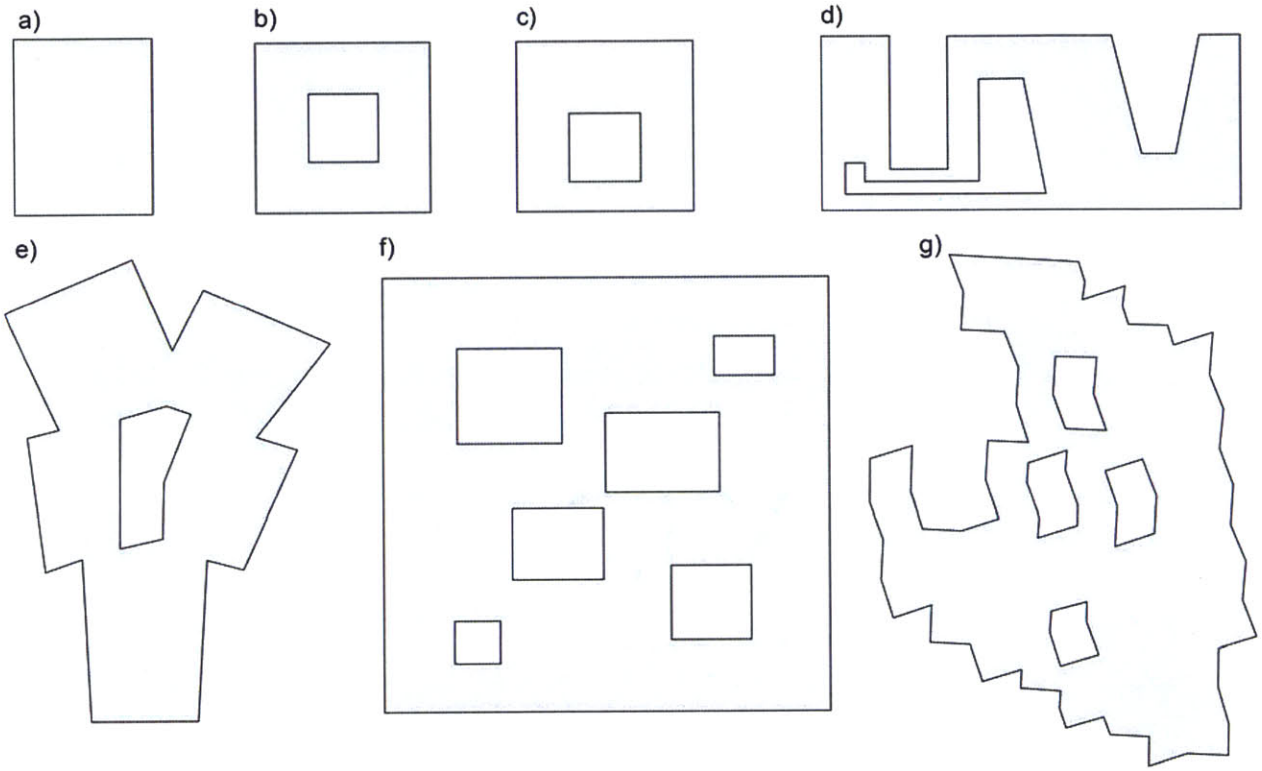

Figure 3-8: Test shapes of varying complexity

$$\omega_i = \frac{A_i}{lf_i} \qquad E\%_i = \frac{\omega_{Ai} - \omega_{Mi}}{\omega_{Mi}} \times 100 \qquad AW\text{-}RMSE = \frac{\sum_{i=1}^{n} [A_i * \sqrt{E\%_i^2}]}{\sum_{i=1}^{n} [A_i]}$$

Formula 1 a,b,c: a) Facade area weight ω b) Percentage error E% c) Area weighted RMSE

3.2.3 Proof of concept implementation and workflow integration:

The algorithm presented in the previous sections was implemented as a proof of concept plug-in for McNeel's Rhinoceros [McNeel, 2012] and Grasshopper [McNeel, 2012] using the C# programming language. McNeel's Rhinoceros is a CAD modeling software that can create,

edit, analyze, and translate curves, surfaces, and solids. Grasshopper is a graphical editor for generative algorithms within the Rhinoceros ecosystem. Both were primarily chosen due to their popularity among architects and urban planners and the extensive support for plug-in development provided through the RhinoCommon SDK [McNeel, 2013]. However, the Autozoner algorithm can be implemented in any modeling environment if the following three geometric algorithms are available:

Offsetting and 2D Boolean addition, subtraction and intersection are used throughout the 2D zoning procedures. This implementation uses the publicly available polygon-clipping library called Clipper by Johnson [2012], which provides this functionality.

For the cellular subdivision, a straight skeleton algorithm is needed. The implementation of a robust straight skeleton algorithm that can handle complex polygons is not a trivial task. This algorithm uses a ported and slightly modified version of an implementation provided by Petr Felkel and has been extensively described by Felkel & Obdrzalek [1998]. Alternatively, Cheng and Vigneron [2007] as well as Huber and Held [2012] describe robust and fast algorithms. An implementation by Cacciola [2004] ships with CGAL [2014], an extensive computational geometry library.

For the 3D zoning (Figure 3-6 (e-h)) 3D Boolean operations are required. This implementation uses the Boolean operations provided by Rhinoceros. However, CGAL offers similar functionality.

The model geometry produced by the Autozoner has to be paired with all non-geometric simulation inputs and zone properties such as construction assemblies, internal loads, schedules and HVAC settings, in order to obtain a fully functional energy model. Automated pairing of geometry and non-geometric simulation properties can be done with Archsim and is explained conceptually in [Cerezo et al., 2014]. Archsim provides a user and programming interface for energy modeling within Grasshopper featuring a thermal model class library containing abstract definitions for zones, faces, materials, etc. that can be translated into a simulation engine specific syntax such as the EnergyPlus [EERE, 2013] IDF format and the TRNSYS [Klein, 1979] BUI format. This allows one to launch a simulation and visualize the simulation results spatially in the Rhino CAD modeling viewport. Once the geometric and non-

geometric data streams are set up correctly, iterating through various geometric design versions and getting simulation-based feedback is only a matter of a few clicks. The proposed workflow is depicted in Figure 3-9.

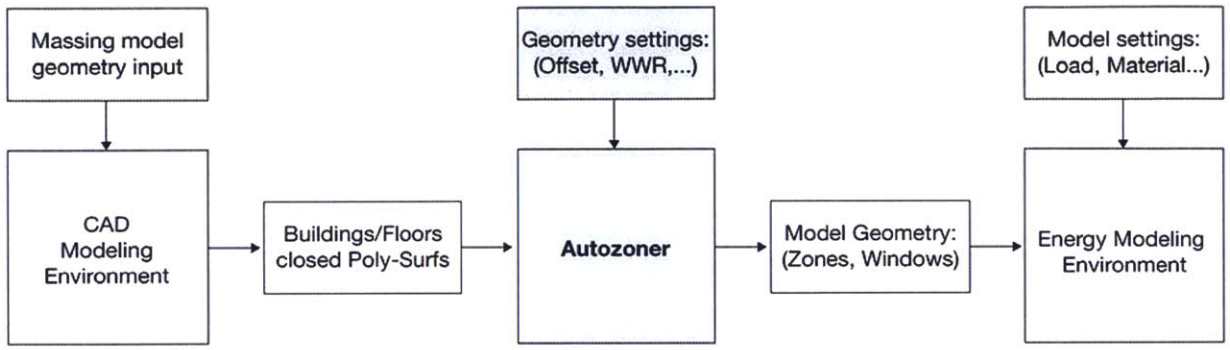

Figure 3-9: Energy modeling workflow integration

3.3 Results

This section shows the results of the automated zoning and compares the outcome with manual zoning. Further, algorithm runtimes are presented. Figure 3-10 shows the automatically zoned test floor plans of Figure 3-8. Simpler shapes such as Figure 3-10(a) result in a subdivision with a zone count of 5. More complex shape outlines yield a higher zone count. An example is Figure 3-10(g) with 58 zones.

While comparing the automatic subdivision shown in Figure 3-10 with a manually generated subdivision, one encounters significant differences in some regions of the shapes. The most prominent cases are highlighted in Figure 3-11. Region 1 shows a detail from shape (c) of Figure 3-10. A manual subdivision would very likely connect both exterior corner points with a straight line with $\alpha=30°$. The straight skeleton approach in this algorithm strictly follows the bisectors of the exterior edges with $\alpha'=45°$. This leads to a difference in normalized area for f_1 to f_1' of 18%. A similar case shown in Region 3 leads to a local disagreement of 43% between f_2 to f_2'. One also observes higher disagreement in regions where the polygon offset that inscribes the core region vanished and many facade edges are in close proximity (Region

2 and 4). The geometric differences for the entire shapes are far less pronounced. The computed AW-RMSEs range from 0%-7% and are given in Table 3-1.

These differences are also reflected in the load simulation comparison. Table 3-1 lists the differences in the results for manually and automatically zoned shapes with the labels $E\%_{DOE}$, $E\%_{LOW}$ and $E\%_{HIGH}$. While, the disagreement does not exceed 1.65% for cases with facade insulation and better glazing ($E\%_{DOE}$, $E\%_{HIGH}$), the deviation can jump up to 8% for the $E\%_{LOW}$ scenario. Here, the difference in floor area, where one assigns all internal gains, to facade length, where major losses occur, has a much bigger impact on the simulation outcome. Due to the different orientations of zones, it is also possible that the deviation levels out, as happened for shape d) were the geometric deviation is at 4% and the simulation-based deviation for all three scenarios is near zero. Table 3-1 also shows the measured runtimes of the presented automated zoning algorithm and each EnergyPlus simulation. For small models, the geometry is computed within milliseconds. Larger models with e.g., 184 zones require 15.5 seconds to compute. EnergyPlus simulation time ranges from 20 seconds to 5 minutes for the largest model.

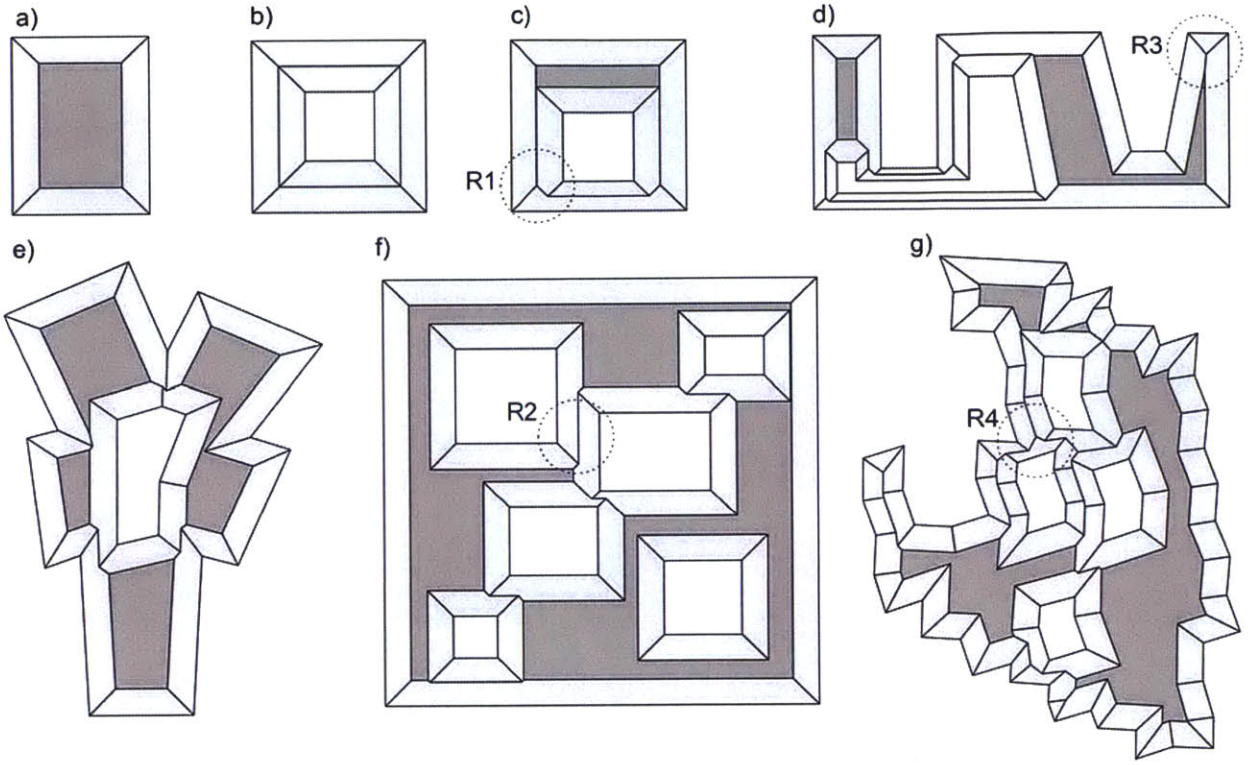

Figure 3-10: Automatic zoning results

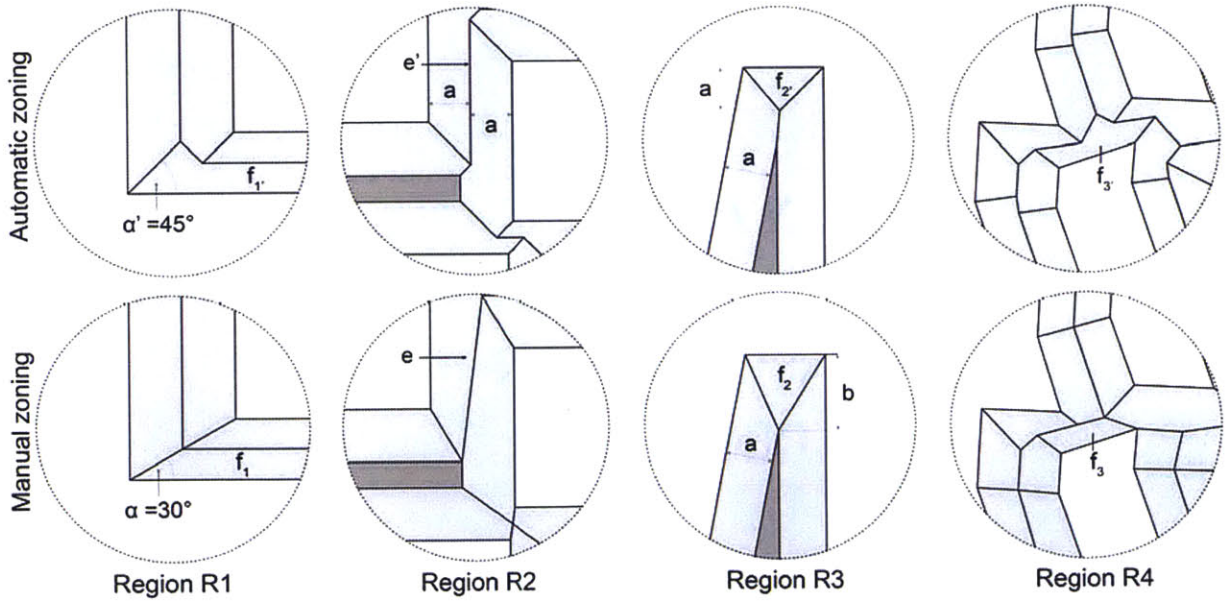

Figure 3-11: Complex massing: Input, floor subdivision, inner subdivision and facade.

Shape	Zones	AW-RMSE	E% DOE	E% LOW	E% HIGH	Autozoning [s]	E+ runtime [s]
a	5	0%	0%	0%	0%	0.29	20
b	8	0%	0%	0%	0%	0.327	23
c	9	4%	-0.78%	-2.19%	0.15%	0.49	24
d	22	4%	0.1%	0%	0.06%	1.4	38
e	26	3%	-1.18%	-4.95%	0.09%	2.8	72
f	28	2%	-1.65%	-8.0%	0.34%	2.1	180
g	58	7%	-0.88%	-6.34%	1.13%	7.7	331

Table 3-1: Algorithm runtime and difference compared to manual zoning

3.4 Discussion

The foregoing section demonstrated that the Autozoner algorithm provides a fast, robust and unambiguous method for automatic zoning of a building according to ASHRAE 90.1 Appendix G. The algorithm is based on standard computational geometry procedures such as offsetting, straight skeleton and 2D/3D Boolean operations and can thus easily be implemented in a variety of energy modeling environments. Arguments in support of using the algorithm during early design are presented next, followed by thoughts on how to set boundary conditions between zones as wells as general limitations of auto-zoning algorithms.

3.4.1 Arguments in favor of using the Autozoner during early design

The two main arguments for using the Autozoner are speed and reproducibility. Given that professional organizations such as the American Institute of Architecture and ASHRAE along with green building rating systems such as LEED [USGBC, 2008], DGNB [DGNB, 2014] BRREAM [BRREAM, 2004] are now encouraging the use of BEM for early design decisions, it seems that the Autozoner, which provides an unambiguous procedure and can be fully automated, has the potential to facilitate the adoption of this recommendation. Indeed, an indication that the use of BEM during design remains problematic is the finding in a recent survey by Samuelson et al. [2012] that 30% of participating AEC firms (Architecture, Engineering, and Construction) who employ in-house energy modelers reported that simulation

based feedback has only "rarely" or "occasionally" an impact on design decisions. Previous studies identified time and resource-intensive workflows as the barriers towards the early use of BPS tools during design, limitations that the Autozoner may help to overcome [De Wilde, 1999][Mahdavi et al., 2003][Ianni et al., 2013].

Apart from individual building design, the Autozoner can also be applied to urban projects that involve dozens of buildings that practically could not be modeled in a reasonable time frame.

The fact that the Autozoner yields unambiguous results seems significant, given that comparing manually and automatically zoned BEMs can yield differences in simulated EUI of up to 8% (Table 3-1). The point here is not to claim that one solution is more "correct" than the other. The point is rather that in a comparative study with multiple variants, a deviation of 8% in the results solely due to inconsistency in the zoning subdivision, can dilute the analysis and thus complicate making suitable design decisions. Thus, it is desirable to employ a zoning method that can compute unvarying and reproducible zone subdivisions for any shape. This consistency is especially desirable if a building energy model is used for envelope studies and when interior space boundaries are not under evaluation.

3.4.2 Boundary Conditions between Zones

Once the geometric boundaries of individual zones have been set, a previously unaddressed question arises, which is how the boundary conditions between touching zones should be modeled by an algorithm such as the Autozoner. ASHRAE 90.1 Appendix G does not provide any binding guidance regarding this topic. The US-DOE Reference Buildings as well as the EnergyPlus Example Files model the zone subdivision with an opaque surface without airflow between zones. What are the consequences of this choice? Figure 3-12 compares annual heating and cooling loads for the same zoning of a square office building but various heat and mass transfer effects at the interior zone boundaries. Beginning with an adiabatic space boundary, conduction, solar radiation and different levels of air mixing are added step-by-step. As one would expect, adding these different modes of inter-zone heat flows successively, the ASHRAE solution is brought closer to the single zone solution. Annual heating and cooling loads vary by up to 41% and 10%, respectively, compared to the building modeled as a single zone. This suggests that an energy modeler and the design team should

be conscious of the likely building layout even during the earliest massing studies using the boundary conditions for the individual or open office scenarios form Figure 3-12 as they may apply.

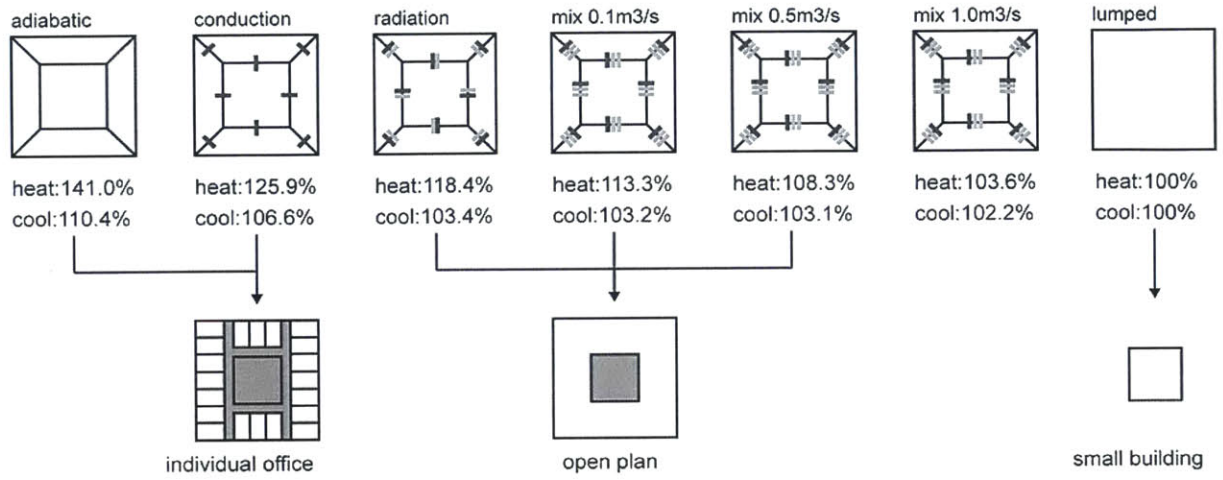

Figure 3-12: Comparison of a perimeter and core subdivision with different inter-zonal heat and mass transfer scenarios versus a single zone simulation and their correlation with architectural floor plan typologies.

3.5 Conclusion

A general algorithm for creating multi-zone energy models for complex building shapes with unknown interior space subdivision is introduced. The algorithm is compliant with ASHRAE 90.1 Appendix G thermal zoning requirements and can easily be implemented in any thermal modeling environment to alleviate time-consuming thermal model preparation and to avoid modeling inconsistencies between different design variants. In practice, the algorithm should be combined with meaningful assumptions regarding the heat transfer through interior boundaries in order to differentiate between single and open plan scenarios. It is important to note that the algorithm should only be used during early massing studies when interior space divisions are indeed still undefined.

4 Automated "typical room" Model Generation

In this chapter, a general algorithm called "Shoeboxer" is presented. It automatically abstracts an arbitrary building massing into a simplified BEM that consists of a set of two-zone perimeter/core shoebox models. The algorithm aims to provide a faster and simpler but yet comparably accurate alternative to the ubiquitous ASHRAE 90.1-compliant multi-zone models in cases when actual interior space divisions and boundary conditions are still undefined. Following a step-by-step explanation of the algorithm, its ability to produce load profiles for equipment electricity, heating, lighting and cooling is validated using an example urban massing model containing 121 buildings. The method yields results that are comparable (RMSE 5-10%) with perimeter and core multi-zone BEMs. The significantly faster simulation times with speed increases of up to 296 times allow building energy modelers to work on UBEM simulations more fluently, effectively and within a feasible time frame.

4.1 Introduction

The Autozoner that was introduced in Chapter 3 can be utilized to auto-generate whole building multi-zone BEMs for hundreds or thousands of buildings. However, one can imagine that the practicality executing multi-zone models generated with the Autozoner is limited to a certain scale due to the computational overhead that is required to simulate models with hundreds of zones. For urban applications, it further seems that an abundance of data would be produced. The benefit of multi-zone models is to be able to spatially resolve differences within buildings such as space orientation, programmatic use and HVAC systems. The use of such a model thus helps the building energy modeler to understand specific energy and mass flows between rooms or zones within the building. However, this suggests that the use of multi-zone thermal models requires a certain amount of knowledge about the interior of a building and becomes for example relevant when heat and air may flow vertically through an atrium. In early design and urban modeling applications such detailed knowledge of the interior qualities of a building are however mostly unknown. This lack of knowledge in combination with the ASHRAE 90.1 Appendix G prescribed zoning conventions often leads to fully conditioned perimeter and core regions with uniform program distribution and uniform set-point temperatures throughout the multi-zone thermal model. This creates a situation where there are only negligible temperature differences across interior zone-boundaries and thus no significant energy flows between zones occur. Therefore, the computational overhead that is invested into simulating hundreds of zones explicitly seems wasteful. Hence, one must question the appropriateness and efficiency of such models for early design and urban applications.

This chapter introduces an algorithm called the Shoeboxer. It explores an alternative methodology that can approximate the results of a perimeter and core multi-zone BEM by dissecting an architectural massing model into a meaningful set of typical room thermal models. The procedure is inspired by the manual methods of Section 2.3.1 that abstract urban modeling tasks into typical street canyons, however, adds improvements such as the complete automation of the abstraction process and spatial result mapping. The introduced method is validated against results produced with the Autozoner. An urban design case study and several use case examples reveal the benefits of using the Shoeboxer versus the Autozoner.

4.2 Methodology

The following section is divided into three main parts: First, a detailed description of the Shoeboxer algorithm is given. Then the validation workflow is described. The third part describes a proof of concept implementation and an urban case study.

4.2.1 Shoeboxer algorithm

Input and input generation: The challenge for early design and urban building performance simulation starts with providing the necessary inputs to run a full climate-based transient energy simulation of multiple buildings. Based on the author's experience in design practice and environmental consultancy, urban and schematic design processes can produce a variety of input data, which are described and categorized in the following section. Given the non-linearity and iterative nature of these design processes, it becomes apparent that the required input data ranging from geometric descriptions of the design to detailed physical and functional descriptions of buildings such as materiality and building use may not be defined or may change constantly while the design moves forward. Hence, the design of an interface and a structure in which the data input can be managed is of significant importance for the Shoeboxer algorithm. One distinguishes between purely geometric input and numeric input that describes building properties [Cerezo et al., 2014]. This allows the user to update each data set independently. The non-geometric data is interchangeable between the geometric data and thus allows automated assignment and modification of building properties and functions. This separation also makes practical sense since the source or authorship of the building properties data can change during the design process. An example could be that an architect or urban designer begins a preliminary design study with standardized building properties, including simple constructions and a simple HVAC system, in order to use energy loads for design feedback. Once the design matured, an environmental engineer could provide more complex building properties that involve specific material improvements, complex fenestration and conditioning systems.

Geometry input availability and categorization: The geometric inputs that are available during an urban design process are best explained using a real world case study. The presented project proposes a master plan for a new urban center for 90,000 inhabitants with a

Net-Zero carbon footprint in Abuja, Nigeria and was collaboratively developed by a team of urban designers and environmental consultants [Holst & Dogan, 2013].

The first concern of the designers was the layout of the street grid. The street grid is the most dominant organizational pattern that defines all kinds of flows (traffic, energy, waste) within a city. The layout and resolution of the grid also defines block size and anticipates, to a certain degree, the built densities and functional distribution within the design. Figure 4-1 shows the first block layout. On top of this structure, a vision of how to fill the blocks with actual buildings needs to be created. The designers began by drawing 2D footprints (Figure 4-2) and assigning a building height or number of floors to each footprint (Figure 4-3). The function and use of each building footprint was indicated by color-coding the footprints and grouping them within a layer hierarchy.

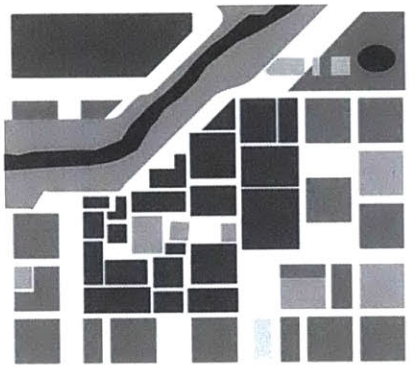

Figure 4-1: Block Layout

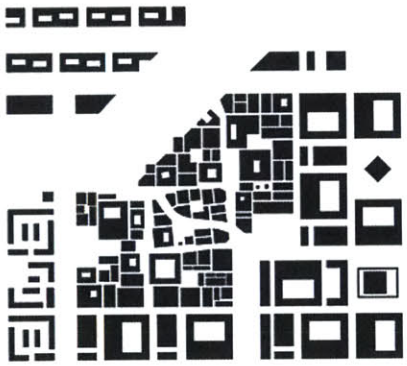

Figure 4-2: Figure Ground Diagram

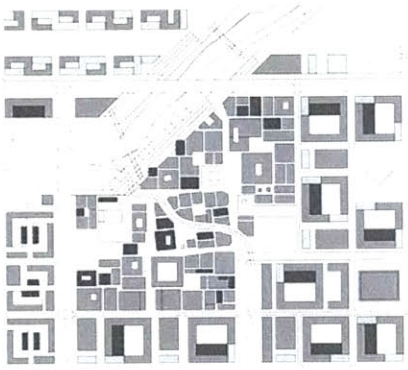

Figure 4-3: Development Plan

These 2D plans were the basis for the first 3D model, generated by simply extruding the building footprints. As the design progressed, the model was updated and refined many times and later included explicitly modeled 3D geometry that went beyond simple extrusions including buildings with setbacks and courtyards (Figure 4-4). Similarly, pitched roofs and non-vertical facades can be added. Despite this added geometric complexity, the models remain *de* facto volumetric, i.e., interior partitions remain undefined and programmatic use remains roughly assigned in volumetric chunks. From a formal design standpoint, the purpose of these models is to understand basic morphologic features. Similar to the functional hierarchy in 2D, the volumes again had a color-coding. However, in 3D the volumes were further subdivided and

differentiated by program and function within the building (*Figure 4-5*), so that floors close to the street level serve as retail and other commercial purposes whereas upper levels are labeled as office and/or residential. Another very common representation involves "stacking" floor-volumes. This adds a notion of "scale" since it immediately allows one to read floor-to-floor heights from the model. This form of representation, however, is usually only generated for smaller sections of a city model such as a neighborhood or block. Due to its level of detail, it can only be visualized effectively at a certain "zoom" level.

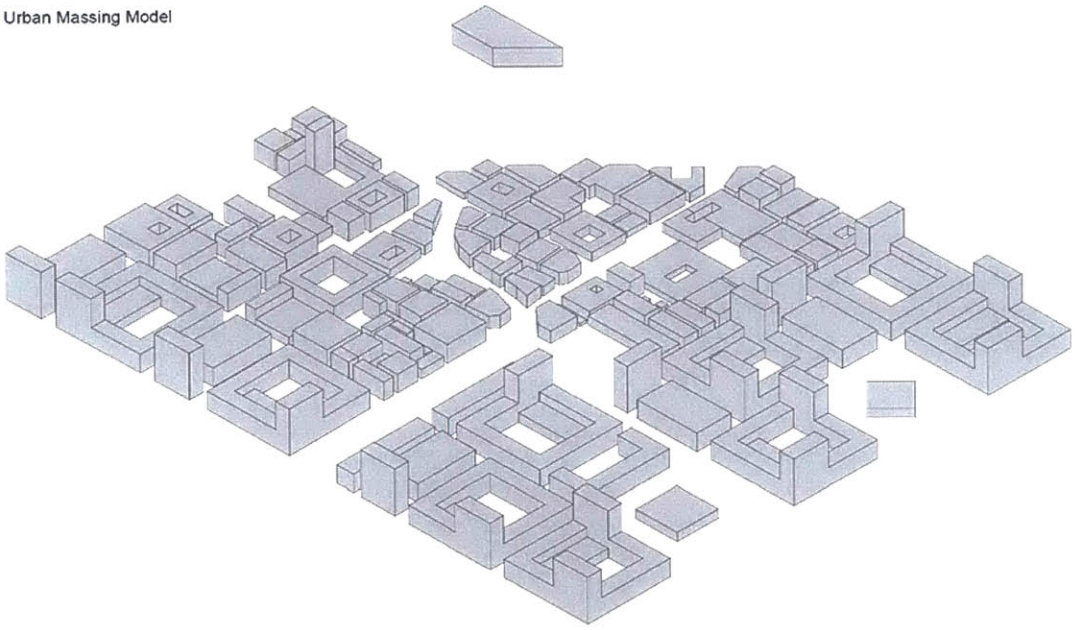

Figure 4-4: Massing model

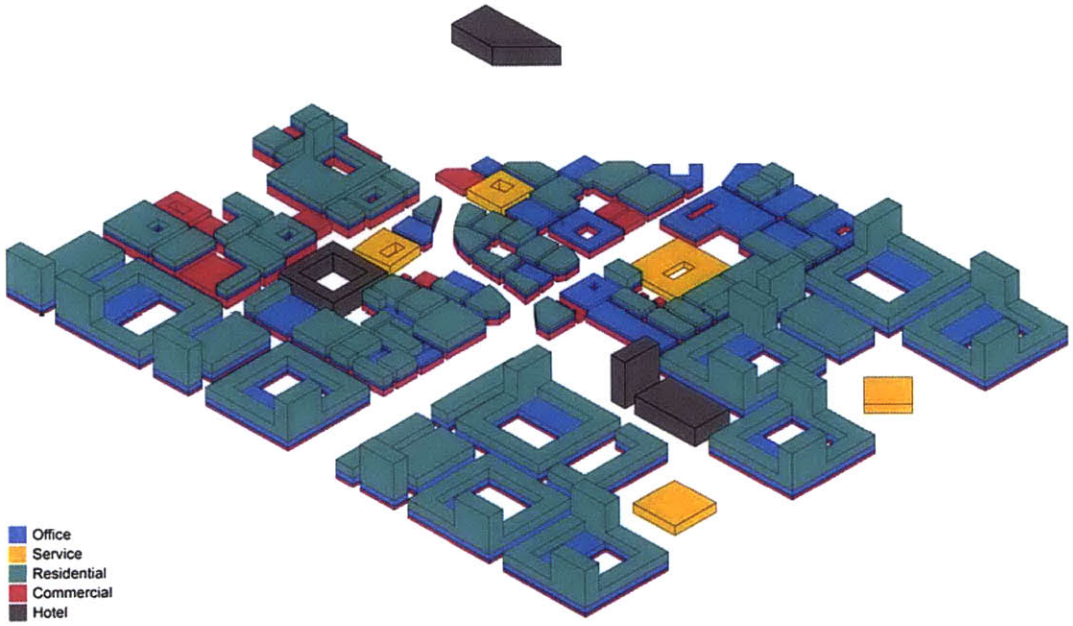

Figure 4-5: Massing model with color-coded architectural program

Geometric input processing: The Shoeboxer algorithm supports all mentioned input geometries. At the earliest stage, the CAD data is 2D and thus not sufficient for BPS. However, critical decisions regarding density and street width that potentially predetermine the environmental performance of the design need to be made in this phase. Consequently, simulation tools should be able to assist decision making at this point. Hence, the Shoeboxer provides helper functions that allow users to process 2D data and convert it into a 3D massing model. The basis for auto-generating 3D data is a set of closed poly-lines describing the building footprints. In case the terrain is not flat, these 2D outlines need to be placed at the correct Z-location within the model. If the terrain is given as a mesh or as a bitmap height-field, the algorithm can auto detect the correct Z-position. This is done by performing a closest point query on the terrain-mesh for each point in the footprint poly-line. The average of the returned Z-coordinates of each test-point is then used as base height for each building. If a bitmap height-field is provided instead of a mesh, the procedure is similar but involves a coordinate query (XY) to read the height information form the bitmap. After the poly-lines are positioned at the right Z-location, one now needs building height information for every poly-line. This data can be provided as array of numbers or in a similar fashion as the height-field bitmap. The later

provides a quick and "fuzzy" interface to design and determine building height. The Shoeboxer can then automatically extrude and cap the footprint poly-lines and produce closed poly-surfaces for each building.

Accordingly, buildings can also be modeled explicitly to represent geometry that goes beyond extrusions. The only two limitations are that surfaces must be planar and volumes must be closed. For models that are subdivided by floor or program, the same rules apply. In addition, the user must be able to group the volumes so that they can be identified as one building later. This can be done by naming the sub-volumes. Procedures that can automatically name hundreds of buildings and their sub-volumes are included as helper functions.

For convenience and clarity, it makes sense to convert this purely geometric data into objects that allow one to attach further information to them and that facilitate querying them later. Therefore, two constructs called "unit" and "face" are introduced. A unit contains the envelope of the volumetric massing of a building or subsection of a building given as the closed poly surface that is described earlier. The face construct describes the envelope sub-surfaces of the closed poly-surface and will be described in more detail in the following paragraphs. Each unit thus also holds a list of faces. Additionally, a unit must contain data so that it can describe a building or a subsection of a building. This data is described in the following paragraph.

Non-geometric input: Besides the volumetric geometry of the buildings, the internal floor-subdivision, the size of perimeter and core regions, the window-to-wall ratio of the facades, materiality, usage profiles and conditioning systems and strategies are highly relevant for a BEM and thus must be attached to each unit within the model. To structure this data, two variable containers called "geometricProperties" and "zoneTemplate" are introduced. The geometricProperties class contains a field for floor-to-floor height, perimeter offset, and an array of doubles for orientation dependent window-to-wall ratios. The zoneTemplate is far more complex. It contains materials and constructions for floors, interior partitions, facades, roofs, ground-facing building elements, glazing properties, descriptions of blind and shading systems. It further contains the use profile of a typical space within the building including the number of occupants, schedules, equipment installed, lighting and conditioning systems.

Linking of units and non-geometric inputs: After defining all possible input types one now has to bring the units and zoneTemplates and geometricProperties together. This organization of the geometric input via color-coding or grouping of geometry by function and program is the fundamental organizational concept that is used throughout the algorithm. Each unit must be assigned to such a group and will inherit one geometricProperties container and one zoneTemplate from it. A second zoneTemplate can be inherited in case the unit has a core region that has a different program than the perimeter.

Building discretization and pseudo-thermal zoning: Based on the necessity to discretize a thermal model into separate zones for different load scenarios (Chapter 2.2), the units have to be further subdivided. ASHRAE 90.1 Appendix G recommendations and the Autozoner implementation would divide a unit into numerous sub-volumes for floors and perimeter-spaces within each floor. The goal of the Shoeboxer, however, is to keep the geometric complexity of the thermal models at an adequate level for urban energy modeling and to reduce the number of zones in a simulation to achieve reasonable simulation runtimes. Hence, the idea is to place a zone (typical-room energy model) only at representative points within the model and then extrapolate its energy demand to emulate a whole unit. Simulating each representative point separately could then have a similar effect as the diagonal partition wall that separates perimeter zones with different orientations in the ASHRAE zoning paradigm.

The algorithm begins with the floor subdivision of the unit. Using the given floor-to-ceiling height, cutting planes are generated at the mid-height of each floor and the intersections with the unit-envelope (poly-surface) are computed. The resulting surfaces are stored in the unit as a list of floors. The floor-surfaces are the basis of the area integration for each unit. The floor area can be further divided into a core and perimeter region by offsetting the floor edges inwards by a specified perimeter-offset. The Shoeboxer uses the publicly available polygon-clipping library called Clipper by Johnson [2012] to perform this operation. Even though the algorithm geometrically computes the offsets (Figure 4-6 A), it only uses the resulting areas to estimate the core and perimeter area ratios within the unit. Hence, it computes a total-floor-area, core-area and perimeter-area and stores the values as doubles inside the unit class.

In a second step the algorithm processes the unit-envelopes' sub-surfaces referred to as faces. Among these faces, there are surfaces that describe the roof, the facades and the ground-facing elements of the building envelope. The goal is to identify them as such. This can be done by checking their normal orientation. Due to the required planarity of each face it is possible to compute the face normal at any location of the surface. Since the initial poly-surface is required to be closed, the face orientation is guaranteed to be outward facing. Therefore, a roof is detected if the face-normal points upwards; if it points downwards, a ground plate or overhang is found. All other normal orientations must then be facades that can be further distinguished by their cardinal direction. This is done by comparing the normal orientation to north, east, west and south with a +- 45 degree tolerance. This information is stored in the form of a type label in each face. To correctly handle sloped surfaces the algorithm allows the user to specify a maximum tilt angle to distinguish floors and ceilings from possibly tilted facades.

Based on the type-labels it is now inferable how much facade area of each unit points to which cardinal direction. Now the total perimeter area of a unit can be virtually divided weighted by this distribution. Intuitively, at least four shoebox models are needed to capture the difference in diurnal and seasonal variations of solar radiation incident on the model. However, it is still unclear where exactly one should place each shoebox within the model. Due to a different Z-position in the building or different urban context even facades with identical orientation might have significantly different solar exposures. Thus, simply sorting the facade surfaces by cardinal direction is not sufficient since microclimatic shading effects could then not be taken into account. Hence, incident solar radiation is used as an additional criterion to group the facades.

Insolation Analysis: In order to compute incident solar radiation, a calculation method that is able to reliably consider local weather data as well as the effects of neighboring buildings is needed. Example methods are described in Duffie and Beckman [2006] and a comparison of selected methods is offered in Ibarra and Reinhart [2011]. This implementation uses the validated backwards ray tracer Radiance [Ward, 1994] along with GenCumulativeSky [Robinson & Stone, 2004] to integrate the annual incident solar radiation. To measure solar radiation, the algorithm needs to discretize the facades into small one-story high pieces (a story is the smallest unit in the Z-direction based on which the algorithm can move shoebox samples

within a unit). The size of those pieces can be controlled by the user with smaller subdivisions being advisable for more complex local shading situations.

The ray tracing requires a set of sensor points (a point and orientation vector construct) and a mesh-based scene of the entire model as input. One can automatically generate these inputs from the units by segmenting the floor-outlines by a given size. The midpoint of each segment represents a slice of the façade that is directly behind it. The segment midpoints are then paired with the face normal to generate the sensors. Figure 4-6 B visualizes a typical radiation analysis result.

Façade Clustering: After the incident solar radiation analysis each facade piece is sorted into bins of similar received radiation within the facade orientation groups of each unit. This is a typical clustering task where one would group a set of objects in such a way that objects in the same group are more similar to each other than to those in other groups. This algorithm uses a k-Means implementation that was first described by Hartigan [1975] and Hartigan and Wong [1979]. An overview and in-depth description of the most commonly used clustering algorithms are available from Zaki and Meira [2014]. The user defines the number of clusters that should be generated per orientation and unit. The algorithm then sorts the facade pieces based on their 1D Euclidean distance of their received radiation (Figure 4-6 C). The accuracy of this sorting is given in a parameter called RD. The parameter describes the sum of all distances of members of a cluster to their centroid. A higher value represents a cluster with diverse members and suggests that more clusters should be used.

In the future additional clustering criteria could be added easily by simply expanding the dimensionality to two or n dimensions. For each cluster, one facade piece is identified as the centroid. This centroid is per definition the closest point to the median of all received radiation values within the cluster. This point or facade segment is the most representative segment of all others within the cluster and hence it is the ideal place to draw a sample and to place the shoebox thermal model (Figure 4-6 C and D). After having identified the most representative façade segments for each unit and orientation, it is now possible to position all the samples/shoeboxes to describe the unit.

Figure 4-6 E shows the perimeter-area that is represented by one typical-room sample (red). This area is computed with a weighing function that virtually partitions the perimeter-area based on the on the aggregated façade area that a cluster occupies.

Shading: Next, contextual- and self-shading within the model must be taken into account. Since the 3D geometry of the urban design is available, one could simply use this geometry as shading surfaces for each shoebox. Doing so would include a large number of surfaces that are most likely not seen by the sample boxes. Unlike the previously used insolation analysis, the simulation time required by the shading algorithm in EnergyPlus increases significantly with the number of polygons in the model. Hence, it would be beneficial to reduce the geometric complexity for EnergyPlus beforehand. Another problem one might face with the shading algorithm in EnergyPlus is stability for complex 3D geometry. Large models tend to throw degenerate shadow polygon errors frequently due to multiple overlapping surfaces in the shadow projection.

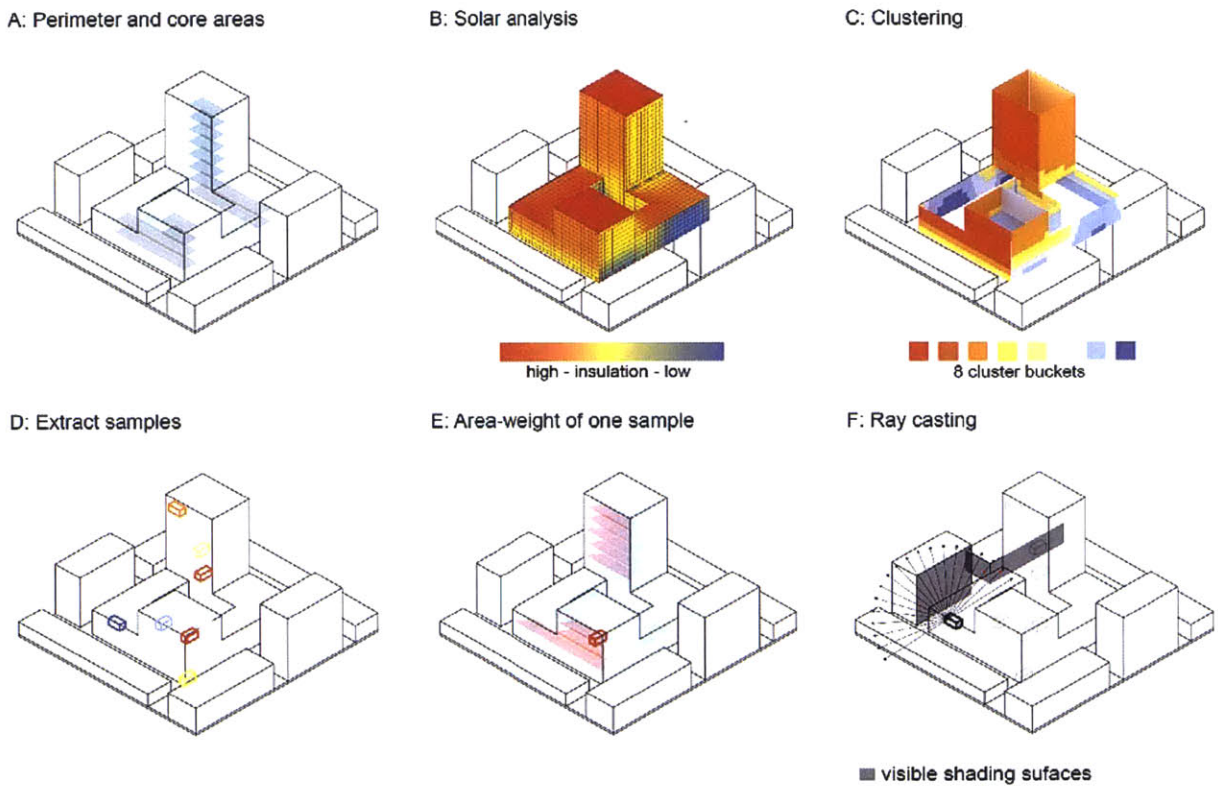

Figure 4-6: Visualization of main algorithmic steps

A more geometry-friendly approach would be to use standard computer graphics methods for the shading calculation. Jones et al. [2012] presented a technique that uses OpenGL buffering and pixel counting in order to compute sunlit areas. However, since the previously mentioned method has never been released publicly and the official EnergyPlus does not provide an interface for "third-party" shading calculations, this approach has been discarded. In the context of this research, a ray casting technique is used to selectively pull only visible shading elements into the simulations. Figure 4-6 F) illustrates a typical shading context for one shoebox with three visible shading surfaces in dark gray.

Shoebox Simulations: To this point, the algorithm has collected units and their settings, has analyzed the incident solar radiation on the unit envelope and has picked facade locations where to place the shoebox models. For each of these locations the algorithm also found all relevant contextual shading surfaces. It is now time to construct the geometry of the shoeboxes and finally combine everything to begin the simulations. The origin for each shoebox within the model is the centroid of the corresponding facade patch. Around this node, the opaque facade rectangle is constructed first. A user defined typical room width and the floor-to-floor distance are used as rectangle dimensions. Then the window geometry is constructed. This can be done by copying the opaque rectangle and then scaling it by the window-to-wall ratio along its horizontal centerline and in Z-direction. Then the algorithm applies the glazing and facade materials, as defined in the unit's zone template. Further, the back face and the sides of the shoebox are constructed. The algorithm determines the depth of the shoebox based on the facade area to floor area ratio of the unit. All three surfaces are then set to adiabatic and the interior partition material is applied to them. The roof and the ground are both constructed out of two surfaces since they will include a portion of the roof- and ground-facing surfaces. The depth of these surfaces is determined according to the roof area to floor area ratio and the ground-coupled area to floor area ratio of each unit. The specified roof material and ground-facing material, are applied respectively. The leftover ceiling and floor surfaces are set to adiabatic and an interior slab construction is applied. In case the unit has a core region, an additional zone is added to each shoebox to represent the core. It is constructed it in a similar fashion. Finally, the zone properties including occupancy profiles, interior gains and conditioning settings are appended and written out as an EnergyPlus input file. Although

EnergyPlus is used for the proof of concept implementation, the Shoeboxer can be used with any other simulation engine that can read text files as input.

Based on the simulation results of each individual shoebox model, the EUI for one unit can be aggregated by weighing the results for each shoebox with the floor area that the pertaining cluster occupies (Figure 4-6 E) within the unit.

Adjacencies: As described thus far, the algorithm could only work for free standing building geometry. In urban settings, however, adjacent buildings are very common. Further, buildings may be split into multiple units to model different architectural programs. Hence, the algorithm searches all units for congruent face pairs and adds them to the adjacency graph of the model.

Adjacencies have a significant impact on each step of the algorithm and they must be computed before the insolation analysis in order to avoid placing sensors inside other neighboring buildings. Adjacencies also influence the area ratio calculation since the algorithm must distinguish between boundaries between buildings and facades. The boundaries are treated as adiabatic surfaces, assuming no heat flow between touching buildings or programmatic volumes. In addition, the algorithm counts the area behind a boundary and adds it to the unit's core area.

Building clustering: Thus far, the Shoeboxer algorithm creates a thermal model that consists of a discrete and user-controlled number of zones for each unit. If a unit represents a massing model for a large building, the Shoeboxer model reduces complexity significantly compared to a core and perimeter multi-zone model that may contain hundreds of zones. This leads to faster simulation runtimes and compact and manageable data sets. However, for very large urban scenes that involve hundreds or thousands of buildings, a building-by-building approximation with the Shoeboxer algorithm might still not be satisfactory. In order to further reduce complexity and simulation time, the Shoeboxer can introduce an additional clustering step that analyzes and then sorts the given units by their geometric similarity. As similarity criteria geometric ratios, such as façade to floor area, roof area to floor area, footprint to floor area as well as core area to perimeter area are utilized. The clustering step is inserted after the units and non-geometric properties have been paired and before the insolation analysis is

performed. Again, the accuracy of the clustering can be measured by the distances of each cluster member to the cluster centroid. This distance is referred to as GD in the following text and graphs.

Since the geometric ratios are used to construct the shoebox models as described in a previous section, the need for the added clustering step becomes apparent. The massing model (Figure 4-4) includes a variety of building typologies and building scales. This is also reflected in the distribution of the geometric ratios. Figure 4-7 shows a histogram of the geometric ratios of the entire massing model. Core-to-perimeter ratios as well as the floor-to-façade ratios are widespread and evenly distributed. The roof and footprint related ratios also spread, however, showing peaks around zero and one. This is due to the fact that multiple units do not have a roof or contact to ground since they are stacked. If these buildings were to be poorly insulated and situated in a cold climate one can expect that a building with more façade surface area versus floor area will have a significantly higher heating demand. This applies to the roof area ratio and footprint area ratios accordingly. It is also important to note that with increasingly good construction standards these area ratios are expected to become less important.

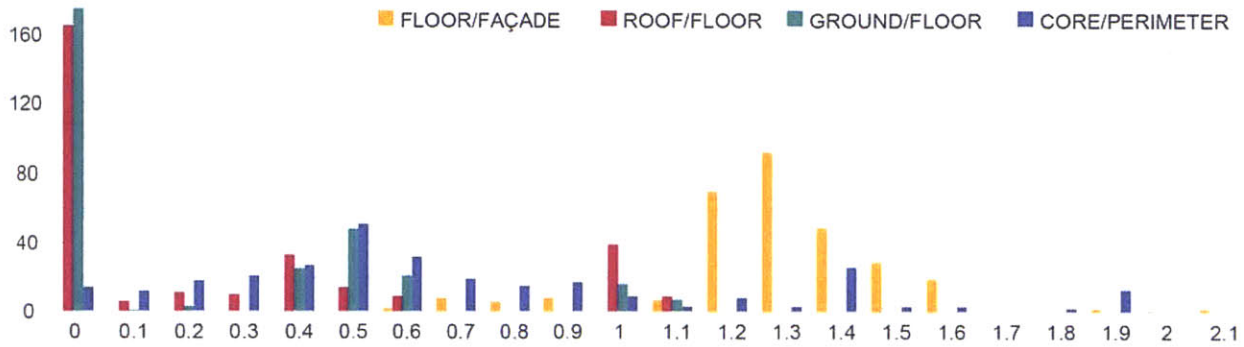

Figure 4-7: Histogram of all relevant geometric ratios of the 296 unit volumes within the massing model.

HVAC Systems: By default the Shoeboxer conditions spaces with an ideal heating and cooling system. While the simulation of pure energy loads is sufficient for most urban modeling tasks, some projects might require simulating more elaborate HVAC systems. This can be done conveniently by swapping out the ideal heating and cooling systems in the EnergyPlus input file with other HVAC templates or components. For HVAC system simulations, the composition of the EnergyPlus input files is of importance. Several options are possible: The

default composition writes every shoebox in a separate EnergyPlus input file so that a maximum degree of parallelization is achieved. Shoeboxes can however also be consolidated in an EnergyPlus input file per usage cluster. Further, the clustering can be set up so that an input file per building is generated. This is equivalent to forcing the building clustering step to create a separate cluster for each building. In this case, the selection, sizing and simulation of an HVAC system does not differ from the workflows that are currently used in BEM simulations. The only dissimilarity is that the BEM consists of fewer zones and the actually incurring energy loads are emulated with zone multipliers.

4.2.2 Validation of the Shoeboxer algorithm

To demonstrate the capabilities of the Shoeboxer, the previously introduced massing model is used as a case study. In order to validate the Shoeboxer algorithm, simulated energy loads modeled with perimeter and core multi-zone models are carefully compared with results generated by the Shoeboxer.

The massing model (Figure 4-4) consists of 121 buildings that are represented as closed volumes (boundary representations). Each building is subdivided into multiple sub-volumes to accommodate and distribute different architectural programs resulting in 296 units (Figure 4-5). The following architectural programs are utilized: hotel, service, commercial, residential, office and core/circulation. Each program definition follows the Swiss architectural norm SIA Merkblatt 2024 [S. I. A., 2006] that defines typical spaces and their internal gains, equipment loads, set-point temperatures and occupancy profiles. Spaces are conditioned with the default ideal heating and cooling system. While the architectural program distribution of the original design was strictly followed, different construction standards and climates are used in the simulations in order to cover a broader environmental spectrum and a variety of materials. Three locations are chosen: Anchorage, Boston and Phoenix representing a heating-dominated, mixed and cooling-dominated climate respectively. Three opening ratios are tested: 25%, 50% and 75% as well as an old (average façade U-Value: 1.5 W/m^2K, double-pane fenestration) and a new (average façade U-Value: 0.2 W/m^2K, double-pane fenestration) construction standard. Static or dynamic shading systems are selectively turned on.

In order to compute energy loads with the Shoeboxer method one simply has to provide the 296 units and the corresponding architectural program definitions to the algorithm. The

Shoeboxer allows the user to adjust several input parameters that have an influence on the accuracy of the algorithm. In order to test the sensitivity of the simulated energy loads with respect to these parameters, each scenario is run with the following accuracy settings: very high (GD:10, RD: 6000), high (GD:20, RD: 22000), low (GD:40, RD: 70000), and very low (GD:60, RD: 130000).

In order to obtain the reference "multi-zone whole building energy models," the previously used building volumes must be further discretized into thermal zones. The Autozoner algorithm (Chapter 3) is used to compute the thermal zones following a core and perimeter subdivision schema as prescribed by ASHRAE 90. The outcome of the auto-zoning algorithm is a set of 4112 closed volumes (BREPs) shown in Figure 4-8. Further, each volume must be sorted so that the various architectural programs can be applied to them. Several scripts are used to automate this task. Then, both zones and the corresponding program definitions are streamed to Archsim [Dogan, 2013], a Grasshopper interface for EnergyPlus. Archsim then batch generates and executes the multi-zone energy models for each building. The urban context is taken into account using a ray-casting technique similar to the one used by the Shoeboxer. Including all test scenarios, results in 3267 individual simulations.

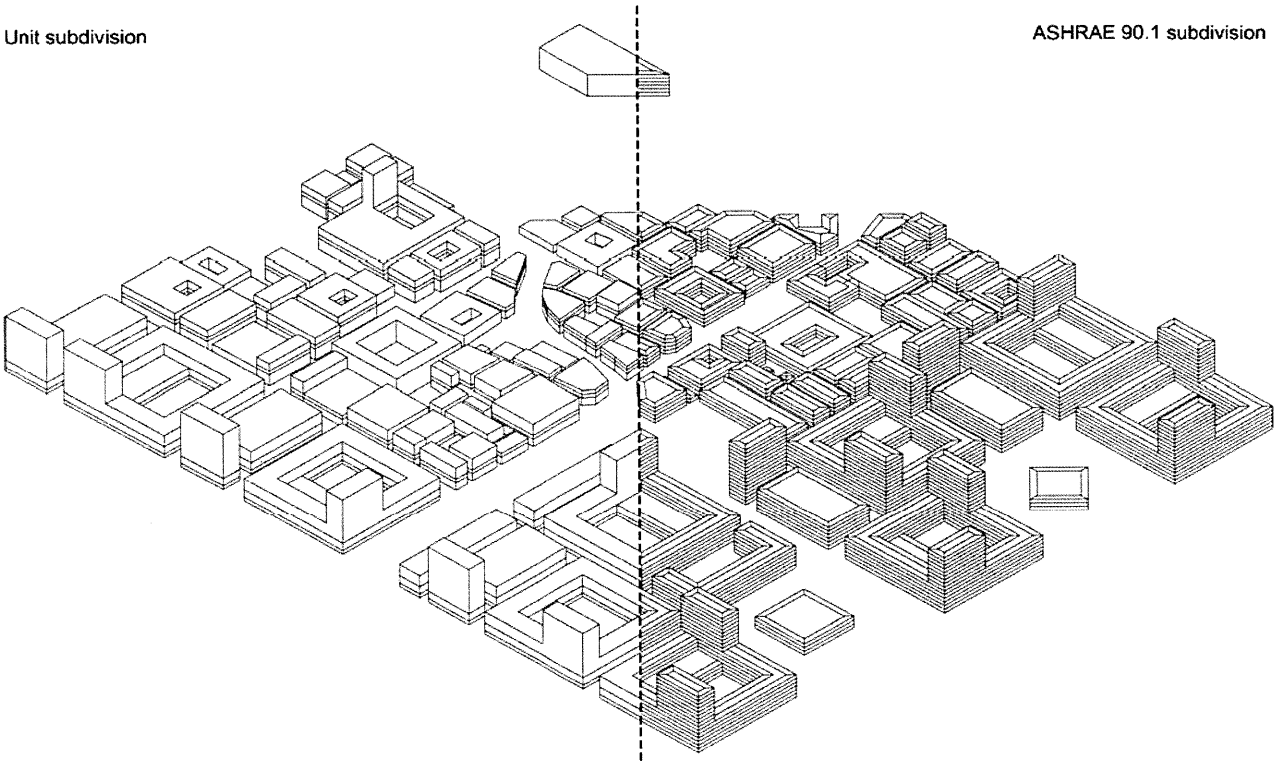

Figure 4-8: Massing model thermal model discretization. The Perimeter/Core subdivision is shown on the right and the simpler unit subdivision for the Shoeboxer on the left.

4.3 Results

For the previously described simulation scenarios and 121 buildings, a total of 8712 simulation result pairs have to be compared. Figure 4-9 compares absolute energy use intensity (EUI) for three scenarios.

In a post-processing step, the percentage error (Formula 4-1) of the temporal sum of all loads for each building of each scenario is computed. Selectively, the percentage error of load components such as solar gains, lighting, electric, heating and cooling are also shown. The computed errors are plotted in form of a histogram with 1% bins ranging from positive to negative 40%. The error distribution for the total EUI is plotted in different colors for each climate and in separate figures for each accuracy setting of the Shoeboxer (Figure 4-10). It can be observed that with a decrease in clustering precision, the peak around 0% Error melts and a much wider spread occurs.

The first histograms (Figure 4-10) show the EUI percentage error distribution for the most accurate Shoeboxer settings tested. This configuration yields 93% of all building level results within a +-15% error margin; 7% lie outside of this margin. The outliers are mostly associated with the Phoenix climate plotted in pink. To further investigate this phenomenon a detailed plot of all loads for one Phoenix scenario is given in Figure 4-11 A. The figure shows that solar gain predictions for some buildings can exceed 40%. It further shows that larger errors in the solar gain prediction have an immediate effect on the cooling load and hence influence the overall energy load prediction. The same scenario, however with dynamic shading systems turned on, is plotted in the Figure 4-11 B. The predicted solar gain error (plotted as yellow dots) drops significantly and with it the overall energy demand error (plotted as black triangles).

In order to summarize all computed errors, an overview in Figure 4-12 is provided that plots overall RMSE (Formula 4-2) and MBE (Formula 4-3) for energy loads including lighting, electric, cooling and heating loads for each scenario. The figure shows that mostly the "old" construction scenario accuracy suffers in case the clustering accuracy is lowered. The different window-to-wall ratios have a small impact on the RMSE and MBE in heating-dominated climates but can lead to deltas in accuracy of ~5% in climates with high direct solar exposure.

$$E = \left(\frac{\left(\sum loads_{New} - \sum loads_{Ref}\right)}{\sum loads_{Ref}}\right)$$

Formula 4-1: Percentage Error

$$RMSE = \sqrt{\frac{1}{n}\sum_{i=1}^{n}\left(\frac{x_i - x_{Ref}}{x_{Ref}}\right)^2}$$

Formula 4-2: Root Mean Square Error

$$MBE = \frac{1}{n}\sum_{i=1}^{n}\left(\frac{x_i - x_{Ref}}{x_{Ref}}\right)$$

Formula 4-3: Mean Bias Error

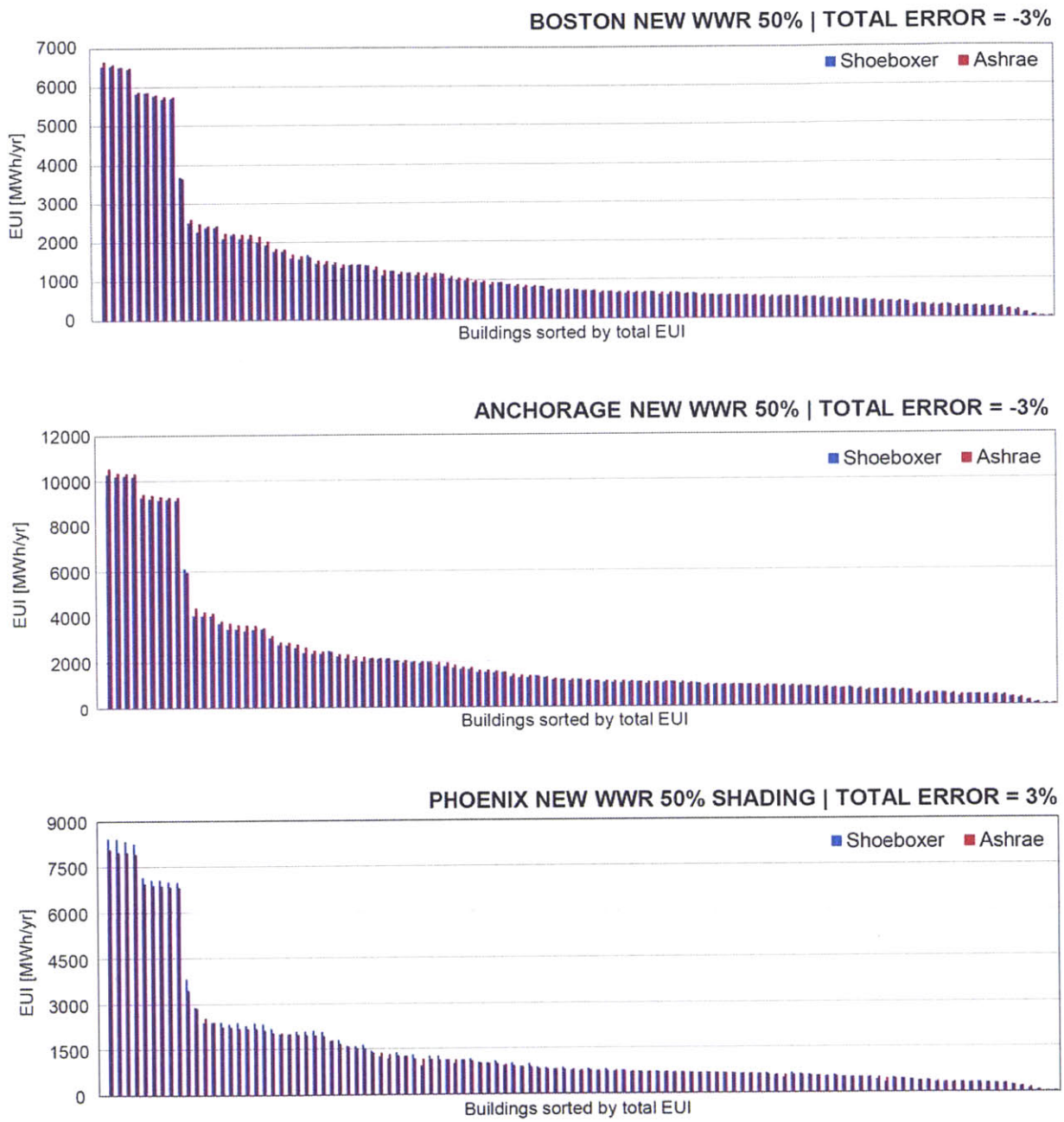

Figure 4-9: Absolute EUI comparison for 3 climate scenarios and 121 buildings. (Clustering accuracy: High)

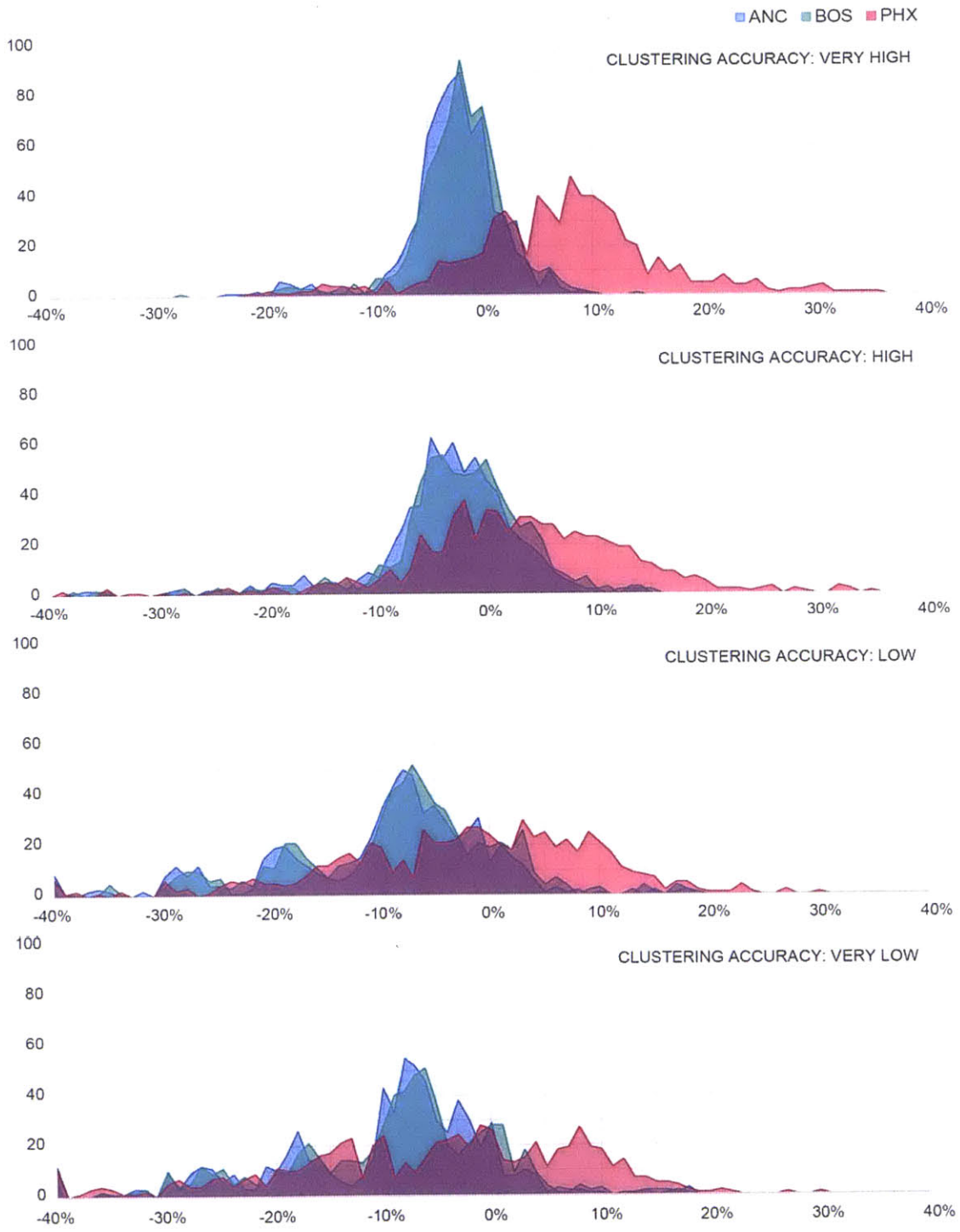

Figure 4-10: EUI percentage error distribution for four accuracy settings

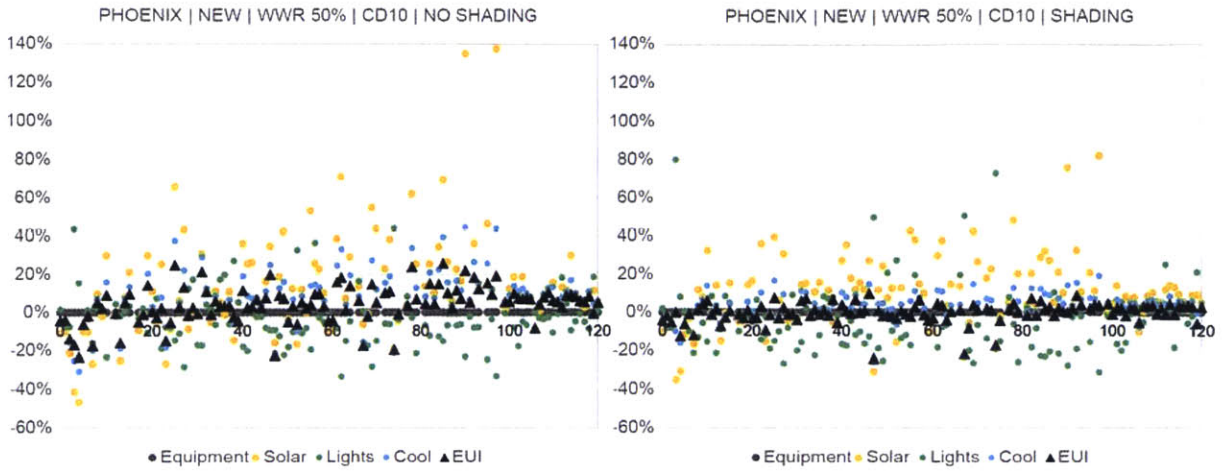

Figures 4-11 A and B: Percentage error per building and end use

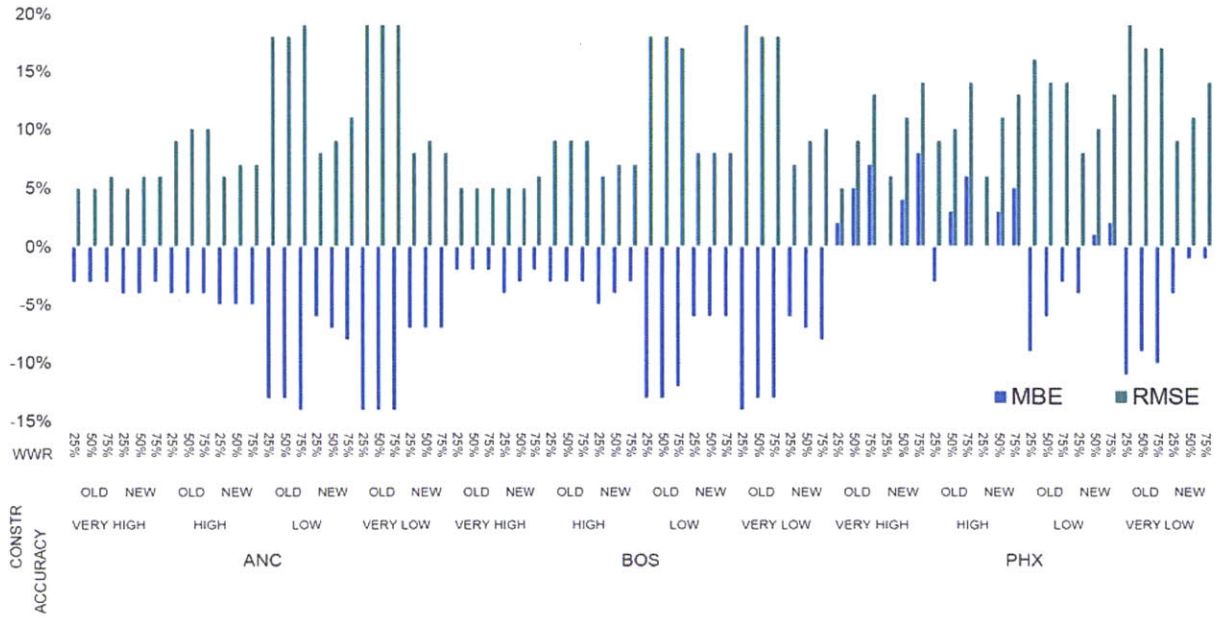

Figure 4-12: RMSE and MBE Overview

Finally, the RMSE (Formula 4-2) of the building EUI data in relationship with the Shoeboxer's clustering accuracy settings is plotted in Figure 4-13. The figure shows a general trend that an increased clustering precision leads to lower RMSEs. The dotted line represents the average of all computed RMSEs and suggests that from the fastest to the most accurate setting an approximate 10% improvement in the RMSE can be expected on average. In the adjacent figure (Figure 4-14) the corresponding Shoeboxer runtimes and the acceleration is

plotted. With the lowest clustering precision, the Shoeboxer can be 296 times faster than the competing whole-building multi-zone model. With added clustering precision the Shoeboxer simulates a much larger sample set and hence the overall acceleration decreases from 296 to 137 to 53 to 20 times. The grey line in Figure 4-14 represents the runtimes in seconds. In the fastest setting, the entire urban model takes 41.25 seconds to compute. The slowest stetting results in a 9.5 minute-long simulation. The simulation time was measured on a 2015 MacBook Pro with an i7 2.8GHz chip, 16GB RAM and SSD hard drive.

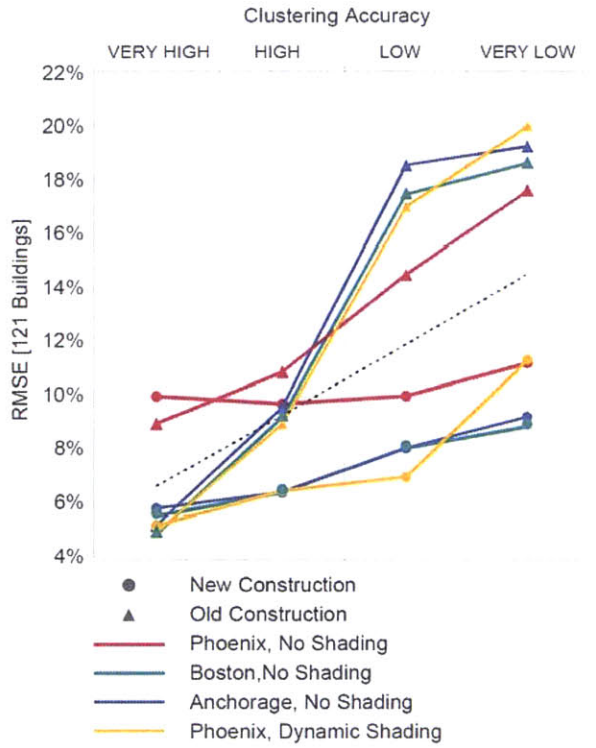

Figure 4-13: Accuracy related to clustering settings.

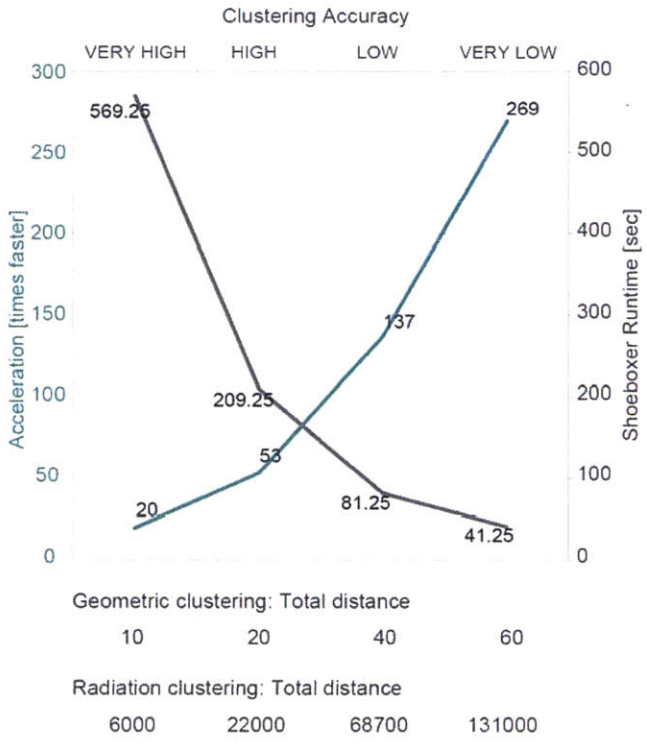

Figure 4-14: Acceleration versus perimeter and core multi-zone model and Shoeboxer runtimes in relation to clustering settings.

4.4 Discussion

4.4.1 Model Comparison

The previous section demonstrated that the Shoeboxer is a fast and reliable method to perform UBEM simulations. Overall, the computed results are comparable with those computed with a perimeter and core multi-zone model in terms of accuracy, spatial and temporal resolution. Given the uncertainties in the design and model inputs that are common in early and urban design processes 5-10% deviation in the results are negligible. While the reference models can provide detailed hourly results per zone and building, the Shoeboxer can provide hourly results per façade cluster, per floor, per unit (architectural program) and per building. For early or urban design processes when floor-plan layouts for the buildings are yet unknown, the Shoeboxer hence presents a more efficient but equally capable method.

However, in certain cases users must be aware that the previously mentioned accuracy strongly depends on the optimal/correct use of the algorithm. Figure 4-13 shows that for scenarios with poor construction standards (high U-Values), a higher clustering accuracy should be selected. This dependency of the clustering accuracy and the energy-load prediction accuracy is intuitive: A lower clustering accuracy leads to less accurate geometric ratios for each building. Due to the higher heat losses and gains caused by higher U-Values, the accuracy of these ratios begins to have a significant impact on the overall results. In cases where the buildings are well insulated (low U-Values), errors in the geometric ratios tend to have a much smaller impact on the overall results.

4.4.2 Usability and responsiveness

The Shoeboxer provides a fully automated and drastically accelerated simulation workflow and hence pushes large-scale urban simulations into a feasible realm. The significantly faster simulation times with speed increases of up to 296 times allow building energy modelers to work on UBEM simulations more effectively and within feasible time and cost constraints. With runtimes for an entire neighborhood model of less than a minute on a standard laptop computer, costly computing power such as server- or Cloud-based simulation clusters are no longer an absolute requirement. Hence, it is the author's hope that the previously mentioned benefits lead to a much broader user group and an increased

applicability of UBEM simulations in education, urban design processes, policy making and infrastructure planning.

4.4.3 Limitations

Solar gains: The results section revealed that in the Phoenix climate the Shoeboxer method can yield percentage errors in solar gain estimation of up to 140% and up to 60% for dynamically shaded windows. In such a climate the difference in solar gains is closely related to under- or overestimation of cooling loads. In extreme cases this can lead to an error in load estimation for certain buildings that are up to 36% different than the reference model prediction. A closer examination of these extreme outliers is hence necessary and presented in the following paragraph.

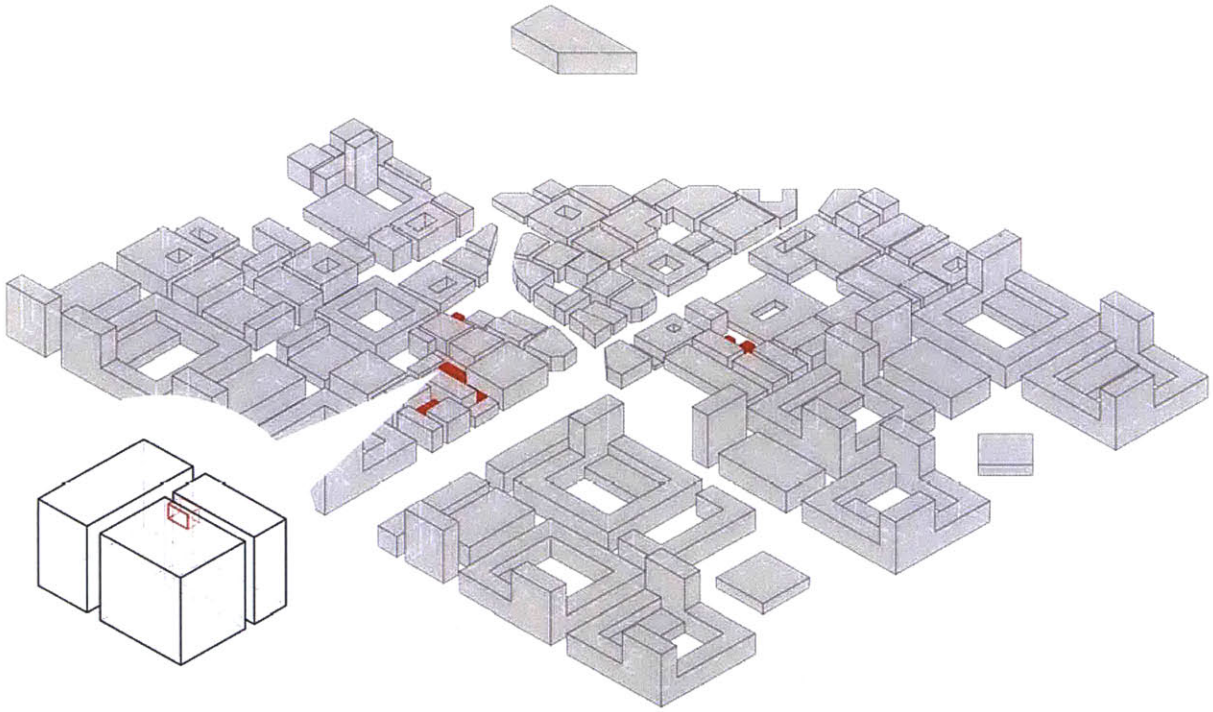

Figure 4-15: Massing model with extreme outliers marked in red and one example magnified.

Figure 4-15 shows the most drastic outliers for estimated solar gains within the whole urban massing model marked in red. Such situations are hard to approximate with a discrete sampling method. The Shoeboxer picks one specific shading situation for each façade cluster based on annual cumulative radiation and hence is not sensitive to fine details and quickly

changing shadows on the receiving surfaces. In addition, the clustering and hence also the selection of the shoebox samples is based on radiation that is evaluated at a point. In contrast to that, the actual shoebox façade that receives incident radiation is a rectangle of significant area (6m x 4m in the simulated cases). These "granularities" can lead to shoebox sample points that capture more or less of the contextual shading projected onto the shoebox façade than the anticipated "averaged" shading for one façade cluster. This is the case for buildings marked in red in Figure 4-15. A close up of one of the situations is given in the magnified area in Figure 4-15. It shows Building #85, its context and one shoebox sample. The shoebox extends about 1.5m outwards and due to the gap in the shading context the sample façade is more exposed to solar radiation than the actual building façade. The resulting differences in solar gains are plotted in hourly resolution for three representative days in Figure 4-16. One should note that these errors occur where they matter the least within the entire urban model. The outlier buildings are among the smallest buildings in the model and are located amid a dense urban context that almost entirely shades the facades.

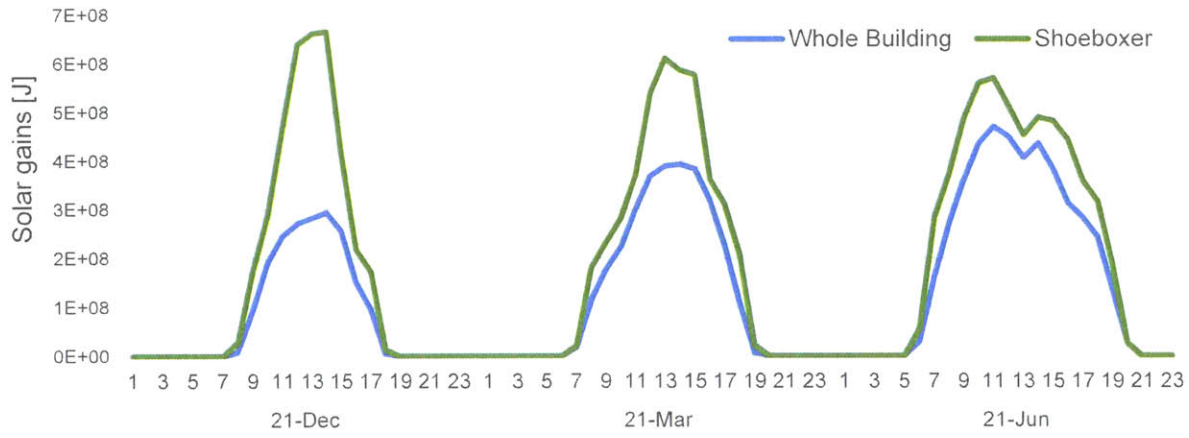

Figure 4-16: Solar gains predicted by the Shoeboxer and the reference model for three representative days of the highlighted building in Figure 4-15

Natural ventilation: Natural ventilation can be modeled as buoyancy-driven flow with the stack equation or as wind driven (cross ventilation) under the assumption of the existence of an ideal exhaust. More complex models such as airflow networks are not supported. Support for such modeling techniques could theoretically be added in future versions of the Shoeboxer by

adding a second perimeter zone on an opposite façade in order to establish an airflow path. However, it is the author's belief that the benefits of airflow network based modeling technique can only be used effectively if the interior space subdivisions are known.

Multi-story interiors: A further limitation of the Shoeboxer is the inability to simulate multi-story interiors such as atria or duplex housing layouts. Future versions of the Shoeboxer could include multiple typical room archetypes that include duplex typologies or specific atria models. Yet again, it is the author's belief that these architectural thoughts on a building and its interior mode of operation are highly specific and suggests that the modeler should neither use the Shoeboxer nor ASHRAE 90.1 subdivision schema for his or her analysis and should instead model the interior subdivisions of the building explicitly.

In the case of an urban modeling task, the need to model some select buildings more explicitly might arise. In such a case, these buildings should be modeled with thermal zones that are derived from their floor plans. The zones can then be fed into the same workflow as presented for the reference buildings. The fact that both the Shoeboxer and explicit workflow live in the same Grasshopper environment also makes it easy to manage and combine both Shoeboxer and explicit results without much effort.

4.4.4 Application Examples

The following section presents three examples of how the presented algorithm could be used. The examples include urban retrofitting, infrastructure planning and an application for urban design.

Impact of urban retrofitting scenarios

For a new design proposal, scenario exploration can be used to provide planners and architects with recommendations for effective energy efficiency measures. In the case of an existing city, the Shoeboxer can be used to identify the "energy hogs" within a community and possible remedies can be tested. This knowledge can then be used for targeted retrofit policies and incentives. Figure 4-17 shows a Shoeboxer simulation-based annual energy cost projection for residential buildings in South Boston. Geographic information system (GIS) data such as building footprint geometry, building height, year of construction, type of construction and building use have been used to generate energy models for all residential buildings in the

neighborhood. Assumptions regarding the construction standard have been calibrated with Residential Energy Consumption Survey (RECS) data provided by the U.S. Energy Information Administration [2009]. The results are mapped in the figure below and reveal several pink and yellow homes as clear underperformers that could be targeted by retrofitting and urban renewal policies.

Figure 4-17: Energy simulation based energy cost predictions and potential urban "energy hogs" in magenta.

Planning aid for district heating and cooling systems

The urban scale is becoming increasingly interesting for energy modelers since the larger scale harbors new untapped potentials. Different agents within a city often have significantly different energy demands that occur at different times of the day and year. Hence, urban energy models can be used to further examine these demands in order to find synergies that can be utilized beneficially. In the following section, an exemplary analysis of simultaneous heating and cooling loads is provided. Figure 4-18 shows the annual heating and cooling hotspots of the previously used massing model. As expected the figure shows that commercial and service buildings are mostly heating load dominated due to their shaded location in the first

floors and lower internal loads. Alongside the office programs, the residential towers tend to be cooling load dominated due to a high insulation standard and more exposed locations. This knowledge could be used to optimize constructions, opening ratios and even program distribution. In this study however, the focus is on identifying synergies between the different agents in the proposal. Hence, the daily energy demand is plotted in Figure 4-19 in order to identify concurrences of both heating and cooling. The different urban agents could balance their contrasting needs in the transitional periods. Under the assumption of an ideal heat exchanger and monthly storage capacity, approximately 13% savings could be achieved (Figure 4-19).

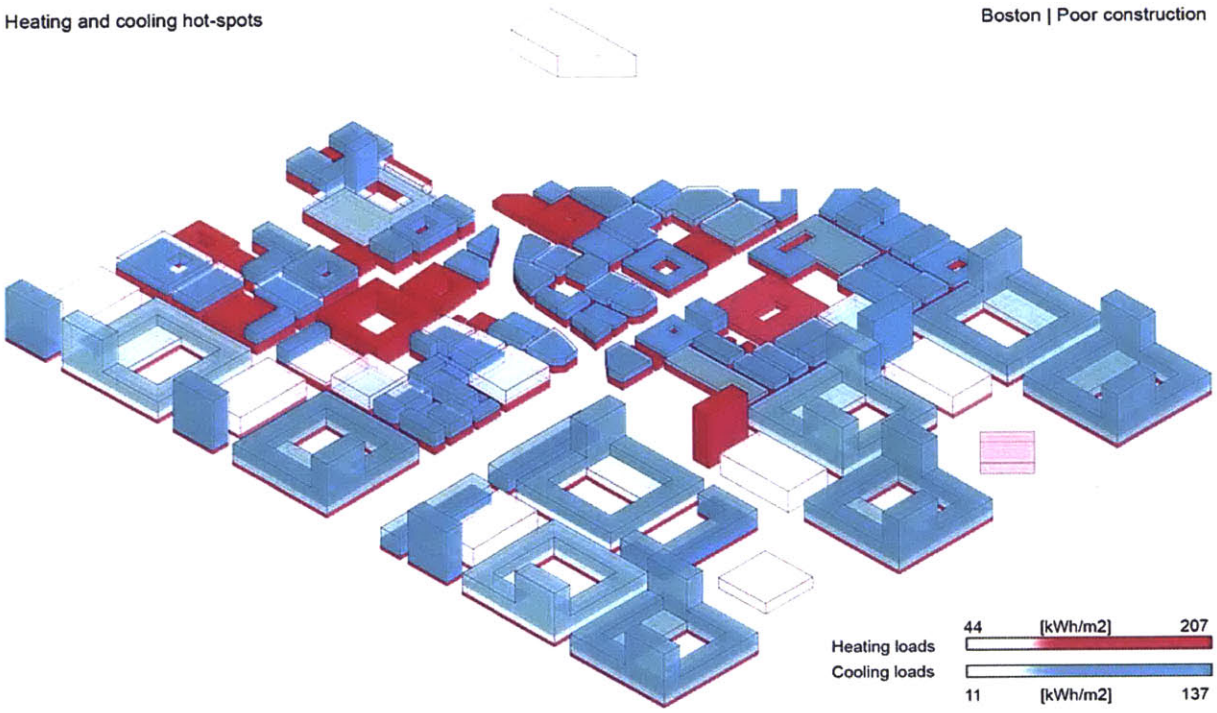

Figure 4-18: Annual heating and cooling hotspots within the urban design.

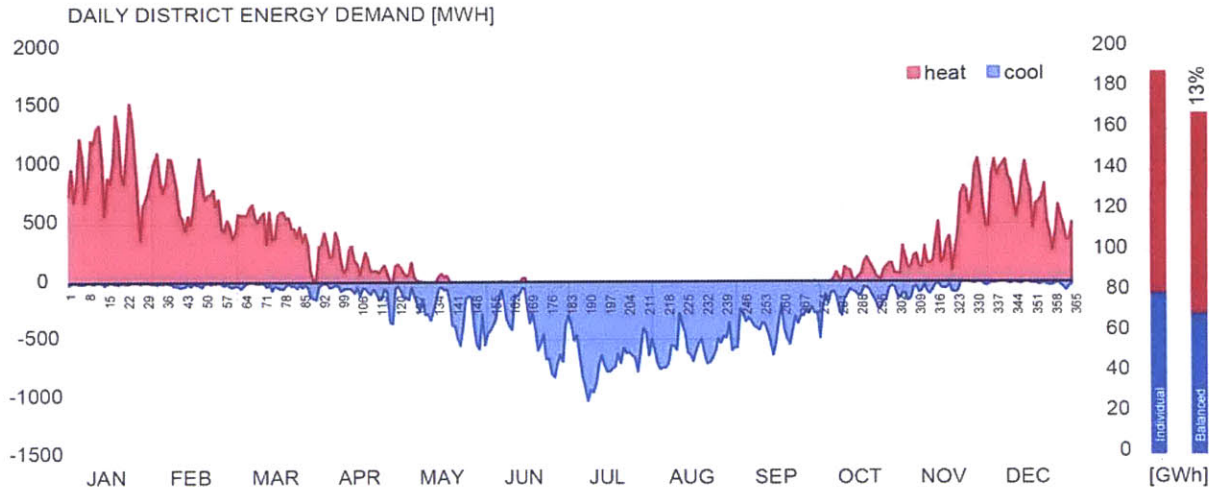

Figure 4-19: Daily district energy demand [MWh] and savings potential due to ideal monthly load balancing.

Design tool

Another field of application for the Shoeboxer are design processes. Simulation times under one minute for an urban design proposal and almost instantaneous feedback for single buildings and smaller building groups provides the chance to smoothly integrate energy simulation feedback into iterative design processes. In combination with optimization algorithms such as those provided in Grasshopper or GenOpt [Wetter, 2011] the Shoeboxer method could serve as a powerful early design or form giver.

The first example is an urban density study. The massing model (Figure 4-4) is manipulated with a scaling function in Z-direction in order to create four different models shown in Figure 4-20. The density is measured as Floor Area Ratio (FAR).

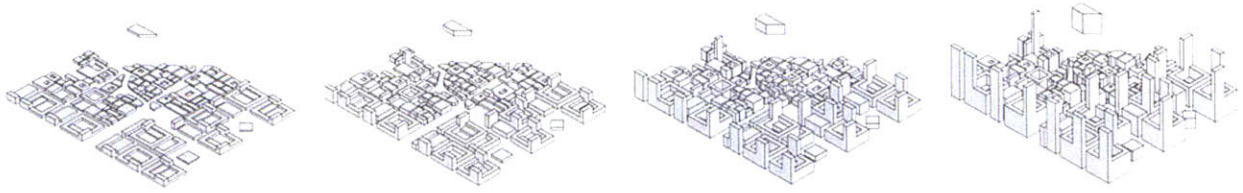

FAR 1 *FAR 2* *FAR 5* *FAR 10*

Figure 4-20: Parametric urban density manipulation

For all four models, the Shoeboxer was used to study the changing densities' effect on energy consumption. Figure 4-22 shows the daily energy demand of the four variants. The higher the density and available floor area, the higher the load. Figure 4-21 shows normalized heating cooling and lighting energy use for the four variants. The higher the density, the more energy is required for electric lighting due to a decrease in daylight availability. Vice versa, the cooling load is reduced due to more self-shading. While the heating load does in general increase with higher densities, it does not behave entirely in a linear fashion. A jump can be observed for FAR 2 where the heating load drops due to a more compact form factor.

An interesting observation is that even with drastically increased FARs the overall normalized energy demand stays roughly constant [Figure 4-21]. While the changes in the end-use energy breakdown such as the increased lighting loads may be used as design hints to improve daylight availability, it remains difficult to clearly identify the most "sustainable" design. However, strategies such as net-zero carbon and 100% onsite renewable energy production as required by the "Active House" standard (Chapter 2), can constitute a limiting factor for higher densities. In this study, it was assumed that all roofs can potentially be used for photovoltaic systems. However, since the gross roof area stays constant throughout the design and contextual overshadowing increases with the higher densities, the renewable energy potential drops significantly [Figure 4-21] and one can imagine that "Active House" design goals are significantly more difficult to reach for the designs with densities 5 and 10.

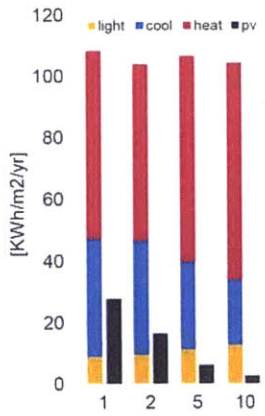

Figure 4-21: Normalized cooling, heating and lighting energy use

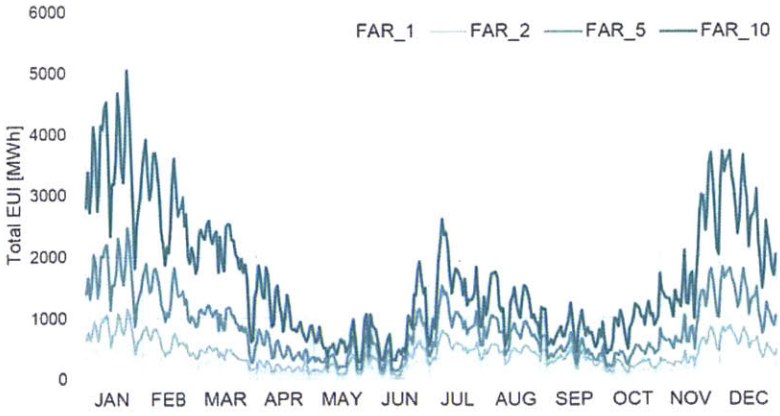

Figure 4-22: Daily total energy use

The Shoeboxer can also be used to provide design feedback at smaller scales. The second example shows a window to wall ratio optimization for the Boston climate for one building. The two competing performance criteria, space conditioning loads (heating/cooling) versus daylight performance in form of electric lighting loads, are chosen. The Shoeboxer is used to cluster the building façade into eight regions of different microclimatic conditions due to orientation and contextual shading. Then an array of different window to wall ratios was simulated for each facade cluster and the best performing opening ratio was chosen and plotted onto the façade of the building as shown in Figure 4-23. The workflow provides feedback that is somewhat expected. The suggested opening ratio is small in areas with a high solar exposure and gradually opens up in more shaded areas. It however also provides unexpected design cues. In heavily shaded regions, the method suggests to close the façade. Here, the daylighting benefits have obviously been overpowered by heat losses due to a larger glass surface.

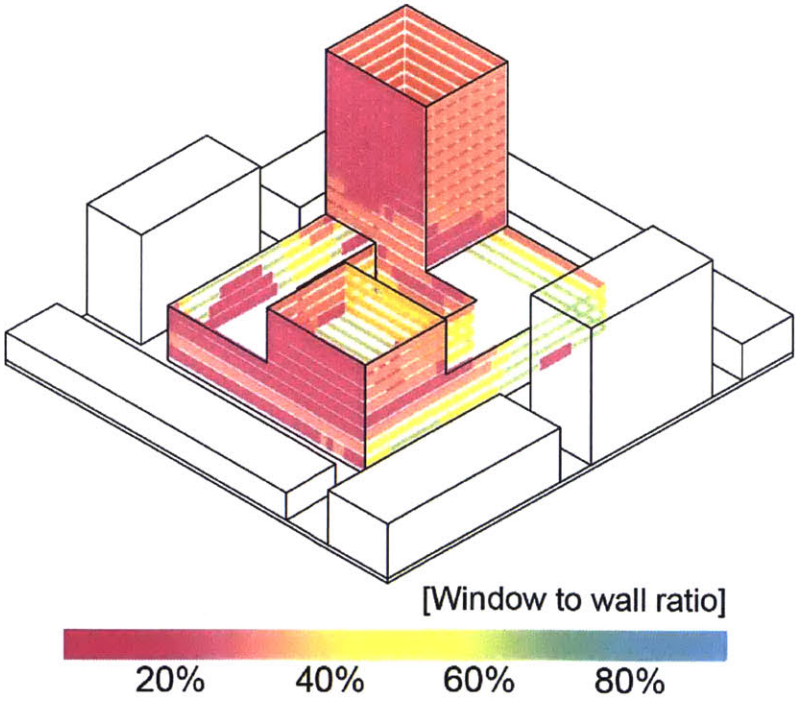

Figure 4-23: Window to wall ratio suggestion based on several Shoeboxer simulations

4.5 Conclusion

A fast and reliable method to perform urban energy simulations at a great spatial and temporal resolution is introduced. The method yields results that are comparable with multi-zone whole building energy models according to ASHRAE 90.1 Appendix G thermal zoning requirements. The method provides a fully automated and drastically accelerated simulation workflow and hence pushes large-scale urban simulations into a feasible realm. The significantly faster simulation times with speed increases of up to 296 times allow building energy modelers to work on UBEM simulations more effectively and within feasible time and cost constraints. Hence, it is hoped that the previously mentioned benefits lead to a much broader user group and an increased applicability of UBEM simulations in education, urban design processes, policy making and infrastructure planning.

5 Typology-Aware Thermal Zoning

In this chapter the ASHRAE 90.1 Appendix G prescribed perimeter and core zoning paradigm, which is fundamental to current BEM modeling approaches including those in Chapters 3 and 4, is validated and critically reviewed from an architectural perspective. The zoning paradigm's accuracy and usefulness in early design are discussed. After a careful comparison with real floor plans, an enhanced design workflow that incorporates key typological characteristics such as the horizontal and vertical circulation layout is presented. A sample set of 1200 simulations reveals an overall RMSE of 15% for total EUI but also inconsistencies such as outliers with RMSEs from -28% to 58%. These results suggests that the ASHRAE zoning scheme may be sufficiently accurate for large-scale applications where occasional errors have only limited influence on the overall results but has only limited applicability for design processes where such inconsistencies can be misleading.

5.1 Introduction

Early design energy modeling as well as the UBEM approaches introduced in Chapter 3 and 4 rely on the prescribed ASHRAE 90.1 Appendix G perimeter and core zoning schema. However, this scheme hardly ever resembles actual interior space subdivisions and thus provokes the question of how accurate and how useful the perimeter and core zoning might actually be for designers. The goal of this chapter is to provide an overview of the implications of the perimeter core zoning on energy simulation results. In the following sections a comparative analysis of 25 carefully selected real floor plans and their perimeter and core counterparts is provided. In the discussion, limits of the ASHRAE zoning methodology are identified and a vision for an alternative early design modeling approach is provided.

5.2 Methodology

The methodology section is divided into two main sections. Firstly, a process of typological sorting for floor plans based on their exterior morphology and interior organization is presented. This process leads to the creation of a comprehensive floor plan typology matrix with samples from contemporary architectural design literature. Secondly, these samples are translated into energy models based on two zoning paradigms:

A. Zoning that strictly follows the form of the architectural plans.
B. The ASHRAE 90.1 Appendix G - prescribed core and perimeter subdivision scheme.

The simulation results of both zoning paradigms are compared.

5.2.1 Typological Sorting

The initial challenge of this study is to develop a representative set of building samples that reflect the typological richness of floor plan designs found in contemporary architectural design. This is a non-trivial task, since the choice of samples to be analyzed is, to an extent, ambiguous and is expected to have a significant impact on the simulation results. In order to respond to this challenge, a two-level process of typological sorting for building floor plans is introduced:

1. Exterior morphology
2. Interior organization

With this categorization scheme, different typological sorting methodologies found in contemporary architectural design theory literature [Neufert 2012, Jocher 2010, Schneider 2011, Ebner 2010] are combined and consolidated. The previously mentioned sources are also used for the selection of the built examples.

5.2.1.1 Level 1: Exterior Morphology

The first level of sorting is the exterior morphology of a building design. The general shape and proportions of a building, reflecting functional characteristics, contextual conditions and environmental considerations can vary significantly. The reoccurrence of certain patterns, however, allows one to sort designs into discrete typological categories. Five different categories called Point, Block/Courtyard, Bar, Poly-line and Freeform are distilled and described in more detail in Table 5-1.

5.2.1.2 Level 2: Interior Organization

The previously described morphologic categories only describe the exterior appearance of a building and hence only indirectly speak to the floor-plan layout of a building. The interior subdivision is mostly driven by the way one enters a building and accesses the individual rooms within it. Consequently, commonly used circulation schemes are characterized and five popular interior organization typologies called Vertical Point, Corridor Center, Corridor Edge, Compartments and Open Plan are identified in Table 5-2.

Table 5-1: Shape typologies

Point: Compact shape for both housing and office use often organized with a core in the center or on the side. This shape typology can be appointed in several scales, ranging from single-family houses to office towers.

Block: Economic and space-efficient layout unifying different spatial qualities: protected, quiet inner courtyards and outward-oriented spaces. This duality allows for multiple spatial distribution options based on different programmatic requirements.

Line: Shape that is made up of a series of rooms organized along a longitudinal corridor or multiple corridors. Well daylit for a single loaded corridor but less economical. Double or triple loaded corridors less likely to be naturally lit.

Poly-line: Similar to the line typology with a mostly linear organization along a longitudinal corridor with varying angles and segment lengths.

Freeform: Shape reacting to contextual conditions or a freestanding solitaire. Facilitates design of non-conventional circulation space. Completion of the interior requires specific non-standard solutions.

Table 5-2: Organization typologies

Vertical Point: Circulation core placed in the center or periphery of the building. The core can house only circulation space or can be designed more generously to incorporate common/shared spaces (e.g., living room/common space as circulation center).

Corridor Center: Linear organization of spaces and services along a central circulation axis that can often be long and narrow. Daylighting can be a challenge for circulation spaces, due to their limited exposure to the facade.

Corridor Edge: Linear organization of spaces and services along a peripheral circulation axis that can either be on the interior or the exterior of a building.

Compartments: Complex 3-dimensional arrangements that might not repeat on every floor. This organization typology can't be represented by lines, but by polygonal shapes generated by the placement of spaces. It is often combined with complex interior voids that span over multiple stories, such as atria or gardens.

Open Plan: Organization typology without space dividers. Separation is subtle and the circulation areas are not designated, allowing for flexible programming and giving the impression of a generous space. Placed elements often encapsulate service spaces such as kitchens and restrooms.

5.2.1.3 Typological Matrix

Both exterior morphology and interior organization describe high-level patterns that frequently reoccur in architectural designs regardless of the building function. Additionally, each exterior morphology type can in theory be freely combined with any interior organization type and create an overwhelming amount of variants. In order to keep the scope of this analysis manageable one built example for each possible combination of the categories was selected. The selected examples are shown in Figure 5-1.

5.2.1.4 Function/Scale

During the search for built examples, the scope was limited to residential and office buildings, since these are the most common functions appointed in an urban setting. This is hence sufficient to showcase the potential of the presented approach. Commercial and special use-cases such as schools, hospitals, and other institutional buildings are not analyzed but could be included in future work following a similar methodology. The function often also greatly influences the scale of a building. A point typology, for example, can range from a single-family home to a large office tower. The selected examples reflect this variety ranging from a 90m^2 single family home to a 3800m^2 office complex.

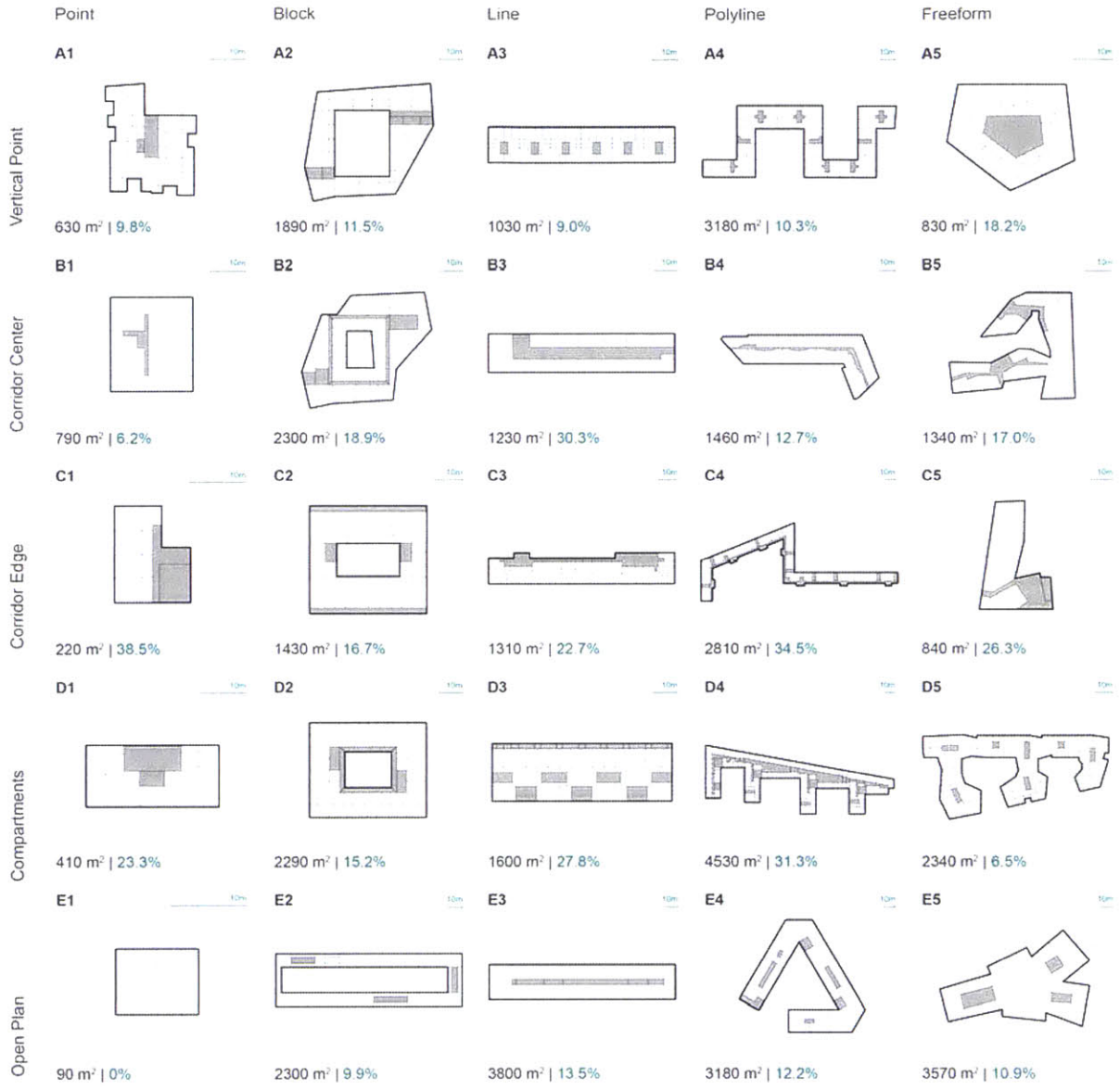

Figure 5-1: Typological matrix of selected floor plans

5.2.2 Modeling and comparison methodology

This section presents how the thermal models are built, configured and compared. Firstly, the thermal zoning scheme for each subdivision paradigm is explained. This is followed by a description of the workflow to convert the zones into 3D multi-zone thermal model geometry. After the geometric setup, this section also describes how the zone geometry is combined with

zone-specific properties such as materiality, loads and conditioning configurations. Lastly, the methodology to compare and analyze the simulation results is detailed.

5.2.2.1 Zone geometry

The first zoning paradigm strictly follows the subdivisions prescribed by the architectural plans. The plan views of the zone subdivisions look identical to the plans given in Figure 5-1. However, it is important to mention that for the 3D thermal model conversion workflow presented in the next section, each zone has to be represented by a closed-polygon outline.

The second zoning paradigm follows the ASHRAE 90.1 Appendix G recommendations. The brief guideline states that a floor should be divided into a "core" and a "perimeter" region. The perimeter is defined as the space within a 5m distance from the facade. Further, perimeter spaces with more than one orientation should be subdivided proportionally. The leftover region in the center of the floor forms the core [ANSI/ASHRAE/IESNA, 2013]. In order to produce the core and perimeter geometry for all floor plans, the Autozoner was used [Chapter 3]. The subdivision of the selected floor plans is shown in Figure 5-2.

To construct the 3D thermal zone geometry, the polygons that describe each zone are extruded by a floor height of 3m. The extrusion of the spaces yields the zone geometry for one floor. In order to emulate a roof, ground and middle floor, the zones are then stacked three times. A critical reader might object and note that not every building included in the floor plan matrix in Figure 5-1 is a three-story building. In this study, however, the main focus is on analyzing the effect of different interior subdivision schemata on energy consumption. Hence, it is not the intention to replicate the exact energy consumption and model representation of the selected buildings.

The window geometry is also automatically generated. The geometric inputs are used as follows: The floor-plan outline is shattered into small segments at each intersection with a zone wall. Then each segment is scaled and extruded to match a 50% window-wall ratio. Each window is positioned above a 1m high balustrade resulting in a window band at each floor that uniformly wraps around the building.

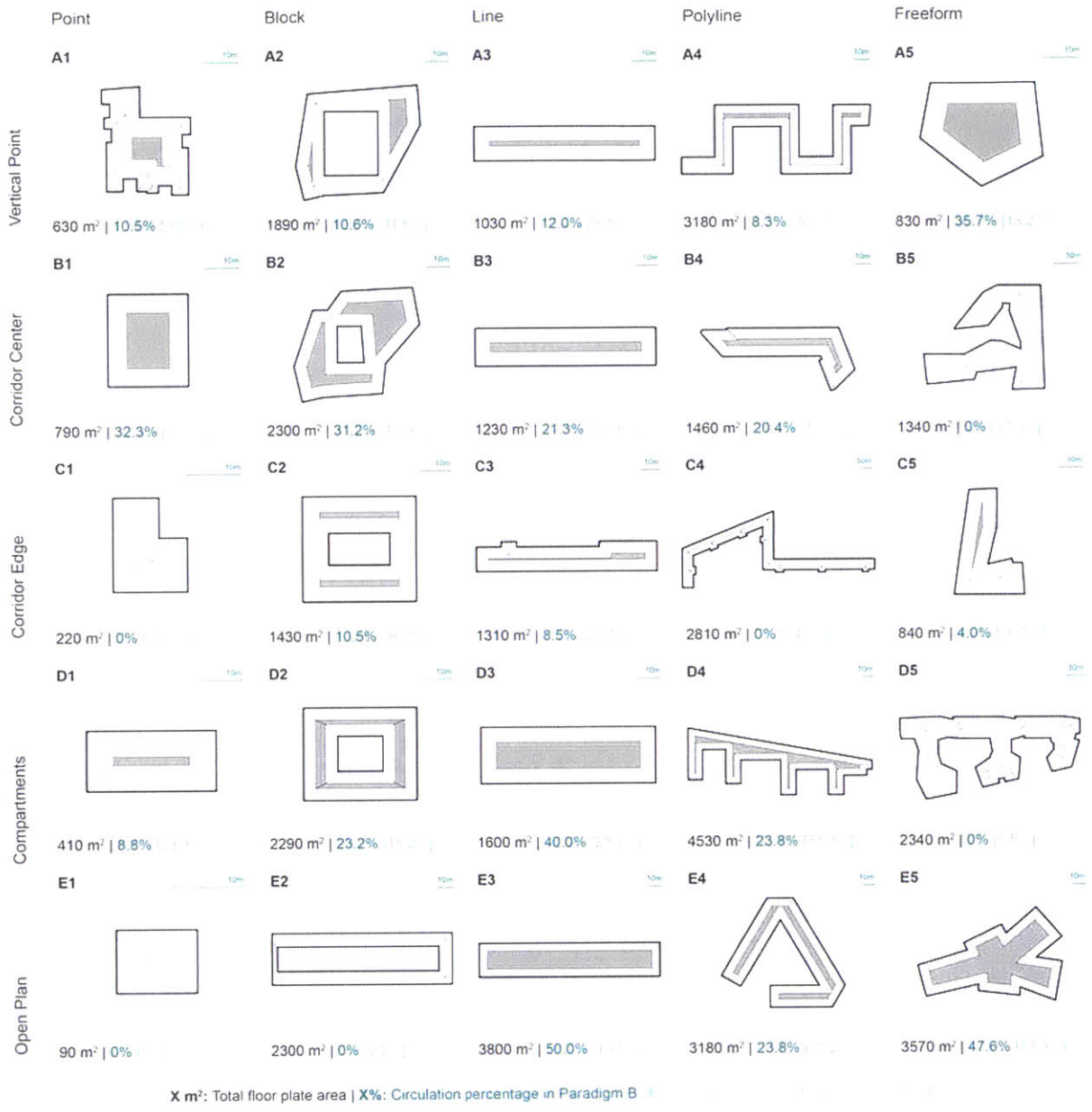

Figure 5-2: Typological matrix with ASHRAE-prescribed zoning

5.2.2.2 Zone configuration:

The zone configuration includes all non-geometric information on a thermal space such as constructions, space loads, occupancy and the configuration of the conditioning systems.

The construction standard is expected to influence the thermal behavior of each zone significantly. Hence, a well-insulated and a poorly insulated scenario are tested. Infiltration rates are altered correspondingly. Separate construction types for the façade, roof, interior partition, exterior ground and interior slab were used and applied uniformly across all zones in the building.

Despite the zone geometry and its materiality, the use-case of each zone must be specified in order to define internal gains, occupancy and control profiles as well as equipment loads. For simplicity, the study is limited to circulation, residential and office space types. Each space type definition loosely followed the Swiss architectural norm SIA Merkblatt 2024 [S. I. A., 2006] that defines the most common spaces and their internal gains, equipment loads, set-point temperatures and occupancy profiles. Each space is conditioned with an ideal-unlimited heating and cooling system with a coefficient of performance of 1, in order to obtain "pure" loads as they occur in space. It is assumed that the spaces are fully conditioned all-year round. The only exception is the circulation space, which is tested in a conditioned and unconditioned configuration.

In order to consistently describe the thermal behavior for each model, this analysis was limited to the energy use intensity [EUI] and its components: heating, cooling, lighting and equipment loads. The loads are given in KWh and are normalized by floor area.

5.2.2.3 Merging the data and running the simulations:

The final task before the simulations are initialized is to combine the previously described parameters with the zone geometry. The geometric and non-geometric input data is hence organized in matching data-tree structures and then streamed to Archsim, a building energy modeling plugin for Grasshopper that utilizes EnergyPlus or TRNSYS. The use of Grasshopper and Archsim lets one completely automate the EnergyPlus input file production and batch execution of the simulations. For the five-by-five matrix with two subdivision schemes, two different use-cases, two different conditioning modes of circulation space and two different construction standards the automated procedure generates 400 energy models. Since each subdivision and space configuration scheme is expected to behave differently in different climates, the process is repeated three times with a cooling-dominated (Phoenix weather), heating-dominated (Anchorage weather) and a mixed climate (Boston weather) resulting in a

total of 1200 Energy Plus simulations. For each of the simulated scenarios, the behavior of the two subdivision paradigms is compared. An overview of the workflow and its information flow is given in Figure 5-3.

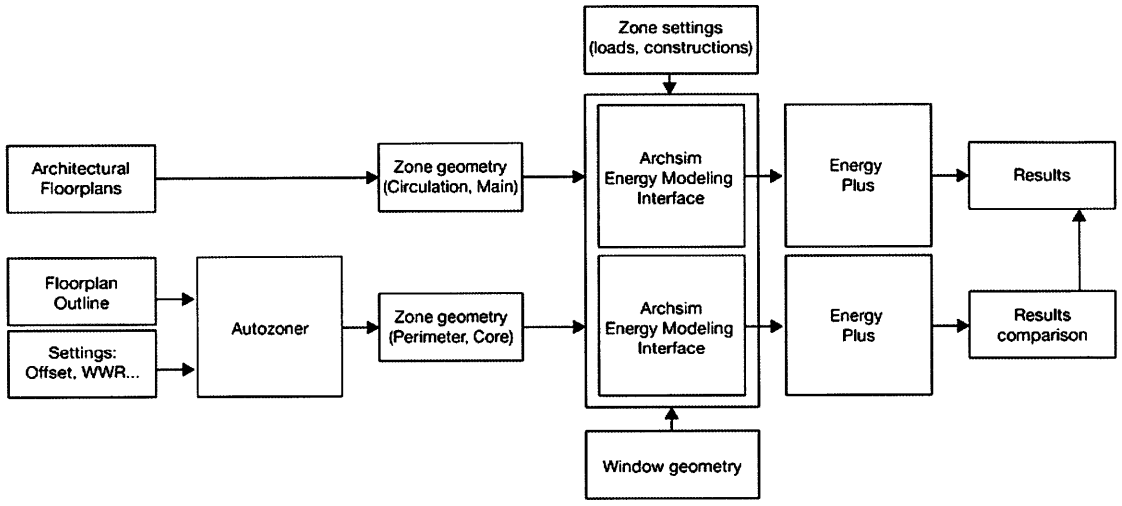

Figure 5-3: Workflow diagram

5.3 Results

The previously described simulations yield 1200 energy load data sets consisting of 600 pairs that describe one building in ASHRAE 90.1 subdivision and the building's original floor plan. In a post-processing step, the percentage error $E=((x_{AHSHRAE} - x_{REAL}) / x_{REAL})$ of the total EUI was computed. The percentage errors for lighting, electric, heating and cooling loads are also given. The computed errors are plotted in a distribution chart with 10% bins ranging from positive to negative 100%. The error distribution for the total EUI is given in Figure 5-4. The distribution chart shows that 75% of the simulated EUI predicted by the ASHRAE zoned models lies within a +-15% margin. The distribution of the error of the EUI components is given in the Figures 5-9. Here the spread in the distribution chart is significantly wider. For predicted electric lighting only 33% are within the bounds of +- 15%. For electric equipment, heating and cooling only 50%, 67% and 58% respectively lie within the margin. Further, the RMSE of the total EUI and its components is computed for all scenarios and each floor plan in order to see the relationship between error and the actual geometry. The result is given in Figure 5-5. It is interesting to note that floor plans such as B3, D4 and D5 report significantly smaller errors

than others. This is mostly due to the geometric similarity of the architectural plan and the ASHRAE subdivision in these specific cases where both variants have similar size core regions. One should also note that similarities in topology do not guarantee consistent results between the two subdivision paradigms. A good example that showcases this effect is case E3. Here the core and perimeter regions are almost identical topologically but differ significantly in proportion and can cause heating and cooling predictions that differ 124% and 265% on average throughout all scenarios. Floor plans with circulation at the edges [Typologies C1-C5] instead of a central corridor have a tendency to produce significant deviation between the two zoning paradigms. Here the circulation spaces serve as a thermal buffer zone and hence lower the predicted energy use. This effect is especially pronounced when the circulation spaces are unconditioned.

Table 5-3 summarizes all computed errors and plots overall RMSE for total EUI, lighting, electric, cooling and heating loads. It also shows the mean bias error MBE and the minimum and maximum errors that were encountered in the data set. The overall RMSE and MBE are at 15% and 2%. However, the data also shows that the overall error is significantly lowered by balancing errors in the EUI components. The overall RMSE and MBE are significantly higher for heating cooling and lighting. The minimum and maximum show that there are extreme outliers in the data set.

Table 5-3: Summary of results

	Total	**Equip**	**Light**	**Heat**	**Cool**
RMSE	15%	24%	37%	175%	105%
MBE	2%	3%	-15%	32%	22%
MIN	-29%	-43%	-84%	-100%	-50%
MAX	58%	61%	118%	2700%	1250%

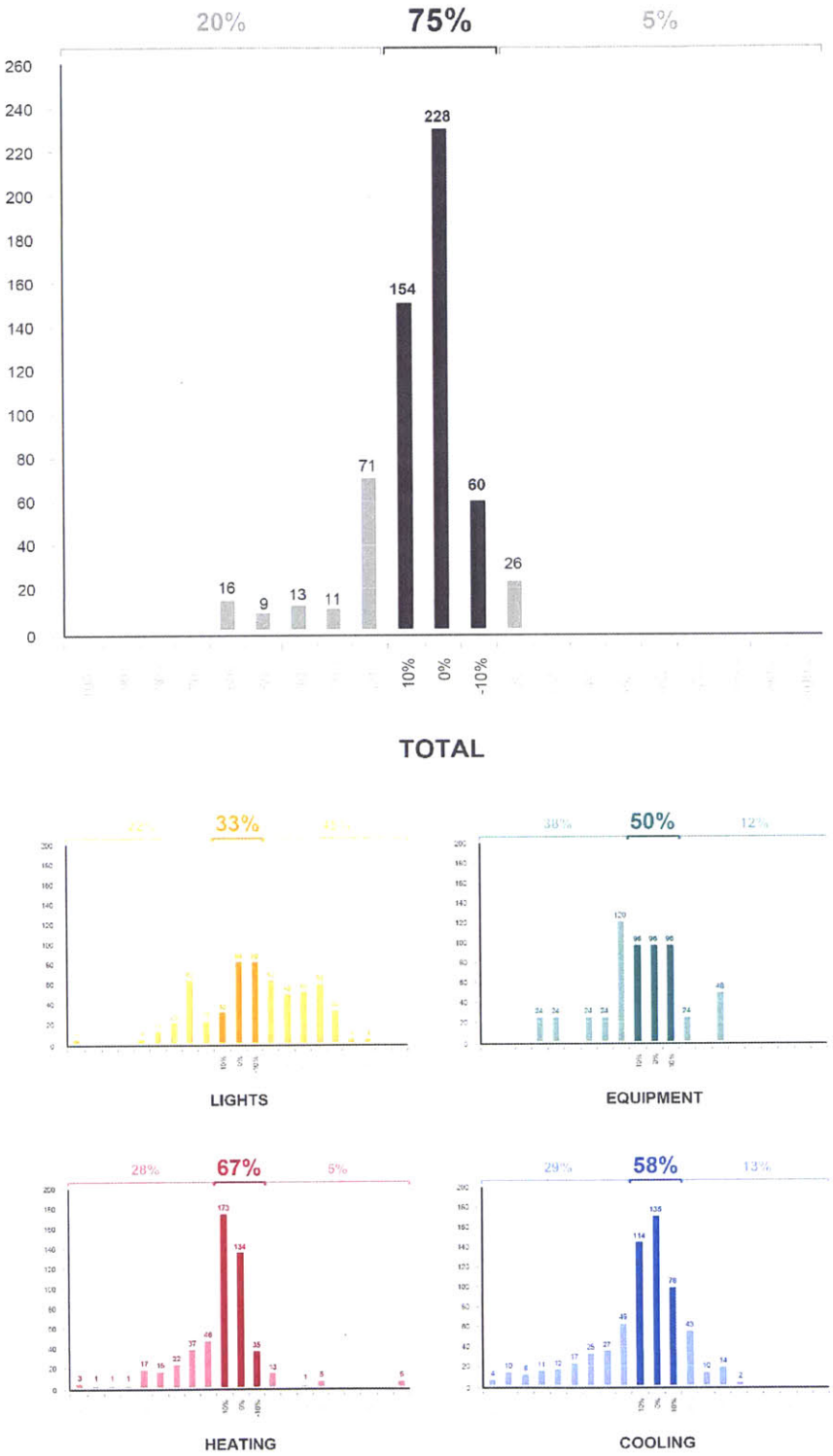

Figure 5-4: Error histograms for EUI, Lighting, Equipment, Heating and Cooling

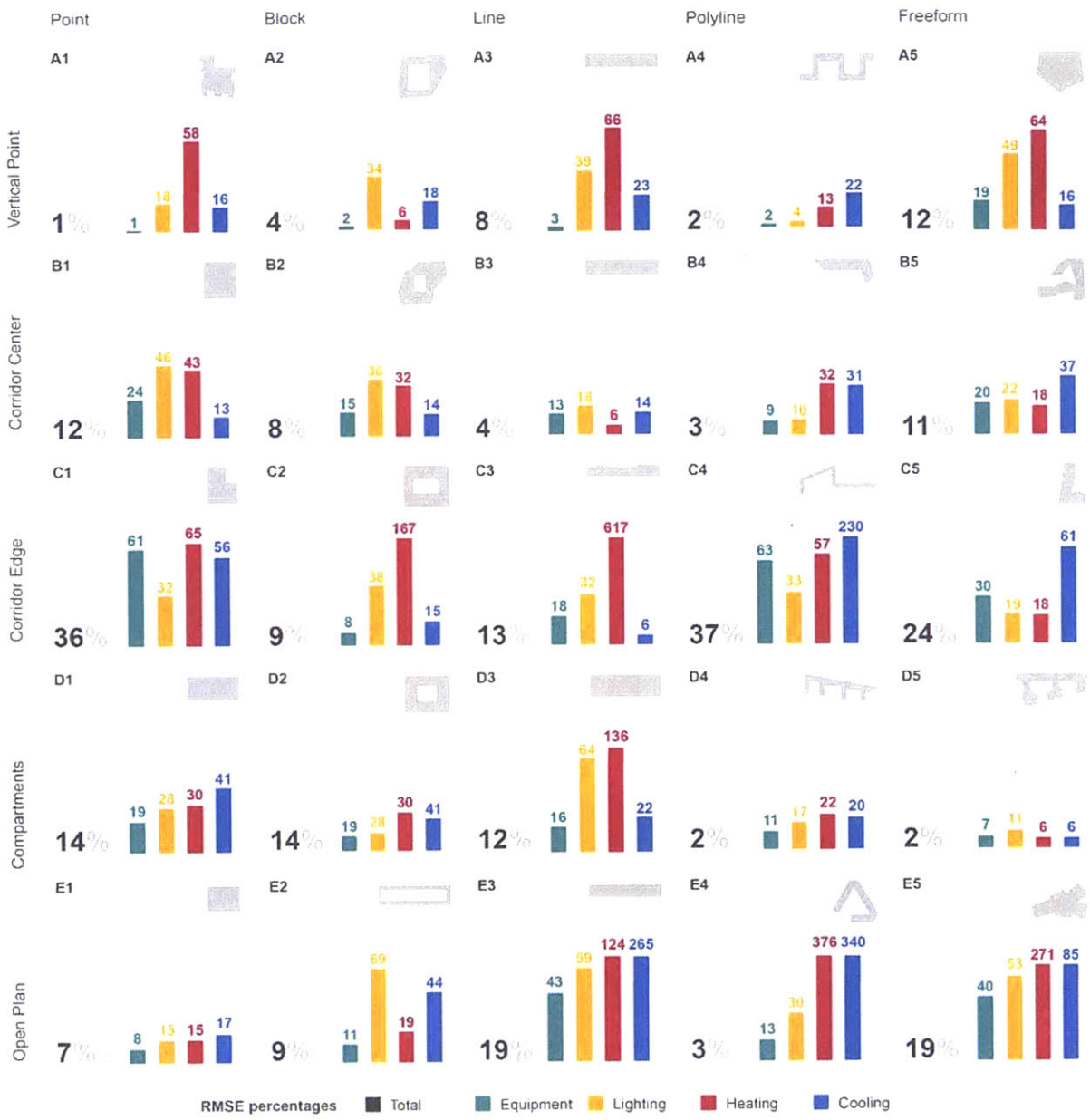

Figure 5-5 RMSE for EUI and sub-metrics plotted on the floor plan matrix.

5.4 Discussion

With an overall RMSE of 15% and with 75% of the 1200 simulated cases within an error margin of +-15%, the perimeter and core zoning paradigm provides a reasonably reliable and consistent energy analysis workflow for buildings with unknown interiors. For urban energy

analyses of existing cities this finding is of significant importance. While floor plan data sets of entire cities are not readily available due to privacy and data management issues, cites do maintain and share detailed GIS data sets that, among other data, contain polygonal representations of building footprints and building height information. In combination with the algorithms presented in Chapter 3 and 4, this data can be used to auto-generate BEM models for hundreds and thousands of buildings. In such a use case the observed outliers with RMSEs from -28% to 58% will have only a limited effect on overall energy demand forecasts and are acceptable errors given the uncertainties that remain in the non-geometric simulation inputs such as infiltration rates, accurate window-to-wall ratios and occupant behavior.

However, for design processes such outliers are significant and suggest that the ASHRAE zoning paradigm has only limited applicability for early design evaluations at the building level. Figure *5-5* reveals that thermally relevant features of a floor plan layout are only sufficiently captured for very specific building types and proportions that are similar to a perimeter and core layout such as Figure *5-5* A1, B3, B4, D4 and E4. The assumptions proposed by perimeter and core paradigm reduce the complexity of architectural design, but also reduce the potential of design to have a positive impact on energy efficiency. How misleading such assumptions can be in a design process is shown in the following example.

Figure 5-6 shows two floor plans of an office building of identical area sizes but with different spatial arrangement of unconditioned circulation area. Both floor plans are compared in an orientation study for the Phoenix climate as is commonly done in early design. The perimeter and core plan (ASHRAE) is symmetric around the north-south and east-west axis and hence yields a sine-wave-like energy demand fluctuation throughout the various orientations. The fluctuation is solely due to a change in area with southern exposure. The plan labeled "ARCH" shows similar behavior from 0 to 45 and 315 to 360 degrees due to symmetry around the north-south axis. Then a significant drop in energy demand can be observed as the circulation area is rotated towards the south. This experiment shows that the ASHRAE prescribed zoning methodology shifts the focus of a simulation towards the envelope and its properties but it fails to capture significant energy saving opportunities based on improved space layouts. As long as modelers are aware of this behavior, the ASHRAE zoning might be a good first approach to test the climate-responsiveness of a massing model. However, the

experiment also reveals a risk that an important design optimization potential, the floor plan layout itself, is overlooked. How could architects tap into this potential?

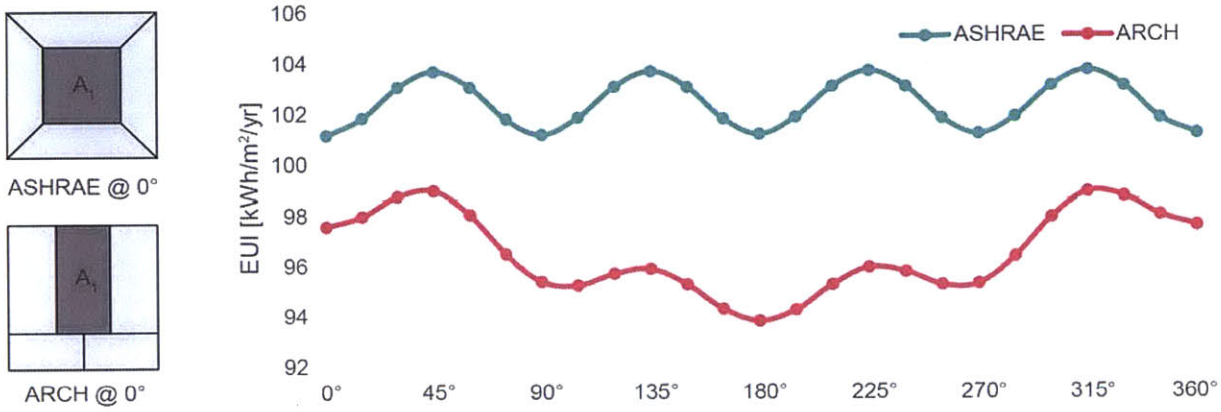

Figure 5-6: Rotation study with architectural and perimeter-core zoning

Unlike other architectural optimization workflows such as structural design or daylight optimization the relationship between energy and form has had the tendency to only provide a fuzzy and indirect sensitivity to morphologic changes of a design. The programmatic proportions and their spatial distribution within a design seem to have a significant influence on energy demand. Hence, a proof-of-concept floor plan optimization workflow is introduced. One floor plan shape is tested with nine different subdivision variants that all maintain the same area for circulation and main use space.

Similar to the previous simulation setup, the floor plan is tested for multiple climates, construction standards and use. A 20m by 60m floor plate is simulated with nine different subdivisions. The plans are shown in Figure 5-7. The zoning consists of a main use area and circulation that is kept constant at 150m^2 per floor in all variants. The circulation area is visualized in light grey. A window-wall ratio of 50% is assumed for both the north and the south facade. The nine zoning variants are tested in the same 24 scenarios mentioned in the methodology section.

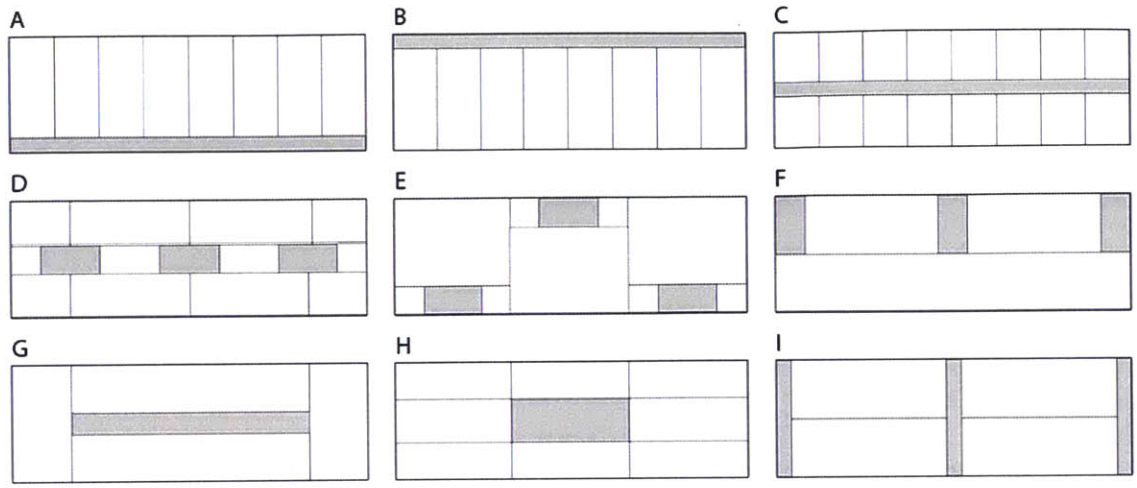

Figure 5-7: Schematic design floor plan design variants with identical circulation area

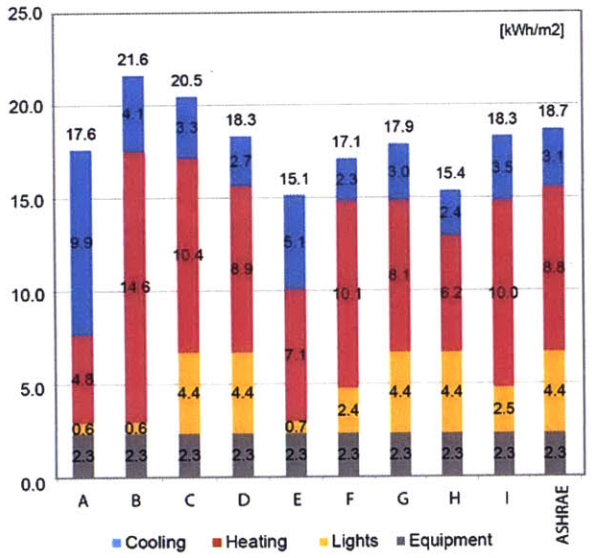

Figure 5-8: Load breakdown for all variants in one simulation scenario

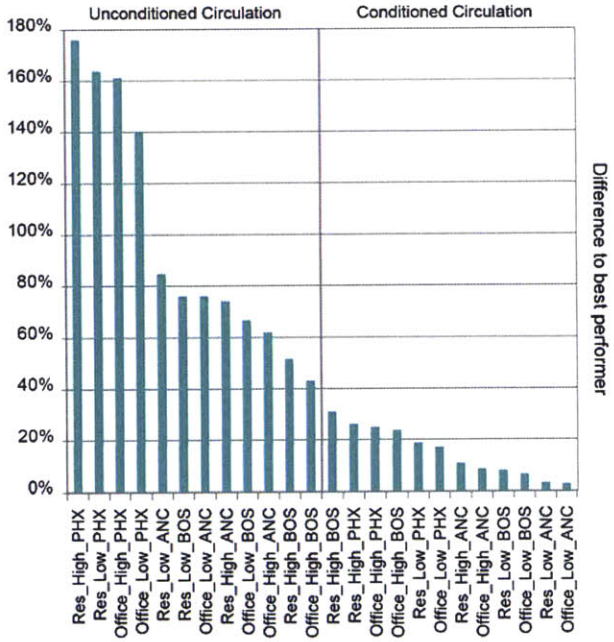

Figure 5-9: Graph visualizing delta of the minimum and maximum energy load divided by the minimum achievable load

The difference in the results is significant. Figure 5-8 shows a load breakdown for one scenario. In this scenario, the choice of the floor plan layout by itself can make or break the LEED credits achievable for building energy load reduction.

In order to evaluate the variance in energy use intensity for all scenarios, Figure 5-9 visualizes the delta of the minimum and maximum energy load among all nine floor plan variants. The delta is then normalized by the minimum-achievable-load. As illustrated in Figure 5-9, the delta of the best and the worst performer within one scenario is as high as 180% of the minimum achievable energy demand. One can thus safely infer that the floor-plan layout can have a significant influence on a building's energy demand. This result sheds new light on the relationship between form and energy in general: whereas the traditional assumption has been that massing orientation and façade design have the greatest impact towards energy efficiency, this study extends the focus on another important parameter of the architectural design domain – the floor plan and its organization typology. The previously presented results show that area proportions and location of the core area have to match only approximately in order to get closely matching results (Typologies A4, B3). Hence, this knowledge should be part of the thermal zoning considerations as early as possible. Ultimately, the form sensitivity that was demonstrated in the workflow may increase the interest of architects in actively pursuing design related efficiency measures.

5.5 Conclusion

This chapter provided an overview regarding the reliability of the ASHRAE prescribed perimeter-core zoning paradigm that is fundamental to the automated BEM and UBEM model generators presented in Chapters 3 and 4. A sample set of 1200 simulations reveals an overall RMSE of 15% for total EUI but also inconsistencies such as outliers with RMSEs from -28% to 58% are observed. These results suggests that the ASHRAE zoning scheme may be sufficiently accurate for large-scale applications where occasional errors have only limited influence on the overall results but has only limited applicability for individual building level design processes where such inconsistencies can be misleading. A significant energy optimization potential is revealed in the floor plan design process. These findings frame the limitations of core and perimeter based zoning for both urban and schematic building design.

6 Conclusion

This chapter discusses the hypotheses from Chapter 1 and provides an outlook for future research.

6.1 Feasibility of contributions

When interior building subdivisions are unknown, modelers rely on the ASHRAE 90.1 Appendix G guideline that prescribes a perimeter and core subdivision schema. In a study including 1200 simulation scenarios, a representative set of floor plans and their perimeter and core counterparts were compared in Chapter 5. With a total RMSE of 15% and 75% of the all simulated cases falling within an error margin of +-15%, the perimeter and core zoning paradigm provides a reasonably reliable and consistent energy analysis workflow for buildings with unknown interiors. Therefore, the current practice of implementing the ASHRAE 90.1 Appendix G thermal zoning guideline for buildings with yet undefined interiors is justifiable for the use in the majority of urban energy modeling tasks.

In Chapter 3 an argument that the ASHRAE zoning guideline effectively follows a straight-skeleton subdivision of a polygon is presented. Based on this finding an algorithm has been introduced that can automatically subdivide arbitrary planar-surface, 3D massing models into ASHRAE 90.1 Appendix G compliant perimeter and core thermal zone geometry. It has been shown that the procedure is robust and can handle simple and complex 2D and 3D shapes including inter-building adjacencies. Based on the algorithmically produced zone geometry it has been shown that multi-zone whole building energy models can be automatically produced and simulated. In Chapter 4, the algorithm has been used to automatically produce 121 individual multi-zone buildings for urban energy simulations. The method introduced in Chapter 3 has hence proven its capability to automatically produce ASHRAE 90.1 Appendix G compliant multi-zone whole building energy models from arbitrary massing models. Therefore, it is possible to develop a robust, fully automated thermal zoning algorithm that converts arbitrarily shaped massing models into ASHRAE 90.1 Appendix G compliant multi-zone "whole building" energy models.

In order to overcome the computational overhead of whole building multi-zone BEMs in large-scale urban applications, Chapter 4 introduced a method that translates arbitrary planar-surface 3D massing models into a meaningful set of "typical room" energy models. A comparison against 8712 BEMs generated with the Autozoner method revealed that results could be approximated with an overall RMSE of 6% and 14% with simulation speed increases of 20 and 269 times respectively. With runtimes on a standard laptop of under one minute for

the use cases presented in the discussion of Chapter 4, it has been shown that users can timely evaluate energy performance related aspects at the urban scale. Therefore, urban massing models can be automatically translated into a meaningful set of typical room energy models to approximate simulation results of fully conditioned ASHRAE 90.1 Appendix G compliant perimeter and core BEMs at a fraction of the computational cost.

6.2 Justifiable effort

The automatic BEM geometry generators Autozoner and Shoeboxer demonstrated that in combination with the simulation interface Archsim, BEM setup and execution can be completely automated. The only required inputs towards an UBEM for the case study in Chapter 4 were BEM space templates and a digital 3D massing model. Space templates are readily available e.g., in the SIA Merkblatt 2024 norm. The 3D massing model was generated for morphologic studies and visualizations in the design process and therefore was also readily available. The Shoeboxer further demonstrated that simulation results for an urban massing model containing 121 buildings can be obtained in just under one minute. Therefore, if BEM space templates and digital 3D massing models are available, the additional effort that is required to produce urban energy models with automatic building energy model generators is marginal and their utilization is hence realistic and justifiable for modelers who are interested in building-level energy simulations.

6.3 Relevance

This thesis has provided several use-case examples for the introduced automated BEM generator algorithms that demonstrate how UBEM simulations can be used to answer relevant societal questions. A Shoeboxer energy analysis of South Boston revealed significant differences in potential annual energy costs of two to three family houses and identified targets for urban renewal policies. A master plan design project from practice was used to indicate the limits of Net-Zero and on-site renewable energy strategies for high urban densities. Simulation results were produced in high spatial and temporal resolution to explore inter-building synergies and district energy management savings potentials. Further, relevant and digestible design feedback was generated such as window-to-wall ratio recommendations that are mapped on

massing model facades. Therefore, improved modeling methodologies can provide relevant energy performance related insights in a high spatial and temporal resolution, which can help to evaluate sustainable design strategies.

6.4 Urban Modeling across multiple scales

This section provides a vision of how the different simulation algorithms developed for this thesis can be used at various stages of urban planning and design. Rather than conclusive and final, this section is meant to be exploratory in nature. Urban design is an iterative and nonlinear process that transcends multiple scales with different levels of detail. Based on typical outputs of this process three main stages can be identified. The land use plan, usually provided in scales around 1:5000, is used to lay out the street layout, establish a first, vague distribution of program and densities. In this stage single-zone shoebox models or the so-called archetype approach seem feasible. The main goal of simulations at this stage is merely to understand the local climate and its implications on materials and construction standards. Based on the definition of the urban program, these shoebox models can also be used to come up with realistic templates for each architectural program. The notion of buildings is first introduced in development plans, layout plans and figure-ground-diagrams that are usually drawn in scales from 1:5000 to 1:1000. At this stage, modelers should transition to using the Shoeboxer in order to provide feedback regarding the layout and morphology. This stage should also fine-tune the prescribed densities and the program distribution from the previous planning step. At the point where designers transition to scales ranging from 1:500 to 1:200, modelers should consider a typology-aware modeling workflow as has been introduced in the discussion of Chapter 5 in order to tap into an additional energy efficiency potential.

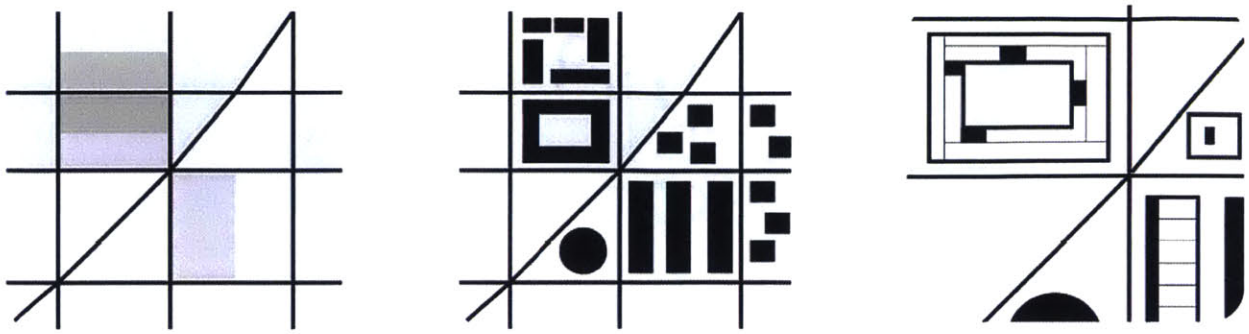

Archetype modeling

Shoeboxer modeling

Typology aware modeling

BEM

Autozoner

Land-use plan	**Development plan** **Layout plan** **Figure-ground plan**	**Detail** **Situation plan** **Ground Floor Plan** **Roof Plan**
Scales: *~1:5000*	*Scales:* *~1:5000 - 1:1000*	*Scales:* *~1:500 - 1:200*
Street layout Vague program distribution Densities Precedents	Building massing Typological ideas Precise program distribution Floor heights	Facades Typology Schematic interiors Entrance locations

Figure 6-1: Urban design process across different scales and levels of data availability

6.5 Outlook

Although this thesis has presented several advances, further work is necessary to foster a wider use of UBEMs in design and planning processes.

Refinement of non-geometric data for urban simulations

This thesis has focused on the production of thermal model geometry and automated workflows for BEM generation and utilized normed space type definitions to auto-populate non-geometric data fields in the UBEMs. While this approach is feasible for new-single-building modeling methodologies, it creates questionable results at urban scales. The use of identical

assumptions per use type such as identical occupancy schedules in all office spaces in an urban model does not reflect reality and produces worst-case load profiles with peak loads that all occur simultaneously. Real energy demand data is noisier since temporal shifts in building peak loads significantly dampen urban energy load curves. Hence, future research should provide methodologies that can generate more realistic non-geometric BEM inputs.

Validation against real urban energy demand

In conjunction with the generation of more realistic non-geometric BEM inputs, validation studies in different climate zones that compare modeled energy use against measured data are necessary to build confidence in UBEM approaches.

Typology-aware zoning for urban design processes

Even though the urban design process does not aim to produce detailed floor plans of every building in a master plan, designing the volumetric shapes of a massing model requires good understanding of architecture and its organizational typologies. Layout of streets, parceling and the depth as well as height of a massing model often predetermine or limit possible interior layouts. Based on these parameters, schematic interior subdivisions could hence become part of the thermal zoning considerations for UBEMs. At the point where designers transition to scales ranging from 1:500 to 1:200 modelers should consider a typology-aware modeling workflow in order to tap into an additional energy efficiency potential that has been revealed in Chapter 5. Future research could provide tools that aid modelers to implement typology-aware BEMs.

7 References

References

ActiveHouse, (2015), ActiveHouse Specifications, Retrieved July 17, 2015, form http://activehouse.info/about-active-house/specification

Aichholzer, O, Franz Aurenhammer, David Alberts, and B Gärtner. (1995). "A Novel Type of Skeleton for Polygons." *Journal of Universal Computer Science* 1: 752–61. doi:10.3217/jucs-001-12-0752.

Aichholzer, Oswin, and Franz Aurenhammer. (1996). "Straight Skeletons for General Polygonal Figures in the Plane." In Computing and Combinatorics, Lecture Notes in Computer Science Volume 1090, pp 117–26. Edited by Jin-Yi Cai and Chak Kuen Wong. Vol. 1090. Lecture Notes in Computer Science. Berlin, Heidelberg: Springer Berlin Heidelberg. doi:10.1007/3-540-61332-3.

ANSI/ASHRAE. (2011). Standard 140-2011, standard method of test for the evaluation of building energy analysis computer programs. ASHRAE, Atlanta, GA.

ANSI/ASHRAE/IES. (2013). Standard 90.1-2013 -- Energy Standard for Buildings Except Low-Rise Residential Buildings, Appendix G Atlanta, Georgia: The American Society of Heating, Refrigerating and Air-Conditioning Engineers.

Autodesk. (2013). "Autodesk Vasari." Retrieved November 1, 2013, from http://autodeskvasari.com/

Barequet, Gill, Michael T. Goodrich, Aya Levi-Steiner, and Dvir Steiner. (2004). "Contour Interpolation by Straight Skeletons." *Graphical Models* 66 (4): 245–60. doi:10.1016/j.gmod.2004.05.001.

Barnaby, C., & Crawley, D. (2011). Weather data for building performance simulation. In Hensen, J. L., & Lamberts, R. (Eds.) Building performance simulation for design and operation. Taylor & Francis US.

Bentley. (2013). "AECOsim", Retrieved November 1, 2013, http://docs.bentley.com/en/AECOsimEnergySimulator/benshelp89.html

Besserud, K., and T. Hussey. (2011). "Urban Design, Urban Simulation, and the Need for Computational Tools." *IBM Journal of Research and Development*. doi:10.1147/JRD.2010.2097091.

Beyeler, F., Beglinger, N., & Roder, U. (2009). Minergie: The Swiss sustainable building standard. innovations, 4(4), 241-244.

Birdsall, B., Buhl, W. F., Ellington, K. L., Erdem, A. E., & Winkelmann, F. C. (1990). Overview of the DOE-2 building energy analysis program, Version 2. 1D(No. LBL-19735-Rev. 1). Lawrence Berkeley Lab., CA (USA).

Bobenhausen, William. (1994). Simplified Design of HVAC Systems. New York: John Wiley & Sons.

BRREAM. (2004). "Building research establishment environmental assessment method." Retrieved April 21, 2014, http://www.breeam.org/index.htm

Bueno, B., Norford, L., Pigeon, G., & Britter, R. (2011). Combining a detailed building energy model with a physically-based urban canopy model. *Boundary-layer Meteorology*, 140(3), 471-489.

Bueno, B., Norford, L., Pigeon, G., & Britter, R. (2012). A resistance-capacitance network model for the analysis of the interactions between the energy performance of buildings and the urban climate. *Building and Environment*, 54, 116-125.

Bundesrepublik Deutschland. (2007). Verordnung über energiesparenden Wärmeschutz und energiesparende Anlagentechnik bei Gebäuden.(Energieeinsparverordnung—EnEV). Energieeinsparverordnung vom 24. Juli 2007 (BGBl. I S. 1519)

Cacciola, Fernando. (2004). "A CGAL Implementation of the Straight Skeleton of a Simple 2D Polygon with Holes." In 2nd CGAL User Workshop. Brooklyn, New York, USA: CGAL. https://cgal.org/UserWorkshop/2004/straight_skeleton.pdf.

CGAL. (2014). "Computational Geometry Algorithms Library." Retrieved April 21, 2014, http://www.cgal.org

Cheng, Siu-Wing, and Antoine Vigneron. (2007). Motorcycle graphs and straight skeletons. *Algorithmica* 47, no. 2: 159-182.

City of Boston. (2014). 2014 Climate Action Plan. Retrieved July 29, 2015, from http://plan.greenovateboston.org/

Clarke, J. A. (1996). The Esp-r system: advances in simulation modeling. *Building Services Journal* pp. 27–9.

Clarke, J. A. (2001). Energy simulation in building design. Routledge.

Clarke, J., Aasem, A., Hand, J., Hansen, J., Pemot, C., & Strachen, P. (1993). ESP-r: A program for building energy simulation. Energy Simulation Research Unit, ESRU Manual U, 93.

Compagnon, R. (2004). Solar and daylight availability in the urban fabric. *Energy and Buildings*, 36(4), 321-328.

Crawley, D. B., Hand, J. W., & Lawrie, L. K. (1999). Improving the weather information available to simulation programs. In Proceedings of Building Simulation'99 (Vol. 2, pp. 529-536).

Crawley, D. B., Hand, J. W., Kummert, M., & Griffith, B. T. (2008). Contrasting the capabilities of building energy performance simulation programs. *Building and Environment*, 43(4), 661-673.

Crawley, D. B., Lawrie, L. K., Pedersen, C. O., & Winkelmann, F. C. (2000). Energy plus: energy simulation program. *ASHRAE Journal*, 42(4), 49-56.

De Berg, M., Cheong, O., van Kreveld, M. & Overmars, M. (2008). Computational Geometry. Berlin, Heidelberg: Springer Berlin Heidelberg. doi:10.1007/978-3-540-77974-2.

De Wilde, P., Augenbroe, G. & Van Der Voorden M. (1999)."Invocation of building simulation tools in building design practice." In Proceedings of IBPSA '99 Buildings Simulation Conference, pp. 1211-1218.

Deru, M., Field, K., Studer, D., Benne, K., Griffith, B., Torcellini, P. & Crawley, D. (2011). US Department of Energy commercial reference building models of the national building stock.

DGNB. (2014). "DGNB Zertifizierungssystem." Retrieved April 21, 2014, http://www.dgnb-system.de/de/system/zertifizierungssystem/

DOE. (2013). "U.S. Department of Energy Commercial Reference Building Models." Retrieved November 1, 2013, from http://energy.gov/eere/buildings/commercial-reference-buildings

DOE. (2015). GREENHOUSE GAS REDUCTION TARGETS. Retrieved July 29, 2015, from http://energy.gov/eere/spo/goals-and-requirements-test-do-not-publish#Greenhouse Gas Reduction Targets

Dogan, T., Reinhart, C., & Michalatos, P. (2012). Urban Daylight Simulation Calculating the Daylit Area of Urban Designs. In SimBuild 2012, Fifth National Conference of IBPSA-USA, 613–20. Madison, Wisconsin.

EERE. (2011) Buildings Energy Data Book. EERE U.S. Department of Energy. Retrieved November 1, 2013, http://buildingsdatabook.eren.doe.gov/TableView.aspx?table=3.1.4

EERE. (2013). "EnergyPlus Energy Simulation Software." Retrieved November 1, 2013, from http://apps1.eere.energy.gov/buildings/energyplus/

EERE. (2013). "EnergyPlus Example File Generator." Retrieved November 1, 2013, from http://apps1.eere.energy.gov/buildings/energyplus/cfm/inputs/index.cfm

EERE. (2013). EnergyPlus Energy Simulation Software. EERE U.S. Department of Energy. Retrieved November 1, 2013, from http://apps1.eere.energy.gov/buildings/energyplus/

European Commission. (2015). European Commission Climate Action, Retrieved July 17, 2015, http://ec.europa.eu/clima/policies/roadmap/index_en.htm

Feist, W. (1989). Forschungsprojekt Passive Häuser; Darmstadt 1989. Kommentierte Neuauflage 1995]

Felkel, Petr, and Stepan Obdrzalek. (1998). "Straight Skeleton Implementation." In Spring Conference on Computer Graphics, 210–18. Budmerice, Slovakia.

Filogamo, L., Peri, G., Rizzo, G., & Giaccone, A. (2014). On the classification of large residential buildings stocks by sample typologies for energy planning purposes. *Applied Energy*, 135, 825-935.

Gaine, K., Duffy, A.: (2010) A life cycle cost analysis of large-scale thermal energy storage technologies for buildings using combined heat and power; Zero Emission Buildings (eds. M.Haase, I. Andresen, A. Hestnes); Conference Proceedings Trondheim, Norway, June 7-8.

Goretzki, P. (1993). Passive Sonnenenergienutzung in der Bauleitplanung, Entwicklung einer computerunterstützten Methode zur quantitativen solarenergetischen Bewertung und Modifizierung von Bebauungs- und Flächennutzungsplänen 1. Aufl. - Stuttgart: Inst. für Bauökonomie.

Goretzki, P. (2013). GSOL, da solar+energetische Städtebausimulationsprogramm, software version 9.x, URL: http://www.gsol.de

Griffith, B. T., & Crawley, D. (2006). Methodology for Analyzing the Technical Potential for Energy Performance in the US Commercial Buildings Sector with Detailed Energy Modeling: Preprint. National Renewable Energy Laboratory.

Hall, I. J., Prairie, R. R., Anderson, H. E., & Boes, E. C. (1978). Generation of a typical meteorological year (No. SAND-78-1096C; CONF-780639-1). Sandia Labs., Albuquerque, NM (USA).

Hegger, M., Fafflock, C., Hegger, J., & Passig, I. (2013). Aktivhaus das Grundlagenwerk–Vom Passivhaus zum Energieplushaus; Verlag Georg DW Callwey GmbH & Co. KG; München 2013. ISBN 978-3-7667-1902-7.

Hensen, J. L., & Lamberts, R. (Eds.). (2011). Building performance simulation for design and operation. Taylor & Francis US.

Hirsch, James. (2010). "eQuest Introductory Tutorial, version 3.64". Retrieved November 1, 2013, from http://www.doe2.com/equest/

Holst, S., Dogan, T., (2013) Transsolar, Abuja Centenary City Project Report. Not publicly available.

Huang, Y. J., & Brodrick, J. (2000). A bottom-up engineering estimate of the aggregate heating and cooling loads of the entire US building stock. Lawrence Berkeley National Laboratory.

Huber, Stefan, and Martin Held. "A fast straight-skeleton algorithm based on generalized motorcycle graphs." *International Journal of Computational Geometry & Applications* 22, no. 05 (2012): 471-498.

Hutchinson, E. J., Wilkinson, P., Hong, S. H., Oreszczyn, T., & Warm Front Study Group. (2006). Can we improve the identification of cold homes for targeted home energy-efficiency improvements? *Applied Energy*, 83(11), 1198-1209.

Ianni, Manuela, and Michelle Sánchez de León. (2013). "Applying Energy Performance-Based Design in Early Design Stages." In Computation and Performance - Proceedings of the 31st eCAADe Conference, Volume 1, 1:31–40. Delft, The Netherlands.

IES. (2015). Software Validation and Approval. Retrieved July 30, 2015, from https://www.iesve.com/software/software-validation

Jentsch, M. F., Bahaj, A. S., & James, P. A. (2008). Climate change future proofing of buildings—Generation and assessment of building simulation weather files. *Energy and Buildings*, 40(12), 2148-2168.

Jentsch, M. F., James, P. A., Bourikas, L., & Bahaj, A. S. (2013). Transforming existing weather data for worldwide locations to enable energy and building performance simulation under future climates. Renewable Energy,55, 514-524.

Johnson, Angus. 2014. "Clipper 6.0 -an Open Source Freeware Polygon Clipping Library." http://www.angusj.com/delphi/clipper.php.

Jones, N. L., McCrone, C. J., Walter, B. J., Pratt, K. B., & Greenberg, D. P. (2013). Automated translation and thermal zoning of digital building models for energy analysis. In Building Simulation Conference.

Keirstead, J., Jennings, M., & Sivakumar, A. (2012). A review of urban energy system models: Approaches, challenges and opportunities. *Renewable and Sustainable Energy Reviews*, 16(6), 3847-3866.

Klein, S. A. (1979). TRNSYS, a transient system simulation program. Solar Energy Laboratory, University of Wisconsin—Madison.

Kolbe, T. H., Gröger, G., & Plümer, L. (2005). CityGML: Interoperable access to 3D city models. In Geo-information for disaster management (pp. 883-899). Springer Berlin Heidelberg.

Korolija, I., Marjanovic-Halburd, L., Zhang, Y., & Hanby, V. I. (2013). UK office buildings archetypal model as methodological approach in development of regression models for predicting building energy consumption from heating and cooling demands. *Energy and Buildings*, 60, 152-162.

Kropf, S., & Zweifel, G. (2001). Validation of the Building Simulation Program IDA-ICE According to CEN 13791 "Thermal Performance of Buildings–Calculation of Internal Temperatures of a Room in Summer Without Mechanical Cooling–General Criteria and Validation Procedures." Hochschule Technik+ Architektur Luzern. HLK Engineering.

Loga, T., Diefenbach, N., & Stein, B. (2012). Typology approach for building stock energy assessment. Main results of the TABULA project.

Mahdavi, A, S Feurer, A Redlein, and G Suter. (2003). "An Inquiry into the Building Performance Simulation Tools Usage by Architects in Austria." In BS 2003, Eighth International IBPSA Conference. 777–84. Eindhoven, Netherlands.

Mata, É., Kalagasidis, A. S., & Johnsson, F. (2013). A modelling strategy for energy, carbon, and cost assessments of building stocks. *Energy and Buildings*, 56, 100-108.

Mata, É., Kalagasidis, A. S., & Johnsson, F. (2014). Building-stock aggregation through archetype buildings: France, Germany, Spain and the UK. Building and Environment, 81, 270-282.

McNeel, R. (2012). Grasshopper - Generative Modeling with Rhino, McNeel North America, Seattle, USA. (http://www.grasshopper3d.com/).

McNeel, R. (2012). Rhinoceros - NURBS Modeling for Windows (version 5.0), McNeel North America, Seattle, WA, USA. (www.rhino3d.com/).

McNeel, R. (2013). "RhinoCommon Plug-in SDK." Retrieved November 1, 2013, from http://wiki.mcneel.com/developer/rhinocommon/

Morbitzer, C., Strachan, P. A., Webster, J., Spires, B., & Cafferty, D. (2001). Integration of building simulation into the design process of an architectural practice. In Building Simulation, Seventh International IBPSA Conference, 697–704. Rio de Janeiro, Brazil.

Nouvel R, Schulte C, Eicker U, Pietruschka D, Coors V. (2013). CityGML based 3D city model for energy diagnostics and urban energy policy support. In proceedings of Building Simulation 2013: Chambery, France; 2013.

O'Rourke, J. (1998). Computational Geometry in C. 2nd ed. Cambridge: Cambridge University Press. doi:CBO9780511804120.

Owen, D. (2009). The Green Metropolis: Why living smaller, living closer and driving less are keys to sustainability. Riverhead Books, New York.

Pratt, K. B., Jones, N. L., Schumann, L., Bosworth, D. E., & Heumann, A. D. (2012). Automated translation of architectural models for energy simulation. In Proceedings of the 2012 Symposium on Simulation for Architecture and Urban Design (p. 6). Society for Computer Simulation International.

Preparata, Franco P. (1977). "The medial axis of a simple polygon." In Mathematical Foundations of Computer Science 1977, pp. 443-450. Springer Berlin Heidelberg.

Remund, J., Müller, S. C., Schilter, C., & Rihm, B. (2010). The use of Meteonorm weather generator for climate change studies. In 10th EMS Annual Meeting, 10th European Conference on Applications of Meteorology (ECAM) Abstracts, held Sept. 13-17, 2010 in Zürich, Switzerland. http://meetings. copernicus. org/ems2010/, id. EMS2010-417 (Vol. 1, p. 417).

Robinson, D. & Stone, A. (2004). Irradiation modelling made simple: the cumulative sky approach and its applications. In PLEA Conference (pp. 19-22).

Robinson, D., Campbell, N., Gaiser, W., Kabel, K., Le-Mouel, A., Morel, N., Stone, A. (2007). SUNtool–a new modelling paradigm for simulating and optimizing urban sustainability. *Solar Energy*, 81(9), 1196-1211.

Samuelson, H., Ghorayshi, A., & Reinhart, C. (2014). Analysis of a simplified calibration procedure for 18 design-phase building energy models. *Journal of Building Performance Simulation*, (ahead-of-print), 1-13.

Samuelson, H., Lantz, A., Reinhart, C. (2012). "Non-Technical Barriers to Energy Model Sharing and Reuse." Building and Environment 54 (August): 71–76. doi:10.1016/j.buildenv.2012.02.001.

Schlueter, A. & Thesseling, F. (2009). "Building Information Model Based Energy/Exergy Performance Assessment in Early Design Stages." *Automation in Construction* 18 (2): 153–63. doi:10.1016/j.autcon.2008.07.003.

Smith, L., Bernhardt, K., & Jezyk, M. (2011). Automated energy model creation for conceptual design. In Proceedings of the 2011 Symposium on Simulation for Architecture and Urban Design (pp. 13-20). Society for Computer Simulation International.

Stanford University. (2015). Innovation - Sustainable Stanford - Stanford University. Retrieved July 29, 2015, from https://sustainable.stanford.edu/sesi/innovation

Strømann-Andersen, J., & Sattrup, P. A. (2011). The urban canyon and building energy use: Urban density versus daylight and passive solar gains. *Energy and Buildings*, 43(8).

Strzalka, A., Bogdahn, J., Coors, V., & Eicker, U. (2011). 3D City modeling for urban scale heating energy demand forecasting. HVAC&R Research, 17(4), 526-539.

The City of New York. (2015). GBEE - The New York City Carbon Challenge. Retrieved July 29, 2015, from http://www.nyc.gov/html/gbee/html/challenge/mayor-carbon-challenge.shtml

Tuominen, P., Holopainen, R., Eskola, L., Jokisalo, J., & Airaksinen, M. (2014). Calculation method and tool for assessing energy consumption in the building stock. *Building and Environment*, 75, 153-160.

U.S. Energy Information Administration. (2009). U.S. Energy Information Administration - Residential Energy Consumption Survey (RECS). Retrieved August 3, 2015, from http://www.eia.gov/consumption/residential/data/2009

UN. (2012). World Urbanization Prospects, the 2011 Revision: Highlights. New York.

UN. (2015). Sustainable Development, Retrieved July 17, 2015, form http://www.un.org/en/ga/president/65/issues/sustdev.shtml

Underwood, C., & Yik, F. (2008). Modelling methods for energy in buildings. John Wiley & Sons.

UNEP. (2015). http://www.unep.org/energy/portals/50177/DES_District_Energy_Report_full_02_d.pdf

UNEP. (2015). Sustainable Buildings and Climate Initiative. Retrieved August 5, 2015, from http://www.unep.org/sbci/AboutSBCI/Background.asp

USGBC. (2011). US Green Building Council. "GREEN BUILDING AND CLIMATE RESILIENCE." Ann Arbor 1001: 48109.

USGBC. (2014). US Green Building Council. LEED rating systems. Retrieved November 2014 from http://www.usgbc.org/leed#rating

Van Treeck, C., & Rank, E. (2007). Dimensional reduction of 3D building models using graph theory and its application in building energy simulation. *Engineering with Computers*, 23(2), 109-122.

Ward, G. J. (1994). The RADIANCE lighting simulation and rendering system. In Proceedings of the 21st annual conference on Computer graphics and interactive techniques (pp. 459-472). ACM.

Wetter, M. (2001). GenOpt®," Generic Optimization Program. In Seventh international IBPSA conference (pp. 601-608).

Wilcox, S., Marion, W. (2008). User's manual for TMY3 data sets. Golden, CO: National Renewable Energy Laboratory.

World Bank. (2015). CO2 emissions from residential buildings and commercial and public services. Retrieved April 6, 2015, from http://data.worldbank.org/indicator/EN.CO2.BLDG.MT

World Commission on Environment and Development. (1987). World Commission on Environment and Development Our Common Future, Oxford University Press, New York.

Publications written in context of this thesis:

Cerezo, C., Dogan, T., & Reinhart, C. (2014). Towards Standardized Building Properties Template Files for Early Design Energy Model Generation. In Proceedings of the ASHRAE/IBPSA-USA building simulation conference (pp. 25-32).

Dogan, T. (2013). Archsim - Energy Modeling Tools for Grasshopper. Retrieved November 1 2013, from http://www.archsim.com/

Dogan, T., & Reinhart, C. (2013). Automated Conversion of Architectural Massing Models into Thermal 'shoebox' Models. In BS2013: 13th Conference of International Building Performance Simulation Association, 3745–52. Chambéry, France.

Dogan, T., Reinhart, C., & Michalatos, P. (2014). Automated Multi-zone Building Energy Model Generation for Schematic Design and Urban Massing Studies. In IBPSA eSim conference, Ottawa, Canada.

Dogan, T., Reinhart, C., Michalatos, P. (2015). Autozoner: An algorithm for automatic thermal zoning of buildings with unknown interior space definitions. *Journal of Building Performance Simulation*. http://dx.doi.org/10.1080/19401493.2015.1006527

Dogan, T., Saratsis, E., Reinhart, C. (2015). The Optimization Potential of Floorplan Typologies In Early Design Energy Modeling, Submitted to BS2015, India.

Dogan, T., Saratsis, E., Reinhart, C. (2015). Towards An Energy Simulation-Informed Design Process, Submitted to BS2015, India.

Reinhart, C. F., Dogan, T., Jakubiec, J. A., Rakha, T., & Sang, A. (2013). UMI-An Urban Simulation Environment for Building Energy Use, Daylighting and Walkability. In Building Simulation 2013, 13th Conference of International Building Performance Simulation Association, 476–83.

Rose, C., Saratsis, E.; Aldawood, S.; Dogan, T.; Reinhart, C. (2015). A Tangible Interface for Collaborative Urban Design for Energy Efficiency, Daylighting, and Walkability, Submitted to BS2015, India

Saratsis, E., Dogan, T., Reinhart, C. (2015). Daylit Density – Simulation-based framework for the development of zoning rules for daylighting, Submitted to the *Journal of Building Research & Information.*

List of abbreviations:

AIA: American Institute of Architects

BEM: Building Energy Model

BIM: Building Information Model

BPS: Building Performance Simulation

BREEAM: Building Research Establishment Environmental Assessment Methodology

BREP: Boundary representation

CAD: Computer Aided Design

CGAL: Computational Geometry Algorithms Library

DCEL: Doubly connected edge list

DGNB: Deutsche Gesellschaft für nachhaltiges Bauen e.V

DGNB: German Sustainable Building Council

DOE: Department of Energy

EERE: Office of Energy Efficiency & Renewable Energy

EnEV: Energieeinsparverordnung (German Energy Savings Directive)

EUI: Energy Use Intensity

GHG: Greenhouse gas

GML: Geography Markup Language

HVAC: Heating, Ventilation and Air Conditioning

IWEC: International Weather for Energy Calculations

LEED: Leadership in Energy and Environmental Design

RAM: Random-access memory

SIA: Schweizerischer Ingenieur- und Architektenverein (Swiss chamber of architects and engineers)

SSD: Solid state drive

TMY: Typical Meteorological Year

UBEM: Urban BEM

UBPS: Urban BPS

UNEP: United Nations Environment Programme

USGBC: U.S. Green Building Council

WSVO: Wärmeschutzverordnung (German Energy Savings Directive)